IMPERIAL COLLEGE OF SCIENCE AND TECHNOLOGY

Department of Electrical Engineering

CONTROLLED GROWTH OF MAGNETIC OXIDE LAYERS BY LIQUID PHASE EPITAXY

by

JOHN EDWARD DAVIES

A thesis submitted for the degree of

DOCTOR OF PHILOSOPHY

January, 1974

ABSTRACT

The process of liquid phase epitaxy for the growth of thin layers of magnetic garnet has received considerable attention during the past three years. The introductory chapter outlines the development of this process during this time and provides a summary of the present state of art.

The fundamental physical properties of the lead oxide/boric oxide flux and its solutions of garnet have been measured. Epitaxial layers have been grown onto non-magnetic garnet substrates using the dipping method. The conditions for obtaining highly perfect epitaxial layers are discussed. An analysis of the growth kinetics has been made and a model for the growth process proposed. Interface instability and its relevance to the growth process has been determined. An investigation of other potential flux systems for garnet epitaxy has been made.

CONTENTS

Cont..

Cont ..

CHAPTER I

1. INTRODUCTION.

1.1 The Need for Single Crystal Garnet Films.

The earliest requirement for single crystal garnet films was for microwave applications. Here the main need was to obtain films with narrow ferrimagnetic resonance linewidths and generally yttrium iron garnet (YIG) proved suitable when fabricated into films of approximately 100 micron thickness. At about 1969 there began a very active interest in the device potential of the magnetic "bubble" domain and two years later it was realised that by appropriate substitution the garnet family would prove a very attractive material for this type of device. At present there is a tremendous amount of research being done in this field in order to get prototype devices into operation.

Another attractive property of the garnet is its magneto-optic effect, about which more will be said later in this chapter. Attractive optical display and data storage can be envisaged in garnet films exhibiting large magneto-optic effects.

1.2 The Magnetic Bubble

Since this research project was undertaken with the aim of producing single crystal films of magnetic garnet suitable for bubble domain applications, it is necessary at this point to define the bubble domain, outline its device potential and state exactly what the

materials requirements are.

One of the simplest descriptions of a magnetic bubble domain has been given by Bobeck and Scovil (1). If a thin section of a ferromagnetic crystal is cut perpendicular to its easy axis of magnetisation and viewed through a polarising microscope then the crystal's magnetic domains rotate the plane of polarisation of the incident light in a direction which depends on their magnetic polarity. This is known as the magneto-optic effect and the magnitude of the rotation is known as the Faraday rotation, which depends on the material, its thickness and the wave-length of the polarised light. For most garnet materials the Faraday rotation is about 0.3^{o} per micron thickness of crystal in the visible spectrum, although bismuth-substituted garnets can have values of a few degrees per micron making them attractive possibilities for optical display and storage devices. Therefore by adjusting the polarising filter to the almost-crossed position, domains of one magnetic polarity will appear dark while those of opposite polarity appear brighter. In the absence of an external bias field, regions of opposite polarity are equal in area and interwoven in a serpentine pattern as illustrated in figure 1.1.A.

If an external bias field is then applied parallel to the easy axis, as the bias field is increased regions which have magnetic polarity in the same sense as the bias field increase in size at the expense of those whose polarity is in the opposite direction (figure 1.1.B). During this process a few isolated

cylindrical magnetic domains may be created and these are referred to as bubble domains. When the bias field is increased to a sufficiently large magnitude, all of the crystal becomes magnetised in the same direction as the field. The value at which this just occurs is known as the run-out field.

A complete hexagonal bubble lattice can be generated by applying an appropriately pulsed bias field. Figure 1.1.C shows such a lattice and it is remarkable that this has a number of anologies with a real crystal lattice. As can be seen in figure 1.1.C, the bubble lattice contains low angle grain boundaries and dislocations. By oscillating the bias field the bubbles can be made to flow and crystallise into a more perfect hexagonal lattice. Finally in highly perfect garnet films, highly perfect bubble lattices can be generated and from these diffraction patterns have been obtained using a Helium-Neon laser (2).

1.3 Device Potential of the Magnetic Bubble.

The simplest use of the magnetic bubble is in data storage, the presence or absence of a bubble providing the necessary information in binary code. It has been shown (1) that by using a rotating magnetic field in combination with appropriate permalloy overlay patterns on the crystal surface, bubbles can be generated, annhialated and moved through the crystal lattice. In addition, bubbles can be detected by a technique based on magnetoresistance; the resistance of a permalloy overlay bar changing when a bubble is immediately beneath it.

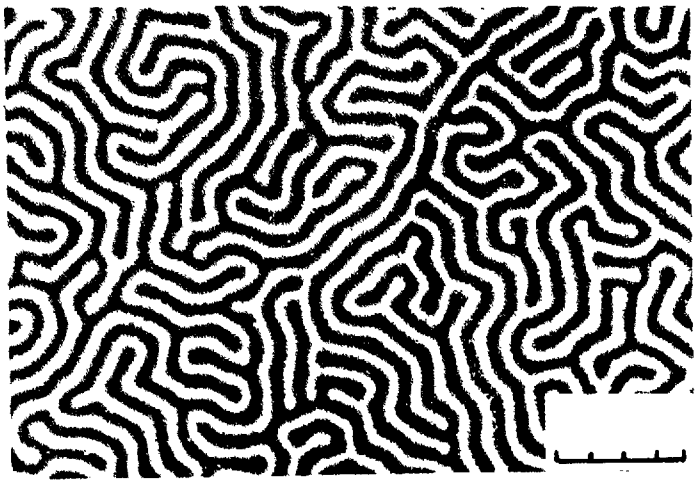

A

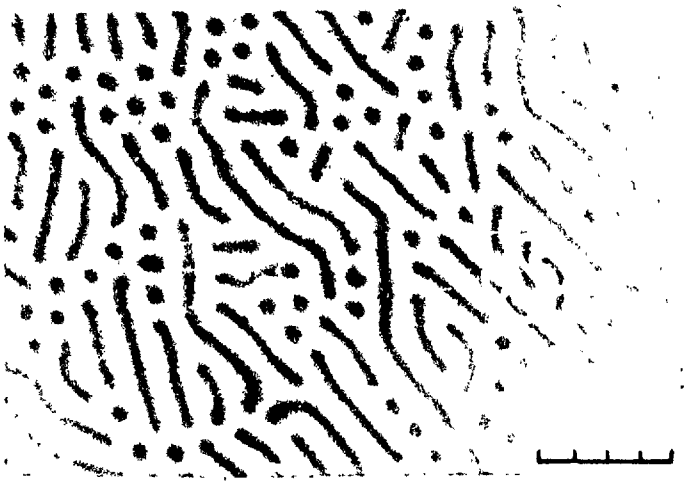

B

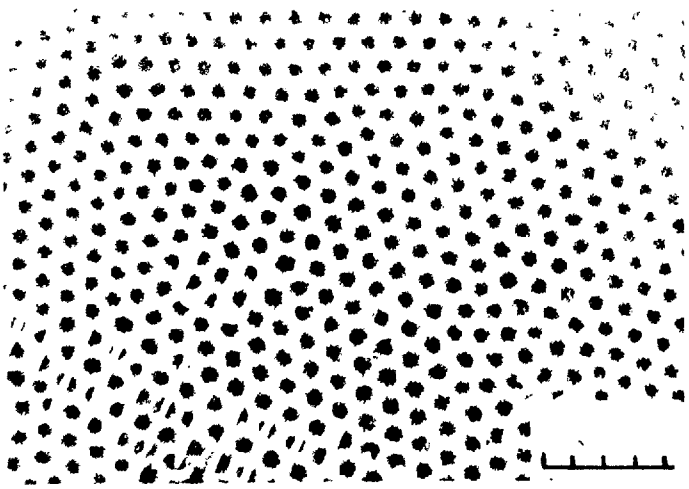

C

FIG 1.1 (1 DIV. = 10 MICRON)

Using these basic steps data storage can be performed, the bubble size governing the density of storage and the domain wall velocity governing the rate at which the data may be read out (i.e. the access time).

Normally the mode of data storage depends on the speed at which the data is required. Extremely fast access times are obtained using ferrite cores or transistors. However since these require a relatively large pulse of energy to switch, they cannot be packed closely together because of the problem of heat dissipation. Magnetic discs and drums provide enormous storage capacities but have the disadvantage that access times are extremely slow. The magnetic bubble mode of storage conveniently fits into the access gap. Since the energy required to move a bubble four diameters, the equilibrium spacing between bubbles, is two orders of magnitude lower than that required to switch tiny transistors, high density storage is clearly possible. Domain-wall velocities of 400 cm. per second per oersted of drive field provide data at the megabit rate, much faster than discs or drums, although not as fast as ferrite cores or transistors.

On a long-term basis, the magnetic bubble storage system has the potential to be extremely reliable since it requires far less mechanical parts than magnetic discs or drums. However, perhaps the greatest long-term asset of the bubble domain is that by using a combination of overlay patterns and ciruits, basic logic functions can be performed "on chip" without the need for the data

to be read out first.

1.4 Materials search.

In order to obtain a commercially attractive mode of storage, a capacity of one million bits per square centimetre is required which can only be satisfied by bubbles whose diameter is less than five microns. To obtain a data access rate in the megabit region the conditions on domain-wall velocities has already been specified. In addition to these device requirements the conditions for stable bubbles to exist have been specified by Thiele (3, 4). They are:

1) The material must have a unique easy axis of magnetisation.

2) The quantity, q, must lie between 2 and 10 where

$$q = \frac{K_u}{2\pi M_s^2}$$

K_u being the uniaxial magnetic anisotropy and M_s the saturation magnetisation.

3) The thickness of the crystal film must be approximately equal to the bubble diameter, although small deviations from this are allowable resulting in less stable bubble domains.

In attempting to meet the first requirement, the garnet family was originally overlooked since, being cubic, the crystals have four equivalent (111) easy axes. Rare earth orthoferrites ($RFeO_3$, where R is the rare earth)

were the first materials to receive wide attention (5, 6). However, these provided large bubbles, typically 100 microns in diameter. The formula relating bubble diameter, d, to the properties of the material is

$$d = \frac{10\sqrt{AK_u}}{\pi M_s^2}$$

where A is the exchange constant (a measure of the force acting to keep adjacent spin vectors aligned). Therefore attempts were made to find orthoferrites with high magnetisations. The composition $Sm_{0.55}\ Tb_{0.45}\ FeO_3$ supported the smallest bubbles found in orthoferrites but even these were approximately 25 microns in diameter. In addition, the dependance of magnetisation was always large for orthoferrites and so they generally proved unattractive for device applications.

Magnetoplumbite ($PbO.6Fe_2O_3$) and its barium and strontium analogs belong to the hexagonal crystal class, possessing a unique easy axis of magnetisation. Upon examination (7) these were found to support bubbles whose diameters were substantially less than one micron. Since submicron bubbles are not easily handled, gallium or aluminium was partially substituted for iron. Although this gave suitably sized bubbles, domain-wall velocities were always too low to be of use. As was the case with orthoferrites, the temperature dependance of magnetisation was fairly steep in almost all cases.

A significant breakthrough occurred when it was discovered by Bobeck et al. (8) that, in addition to

the magnetocrystalline anisotropy exhibit by orthoferrites and magnetoplumbites, anisotropy could be introduced into the ordinarily cubic garnets during the growth process. When two or more rare earths are competing for the dodecahedral sites they often do not distribute randomly (9) producing a garnet crystal which is distorted slightly from cubic symmetry with respect to both its crystallographic and magnetic properties. Hence one of the four equivalent (111) axes becomes a unique easy axis and Thiele's first requirement for the existance of stable bubble domains is satisfied.

Although the mechanism of growth-induced anisotropy is not fully understood, it is probable that when rare earths of different sizes enter the garnet lattice, each distorts the lattice around it in such a way as to favour one particular rare earth to be accommodated in that part of the lattice. It has been predicted by Rosenwaig (10) that the greater the size difference in the rare earths the larger is the growth-induced anisotropy and this general trend is found to be true in practice. Further supporting evidence is gained from the fact that lower growth temperatures produce garnets with higher anisotropies. In garnets grown by chemical vapour deposition (CVD) the temperatures used are in excess of 1200^{o}C. At these temperatures there is enough thermal energy to disrupt any site preferences of rare earths and no growth-induced anisotropy is found. Garnet layers grown by hydrothermal epitaxy (11) at around 400^{o}C generally have larger anisotropies

than comparable garnet layers grown by liquid phase epitaxy at about 900°C. Annealling of garnets at 1200°C or greater reduces and may even eliminate their growth-induced anisotropy. This is also consistent with the site-preference mechanism.

Garnets have a number of important advantages over orthoferrites and magnetoplumbites as bubble domain hosts. Although the magnetisation of rare earth iron garnets is sufficiently high to support submicron bubbles, partial substitution of gallium or aluminium for iron can be used to lower the magnetisation and provide suitably sized bubbles. Many of these gallium-substituted garnets have high domain wall velocities making them suitable for fast access storage. In addition, the variation of magnetisation with temperature is extremely small for many garnets in the vicinity of room temperature.

In order to understand the insensitivity of magnetisation with temperature it is necessary to consider the garnet structure in detail. The garnet structure belongs to the most complex of the cubic point groups, Ia3d. There are eight formula units and consequently 160 atoms, per unit cell. Unsubstituted rare earth iron garnets can exist with rare earths ranging from lutetium to samarium. Rare earths larger than samarium do not form iron garnets by themselves although they may be partially substituted in iron garnets containing smaller rare earths.

In the unsubstituted rare earth iron garnet of formula $R_3Fe_5O_{12}$, there are two types of site which

the iron atoms can occupy, octahedrally or tetrahedrally coordinated with oxygen atoms. In the unit garnet forumla two iron atoms occupy octahedral sites and three occupy the smaller tetrahedral sites. Since trivalent iron has five unpaired electrons whose spin vectors are antiparallel on octahedral and tetrahedral sites the net magnetic moment due to the iron sub-lattice is five Bohr-Magnetons at $0^{o}K$. However most rare earths (yttrium is an exception) also contain unpaired electrons whose spin vectors tend to align with those of the octahedrally-coordinated iron atoms. These rare earths occupy the dodecahedrally-coordinated sites and so in general the magnetisation of the garnet may be represented as follows.

Fig. 1.2

Site	Number of unpaired electrons	Spin Vector
3 (Rare earth)	Depends on the rare earth	↓
2 (Iron, octahedral)	5 x 2	↓
3 (Iron, tetrahedral)	5 x 3	↑

Clearly, depending on the tendancy of the rare earth spins to align with those of the octahedrally-coordinated iron and the number of unpaired electrons supported by the rare earth, there is a temperature at which the net magnetisation of the garnet is zero. This is known as the compensation temperature and is shown

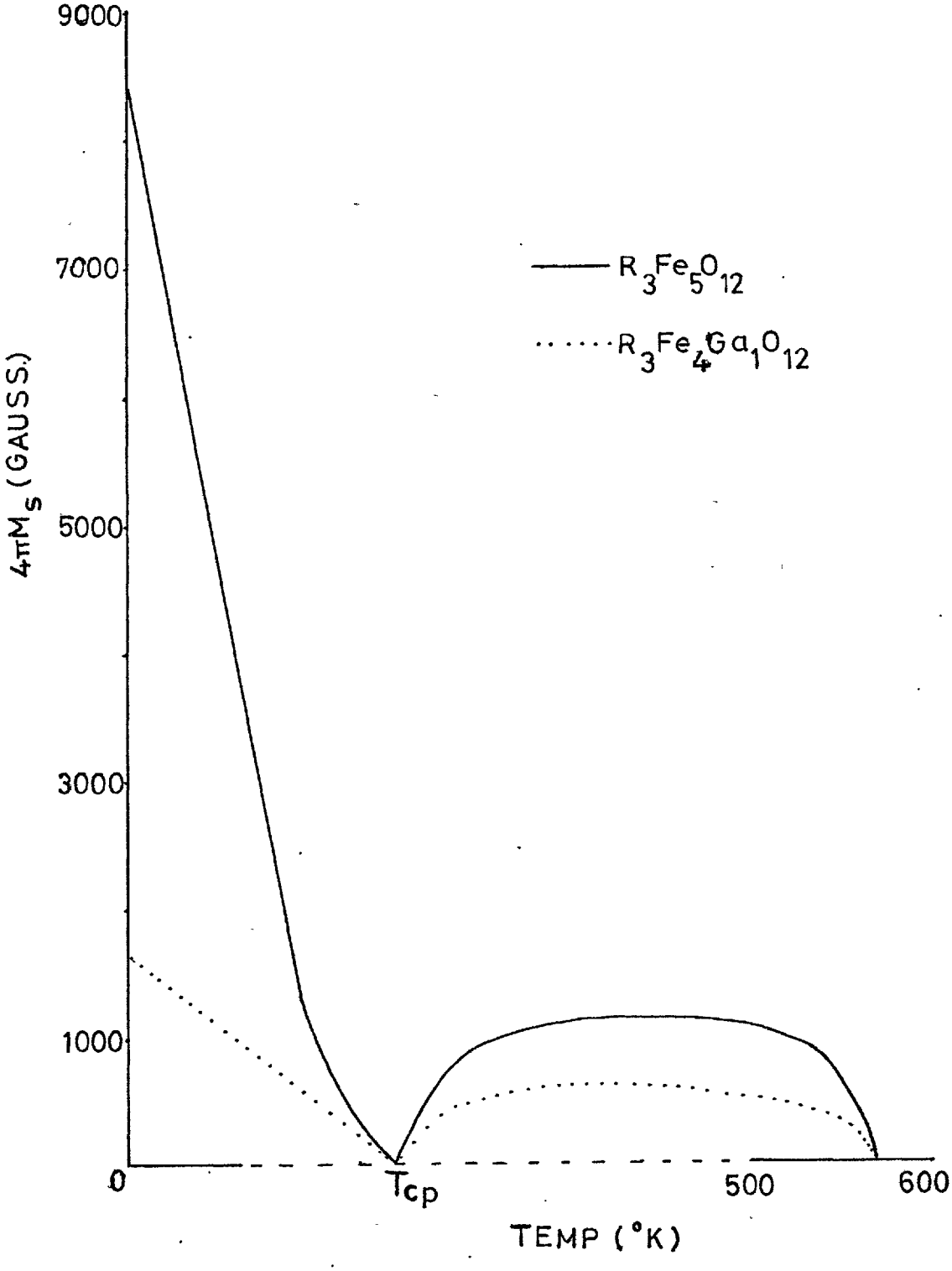

Fig. 1.3 Variation of Garnet Magnetisation with Temperature

by the symbol T_{cp} in figure 1.3. This temperature is below room temperature for most rare earths. As can be seen in figure 1.3, above the compensation temperature the garnet magnetisation is fairly insensitive to small temperature changes, gradually decreasing to zero at the Curie temperature. For most rare earth iron garnets the Curie temperature is in the region of 550°K and is the temperature at which there is enough thermal energy to randomise the spin vectors of the unpaired electrons. Although the magnetisation of garnets does slightly decrease with increasing temperature, so does that of the barium hexaferrite ($BaO.6Fe_2O_3$) magnet providing the external drive field. It is extremely fortunate that these two magnetisation/temperature curves can closely match in the vicinity of room temperature so that a small temperature change produces proportionately the same changes in both materials producing an almost "temperature-independant" device material.

1.5 The Need for Substrates.

As mentioned in the previous section, partial substitution of gallium on the iron sites is necessary to give garnets with sufficiently low magnetisations, typically 200 gauss, to support bubbles with a diameter of five microns. However, in growing gallium-substituted iron garnet crystals, two problems are encountered. Firstly, rare earth iron garnets are incongruently melting and therefore large crystals, suitable for fabrication

into thin slices, are usually grown by a fluxed melt technique involving a solution of the constituent oxides in a lead-based solvent. From these lead oxide/lead fluoride solvents the garnets grow in such a way that the gallium to iron ratio taken up by the growing crystal at any time is about twice that in solution. Therefore as the crystal grows the solution becomes depleted of gallium and the resulting crystal is richer in gallium at the centre than at the outside. When thin slices of these crystals are cut they exhibit large magnetisation gradients and are completely useless for bubble domain applications. Control of a procedure which tops up the gallium oxide content in the solution as the crystal grows would be extremely difficult.

Secondly, since the crystals are usually grown by slow cooling of the solution this also presents a problem. Gallium shows a distinct preference for tetrahedral sites when substituting for iron. The magnitude of this preference is shown in figure 1.4 which is representing yttrium iron garnet.

Fig. 1.4

Garnet	Coordination with oxygen.			Net magnetic Moment at $0^{o}K$
	8	6	4	
$Y_3Fe_5O_{12}$	3Y	2Fe(↓)	3Fe(↑)	5 BM. (↑)
$Y_3Fe_{3.66}Ga_{1.34}O_{12}$	3Y	1.84Fe(↓) 0.16Ga	1.82Fe(↑) 1.18Ga	0.1 BM. (↓)

(BM. = Bohr-Magneton)

The distribution of gallium between octahedral and tetrahedral sites depends on the growth rate, temperature and the orientation of the growth face. Therefore it is virtually impossible to grow large crystals of gallium-substituted iron garnets from which large slices of uniform magnetisation can be cut. Even if this is achieved the problem of fabricating large area slices of only five microns thickness is formidable.

In order to obtain garnet slices of uniform magnetisation suitable for bubble domain device applications the growth process must have the following features:

1) Growth takes place on one crystal face only.

2) The temperature, supersaturation, growth rate and composition of the melt remain unchanged throughout the growth period.

3) The growth process provides crystals from which large area slices of thickness five microns can be fabricated and easily handled.

All of these conditions can be met if, rather than fabricating the thin slices from bulk crystals, a thin epitaxial layer of magnetic garnet is grown isothermally onto a non-magnetic substrate.

It was fortunate that, prior to the interest in garnets as bubble domain hosts, Linares (12) had already determined the characteristics of suitable substrates for garnets in connection with the growth

of thick (100 micron) epitaxial layers of yttrium iron garnet for microwave applications. All of the substrates tried by Linares were transparent, non-magnetic, cubic oxides, ranging from garnets and spinels to magnesium oxide. All had lattice parameters or multiples of them which closely matched the lattice parameter of yttrium iron garnet. It was found that structural compatibility was essential for epitaxial growth since garnet would only grow epitaxially on garnet substrates. In addition if the room temperature lattice parameters did not match closely, then cracking of the epitaxial film always resulted. Gadolinium gallium garnet (GGG) with a lattice parameter of 12.376Å was found to be a suitable substrate for yttrium iron garnet (YIG) which also has a lattice parameter of 12.376Å.

The use of rare earth gallium garnets as substrates is quite versatile since by varying the rare earth or even using a combination of rare earths, substrates can be designed to fit a given composition of magnetic garnet. However, it is interesting that since GGG was the first substrate to be grown in large quantities of sufficiently high perfection, almost all compositions of magnetic garnet have been designed so that their lattice parameter closely matches that of GGG. When special requirements on the properties of the epitaxial layer (epilayer) rule out the possibility of using GGG, then either samarium gallium garnet or neodymium gallium garnet, having lattice parameters of 12.437Å and 12.506Å respectively, are used.

1.6 The Growth and Preparation of Substrates.

Since it has been established by Linares (12) that defects in the substrate will propogate into the epilayer where they adversely affect the motion of domain walls, it is necessary to briefly consider the processes available for the growth of substrates with particular emphasis on their methods of producing low defect densities over large areas of substrate.

Rare earth gallium garnets, unlike the corresponding iron garnets, are congruently melting and therefore can be grown from the pure melt as well as by fluxed melt techniques. Large single crystals of GGG have been grown from lead oxide/lead fluoride fluxes (13) and have proved suitable for fabricating into substrates. Typically they contain 0.1 atomic % lead and have a lattice parameter of 12.376Å. However, since growth rates are slow (approximately one micron a minute) and the larger crystals nucleated early in the growth run when the superstaturation was high, causing them to have large dendritic cores, then growth from the pure melt is advantageous. In this case growth rates approaching 1cm. an hour are achievable and the wastage of grown crystal is much less than for crystals grown by the fluxed melt technique.

Techniques such as float-zoning (14) and the edge-defined film fed method have been used for the growth of substrate material from the pure melt. However, by far the most common technique is Czochralski pulling. This has the advantage that it had already been applied

to one member of the garnet family, yttrium aluminium garnet, a laser host which was required in long, highly-perfect boules. The growth of GGG is extremely similar to that of yttrium aluminium garnet and the expertise associated with the growth of the latter is directly applicable to the former. Although a fairly thorough account of the growth of GGG is given by Cockayne et al.(15, 16), a summary of the ways of producing low defect densities will be given here since highly perfect substrates are essential for producing highly perfect epilayers.

Rare earth gallium garnets melt congruently in the region of 1700°C and the melts must be contained in iridium crucibles. Care is needed in controlling the atmosphere above the crucible since oxidation of the iridium crucible easily occurs, producing iridium oxide which can diffuse through the melt and be reduced at the crystal interface to form metallic inclusions in the final boule. A scheme for this process has been proposed (17) and is as follows:

1.1 $Ga_2O_3 = Ga_2O + O_2$

1.2 $Ir + O_2 = IrO_2$ (at the crucible wall)

1.3 $IrO_2 + Ga_2O_3 = Ir + Ga_2O_3$ (at crystal interface)

Since the complete absence of oxygen promotes reaction 1.1 and too much oxygen promotes reaction 1.2 and consequently 1.3, atmospheres of nitrogen with just

a few percent oxygen are used.

A GGG seed of the required orientation, usually (111), is dipped into stoichiometric melt of gadolium and gallium oxides and the crystal pulled from the melt typically at the rate of 0.5 cm. per hour. Final boules have a lattice parameter of 12.382Å as compared to 12.376Å for the flux-grown material. This, together with the chemical analysis (18), indicates there is always a small excess of gadolium which occupies gallium sites. During growth the rate of rotation of the seed about its vertical axis determines the shape of the crystal/melt interface. Low rotation rates (30 rpm) give a convex interface as shown in figure 1.5. This is undesirable since certain points on this interface are parallel to the equilibrium garnet (110) and (211) faces. At these points the curvature of the interface is interrupted by flat region corresponding to these faces. This is known as facetting and typically in figure 1.5 the regions marked A and B correspond to (211) and (110) facetting respectively. Clearly the gadolinium to gallium ratio and the oxygen segregation will be slightly different on the (211) and (110) planes and the curved surface of the boule. Accurate lattice parameter measurements (15, 16) for one particular boule showed the curved surface, the (211) and the (110) facetted regions to have lattice parameters of 12.3824Å, 12.3841Å and 12.3839Å respectively. Although the difference in lattice parameter across the substrate is usually

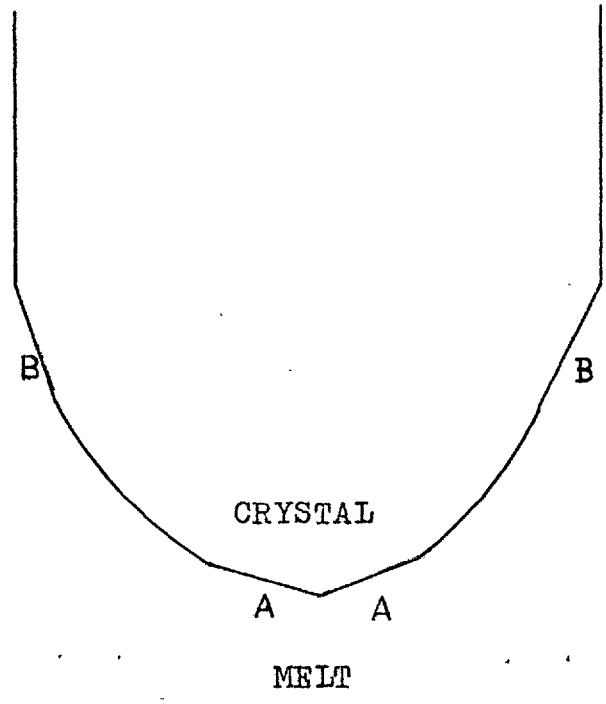

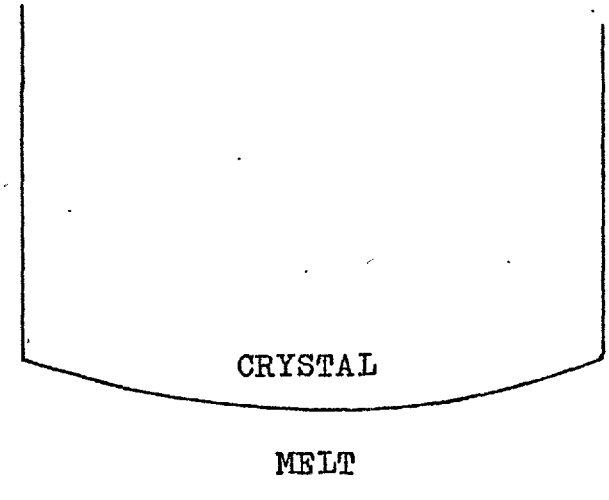

Fig. 1.5 Interface Shape when pulling GGG

smaller than the substrate/epilayer lattice mismatch, straining of the substrate must result and so it is preferable to have facet-free substrates.

As with yttrium aluminium garnet, faster seed rotation (80 rpm) produces an almost flat crystal/melt interface as shown in figure 1.5. However, it has been shown (15, 16) that fast rotation of the seed at the beginning of the pulling process produces a high concentration of dislocations which can also propogate into the epilayer. Therefore a process which produces facet-free crystals of low dislocation density involves slow rotation of the seed at the beginning of pulling and then gradually increasing the rotation rate up to 80 rpm. The portion of crystal pulled after the faster rotation rates has been reached is facet-free and has a low dislocation density. Since the strain energy associated with a dislocation is proportional to its Burger's vector squared it is extremely difficult to nucleate dislocations in the huge garnet lattice during growth as long as the interface does not become concave for long periods. Consequently, as long as adequate precautions are taken, substrate boules with almost zero dislocation density can be grown.

As previously stated, neodymium and samarium gallium garnets may be used as substrates and , much less commonly, the dysprosium and terbium analogues. It is interesting to note that gallium garnets containing a a mixture of two rare earths are now being grown and

investigated as potential substrate material. In this case growth from an impure melt is taking place and, for reasons which will be discussed fully in Chapter 5, constitutional supercooling becomes a problem and interface instability may result. In order to overcome this, growth rates of only 0.1 cm. per hour are the maximum that can be used. Consequently a continuous growth run of at least twenty hours is needed to produce a reasonably sized boule. Automatic methods of controlling the diameter of the boule are almost essential when such long pulling times are necessary.

Substrate discs of approximate thickness 0.5 mm are cut from the boule using the Laue technique to ensure correct crystallographic orientation. The slices are polished with successively finer grades of diamond paste and finally given a chemical-mechanical polish with "Syton" to remove the last traces of surface damage.

1.7 Tailoring of the Epilayer Properties.

Many of the requirements for producing stable bubbles of about five microns diameter have already been outlined in previous sections. Partial substitution of gallium for iron is necessary to provide the correct magnetisation and two or more rare earths provide the necessary growth-induced anisotropy. In addition, the combination of rare earths is chosen to provide the best balance of the epilayer properties such as coercivity, lattice parameter, domain wall velocity and temperature dependance of magnetisation.

A large number of successful epilayer compositions are based on yttrium iron garnet since their lattice match with GGG is easily controlled and they give high domain wall velocities. Two such compositions have been investigated in detail by Giess et al. (19) using polycrystalline samples prepared by conventional ceramic techniques. These have the advantage over single crystal samples in that they are far easier to prepare and their compositions are always accurate, controllable and precisely known. For the general composition $R_yY_{3-y}Fe_{5-x}Ga_xO_{12}$ where the rare earth R was europium or gadolinium, Giess et al. varied both the parameters x and y finding that the lattice parameters obeyed Vegard's law. Compositions which had a close lattice parameter match with GGG and suitable magnetisations were found to be in the region of $Eu_{0.5}Y_{2.5}Fe_4Ga_1O_{12}$ and $Gd_{0.5}Y_{2.5}Fe_4Ga_1O_{12}$. The variation of magnetisation with temperature is small for both of these compositions. Since yttrium does not possess any unpaired electrons only the composition containing gadolinium, which contains a sufficiently large number of unpaired electrons strongly aligned with those of the octahedrally-coordinated iron, has a compensation temperature, approximately 200°K.

Using Vegard's law, the lattice parameter of the garnet $Y_3Fe_4Ga_1O_{12}$ can be calculated as 12.361Å which is 0.021Å less than Czochralski-pulled GGG. Blank and Nielsen (20) have shown that when the epilayer has a lattice parameter more than 0.013Å less than the

substrate, cracking will occur. Therefore compositions based on yttrium iron garnet must contain a rare earth of larger ionic radium than yttrium to give a suitable lattice parameter. This rare earth may be europium or gadolinium as reported by Giess (19) or samarium or lanthanum as reported by Tolksdoft (18). Lanthanum is not as commonly used as the other three alternatives in view of its extremely large size. Small variations in lanthanum concentration produce large variations in the lattice parameter and, since lanthanum does not form an iron garnet alone, large quantities of it are needed in the melt to force it into the garnet lattice.

Accurate control of the epilayer lattice parameter is essential because, as well as cracking when the substrate/epilayer mismatch is too large, the magnitude of the mismatch gives rise to another contribution to the anisotropy, namely stress-induced anisotropy. This contribution, although usually smaller than the growth-induced anisotropy, can act with or against the growth-induced anisotropy depending on the epilayer composition, substrate orientation and if the epilayer is in tension or compression. Giess et al. (21) have grown the same epilayer composition onto a variety of substrates all of the same orientation and were therefore able to separate the anisotropy contributions due to growth and stress in their particular system.

As well as the compositions based on yttrium iron garnet, a few other compositions have been investigated and have been shown to be suitable for devices applications. Blank and Nielsen (20) have reported the

composition $Er_2Eu_1Fe_{4.3}Ga_{0.7}O_{12}$. Very recent work has moved towards decreasing bubble diameters and in particular, one paper on submicron bubbles is noteworthy (22). High magnetisations are necessary to support submicron bubbles and so gallium substitution is unnecessary. However, in Thiele' second criterion for the existance of stable bubble domains (section 1.4) the quantity, q, must lie between 2 and 10. Therefore garnet compositions capable of supporting submicron bubbles must have large anisotropies. For this reason the two rare earths must have a large difference in size, giving rise to a large growth-induced anisotropy. The compositions reported by Giess et al.(22) are consistent with this in that they contain either samarium or europium, two large rare earths, coupled with either ytterbium or lutetium, the two smallest rare earths.

1.8 Growth of the Epitaxial Layer.

Three basic methods of growth of the epitaxial layer exist; liquid phase epitaxy (LPE), chemical vapour deposition (CVD) and hydrothermal epitaxy (HE). LPE has found the widest application because it is easier to control precisely and generally produces epilayers with lower defect densities than can be obtained from the other two growth processes.

Hydrothermal epitaxy has never been considered as a serious rival to LPE and CVD. Kolb and Landise (11) have reported its use for the growth of orthoferrites and for the garnet composition $Er_1Eu_2Fe_{4.3}Ga_{0.7}O_{12}$

using $Nd_{0.6}Gd_{2.4}Ga_5O_{12}$ substrates, in which case cracking of the epilayer was found to be a problem. The technique employed a platinum-lined autoclave placed in a temperature gradient. The constituent oxides were dissolved in concentrated sodium hydroxide solution and garnet deposited on substrates at the cooler end of the autoclave (400°C). The pressure in the autoclave was approximately one kilobar. Attack on the substrates by the strong alkali was found to be acute. Ferrand and Daval (23) overcame this problem by making use of the following reaction:

$$5FeNaO_2 + 3Y(OH)_3 = Y_3Fe_5O_{12} + 5NaOH + 2H_2O$$

The yttrium iron garnet was produced before the alkalinity of the solution was strong enough to attack the substrate. Although hydrothermal epitaxy has the advantage that growth can occur on a large number of substrates simultaneously under the same conditions, cracking of the epilayer is a problem and defect densities are relatively high.

Chemical vapour deposition was originally considered as a serious rival to LPE but recently it has been attracting less interest. An extensive review of its advantages and limitations for the growth of spinels, ferrites and garnets onto suitable substrates has been given by Mee et al. (24). Basically the process depends on the oxidation of the constituent chlorides according to the following equation:

$$3RCl_{3(g)} + (5-x)\,FeCl_{2(g)} + xGaCl_{(g)} + {}^{6}O_{2(g)} =$$

$$R_3Fe_{5-x}Ga_xO_{12(s)} + \tfrac{1}{2}(19-x)Cl_{2(g)}$$

Clearly control of the composition of the epilayer can only be achieved by accurate control of the vapour pressures of the constituent chlorides. To achieve this it is necessary to have a separately-controlled volatilisation chamber for each of the chlorides. Iron dichloride and gallium monochloride are generated by passing chlorine gas over the metallic elements and recently this in-situ production has also been applied to the rare earth trichlorides (25, 26) which had previously needed purification by sublimation and careful handling techniques to prevent hydrolysis. Argon or helium is used as a carrier gas. The chloride streams are then mixed with oxygen immediately above the substrates at temperatures in excess of 1200°C. Deposition takes place and growth occurs at two microns per hour. In order to obtain reasonably uniform thickness of epilayer, high gas flow rates must be used.

At the high temperatures used in CVD no site preference of the rare earths occurs and so the uniaxial anisotropy must be generated by a substancial epilayer/substrate lattice mismatch. This calls for careful control since if the mismatch is greater than 0.013Å cracking of the epilayer occurs. CVD has the advantages that growth may occur simultaneously on a large number of substrates which can be moved in and out of the growth zone thus minimising attack prior to growth. In addition, no corrosive fluxes are used. It has the disadvantages of requiring stringent control and, more important, produces higher defect densities than does

the LPE process, partly because of the higher temperatures involved.

The liquid phase epitaxy growth process has received an enormous amount of attention and may be summarized as follows. The constituent rare earth, iron and gallium oxides are dissolved in a flux, almost invariably lead oxide/boric oxide in a 15.5 : 1 mole ratio, in the correct amounts to crystallise garnet of the desired composition as the primary phase (a detailed account of the relationships between the compositions of the fluxed melt and that of the epilayer is given in sections 2.1 and 3.3.1). The solution is cooled until it becomes saturated and then is brought into contact with a suitable substrate. When an epilayer of desired thickness has been grown, the substrate is removed from the solution.

The various geometries that can be used for bringing the substrate and supersaturated solution into contact are shown in figure 1.6. They are so-called tipping, flipping and dipping. Tipping has been used by Linares (12) for the growth of yttrium iron garnet (YIG) on GGG. Flipping has been used by Tolksdorf (13) for the homoepitaxial growth of YIG on YIG seeds. However, both of these techniques are not as suitable for controlled growth of the epilayer as the dipping process. As pointed out by White and Wood (27), tipping suffers from the disadvantages that it is difficult to hold the boat in a strictly maintained thermal environment, solution flow relative to the substrate surface can only be obtained by convection, itself an uncontrollable process, and homogenisation of the solution by stirring is difficult to achieve. The same disadvantages, namely the lack of

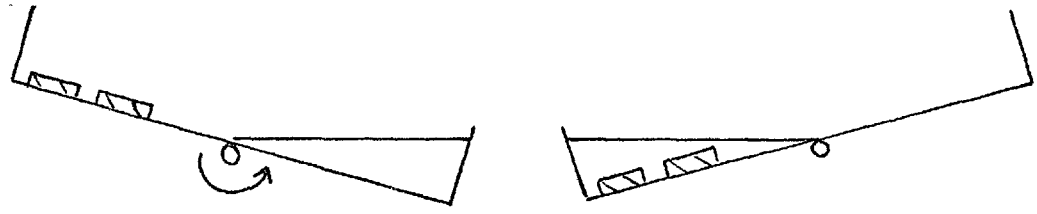

TIPPING

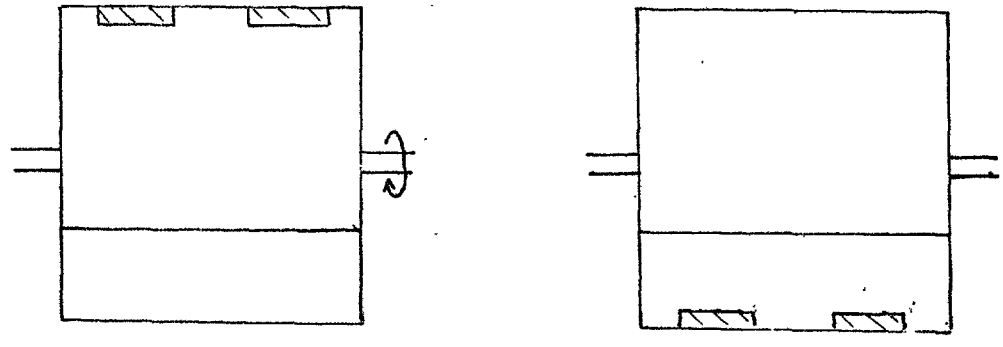

FLIPPING

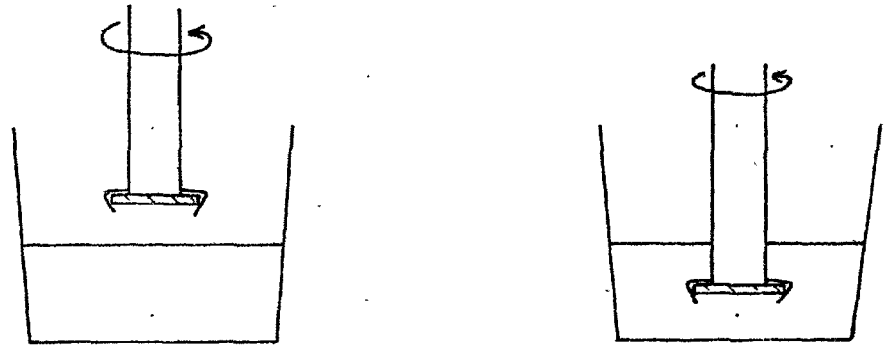

DIPPING

Fig. 1.6 Various Geometries for LPE Growth of Garnets

control of heat and mass flow, also apply to flipping.

The dipping technique is easily adapted to overcome the shortcomings of the other two geometries. If the substrate disc is rotated in the horizontal plane during growth it serves to provide the stirring. In addition, a rotating disc has unique hydrodynamic features which have been analysed mathematically by Cochran (28). Cochran showed that not only are the momentum, thermal and solutal boundary layers uniform over the whole area of the disc, but also may be expressed in terms of the physical parameters of the solution and the rotation rate of the disc. Although the implications of this are discussed fully in Chapter 4 where a full definition of the term boundary layer is given, essentially it means that the whole area of the disc receives solute at the same uniform rate and can dissipate heat at the same uniform rate. Consequently the system is ideal for growing epilayers which have minimal variations both in thickness and composition over the whole of this area and is especially important for the multicomponent garnet systems where small changes in composition produce large irreproducible variations in the magnetic properties. Cochran's mathematical treatment for a rotating disc has successfully been applied to the Czochralski growth of uniformly doped germanium crystals by Burton, Prim and Slichter (29).

An additional advantage of dipping is that on removal of the epilayer from the melt, any small droplets of solution can be spun off the surface by rapid rotation.

For tipping and flipping these droplets remain adhered to the epilayer and growth continues underneath these so that small circular thickness discontinuities result. These are referred to as mesas and their presence affects both the stability and mobility of a bubble in their vicinity.

In view of the fact that the LPE dipping process appears to be the most controllable and versatile method of producing magnetic epilayers suitable for device purposes, the remainder of this thesis is devoted to the process with particular emphasis on the understanding and subsequently control of the complete growth mechanism.

CHAPTER 1 : REFERENCES.

1) A.H.Bobeck and H.E.D.Scovil,
Scientific American, June, 1971

2) K.Papworth, Conference on Magnetic Bubbles, LONDON,1973

3) A.A.Thiele, Bell System Technical Journal 41,(1970), 1139

4) A.A.Thiele, Bell System Technical Journal 50,(1971), 725

5) A.H.Bobeck, R.F.Fischer, A.J.Perneski, J.P.Remeika and L.G.Van Uitert,
IEEE Trans. Mag. MAG-5, (1969), 544

6) D.Treves, J. Appl. Phys. 36, (1965) 1033

7) L.G.Van Uitert, D.H.Smith, W.A.Bonner, W.H.Grodkiewics and G.J.Zydzik.
Mat. Res. Bull. 5, (1970) 455

8) A.H.Bobeck, E.G.Spencer, L.G.Van Uitert, S.C.Abrahams, R.L.Barns, W.H.Groskiewics, R.C.Sherwood, P.H.Schmidt, D.H.Smith and E.M.Walters.
Appl. Phys. Letters 17, (1970), 131

9) H.Cullen, Appl. Phys. Letters 18, (1971), 711

10) A.Rosenwaig and W.J.Tabor, J.Appl. Phys. 42,(1971), 1643

11) E.D.Kolb and R.A.Laudise, J.Appl. Phys. 42, (1971), 1552

12) R.C.Linares, J.Cryst. Growth 3/4, (1968), 433

13) W.Tolksdorf, J.Cryst. Growth 3/4, (1968), 463

14) J.A.Beswick and F.W.Ainger,
Conference on Magnetic Bubbles, LONDON,1973

15) B.Cockayne, J.M.Roslington and A.W.Vere,
J.Mat. Sci. 8, (1973), 382

16) B.Cockayne and J.M.Roslington,
J.Mat. Sci. 8, (1973), 601

17) C.D.Brandle, D.C.Miller and J.W.Nielson,
J. Cryst. Growth 12, (1972), 195

18) W.Tolksdorf, G.Bartels, G.P.Espinosa, P.Holst, D.Mateika and F.Welz, J.Cryst. Growth 17, (1972), 322

19) E.A.Giess, R.E.Argyle, B.A.Calhoun, D.C.Cronemeyer, E.Klokholm, T.R.McGuire and T.S.Plaskett, Mat. Res. Bull. 6, (1971), 1141

20) S.L.Blank and J.W.Nielsen, J.Cryst. Growth 17, (1972), 302

21) E.A.Giess and D.C.Cronemeyer, Appl. Phys. Letters 22(11), (1973), 601

22) E.A.Giess, C.F.Guerci, J.D.Kuptsis and H.L.Hu, Mat. Res. Bull. 8, (1973), 1061

23) B.Ferrand and J.Daval, J.Cryst. Growth 17, (1972), 312

24) J.E.Mee, G.R.Pulliam, J.L.Archer and P.J.Besser, IEEE Trans. Mag. MAG-5, (1969), 717

25) G.A.M.Janssen and W.A.Striker, Conference on Magnetic Bubbles, LONDON, 1973

26) C.W.Wilkins, Conference on Magnetic Bubbles, LONDON,1973

27) E.A.D.White and J.D.C.Wood, J.Cryst. Growth 17, (1972), 315

28) W.G.Cochran, Proc. Camb. Phil. Soc. 30, (1934), 365

29) J.A.Burton, R.C.Prim and W.P.Slichter, J. Chem. Physics 21(11), (1953), 1987

CHAPTER 2

2. Measurement of the Physical Properties of the Growth System.

The use of high temperature solution techniques for the growth of single crystals is extremely common. However, in very few cases (1, 2, 3) has a systematic study of the relevant physical properties of the growth solution been carried out. Since such a large industrial effort is at present being concentrated on the production of LPE grown magnetic garnet layers, a knowledge of the relevant parameters would seem vital. Once these are known, calculation of the dimensionless numbers which characterise the hydrodynamic conditions in the melt can be carried out and the exact growth mechanism can be determined. This is essential in order that a high degree of control and hence reproducibility can be established for this system, and may, in addition, prove useful for other systems which employ the same lead oxide/boric oxide flux for growth of a wide variety of oxide crystals.

The whole of this chapter is devoted to the measurement of these physical parameters and use will be made of these in chapters 4 and 5 to obtain quantitative information relevant to the growth process. The growth system used is a slight modification of the one described by Giess et al.(4) and employs a fluxed melt of the following composition;

Fig. 2.1

CONSTITUENT	WEIGHT (g)	MOLE %
PbO	200.000	84.92
B_2O_3	4.000	5.40
Eu_2O_3	0.621	0.17
Y_2O_3	1.309	0.55
Fe_2O_3	13.185	7.83
Ga_2O_3	2.237	1.13

From this melt, films of approximate composition $Eu_{0.65}Y_{2.35}Fe_{3.9}Ga_{1.1}O_{12}$ can be grown. (A full account of the preparation of this melt is given in chapter 3 along with full details of the furnace and the relevant growth procedure.) The following measurements in this chapter all refer to the melt given in figure 2.1, except where the flux is referred to which is simply the lead oxide and boric oxide components.

The actual methods for measuring the physical parameters and observing the growth process are somewhat different from those used for room-temperature solution growth where temperature control can be better than $\pm 0.02^{\circ}C$, the solutions are usually non-corrosive and visual observation of the crystal during growth is possible. In high temperature solution growth temperature control is rarely better than $\pm 1^{\circ}C$, so that the effect of small temperature changes on the growth process is hard to detect. The flux is corrosive to almost all metals except platinum so that all apparatus coming into contact with the flux must be made of platinum, which presents problems both in

fabrication and cost. Consequently the apparatus used for measuring the relevant physical parameters must be kept as simple as possible. In addition, the crystal cannot be visually observed during growth or dissolution so that any inferences about the rates of these processes can only be the average values over the whole time that the process is occurring. Bearing these severe limitations in mind, the methods for measuring the physical parameters are described in the following sections and these methods are generally applicable to many high-temperature solution growth processes.

2.1 The Solubility of Garnet in the Lead Oxide/Boric Oxide Flux.

As can be seen from figure 2.1, in order to crystallise garnet as the primary phase from the melt we must have a large excess of the iron and gallium oxides compared to the rare earth oxides. In order to understand this multicomponent system it is simplest to reduce it to a pseudo-ternary in a manner analogous to that of Blank and Nielsen (5). For simplicity the gallium oxide and europium oxide are omitted and the resulting pseudo-ternary of the flux, yttrium oxide and iron oxide is shown in figure 2.2. It is immediately evident that yttrium iron garnet is incongruently saturating in this system (i.e. when the flux dissolves yttrium oxide and iron oxide in a 3:5 molar ratio, garnet is not the primary phase).

Depending on the composition of this system there are four primary phases which can be crystallised:

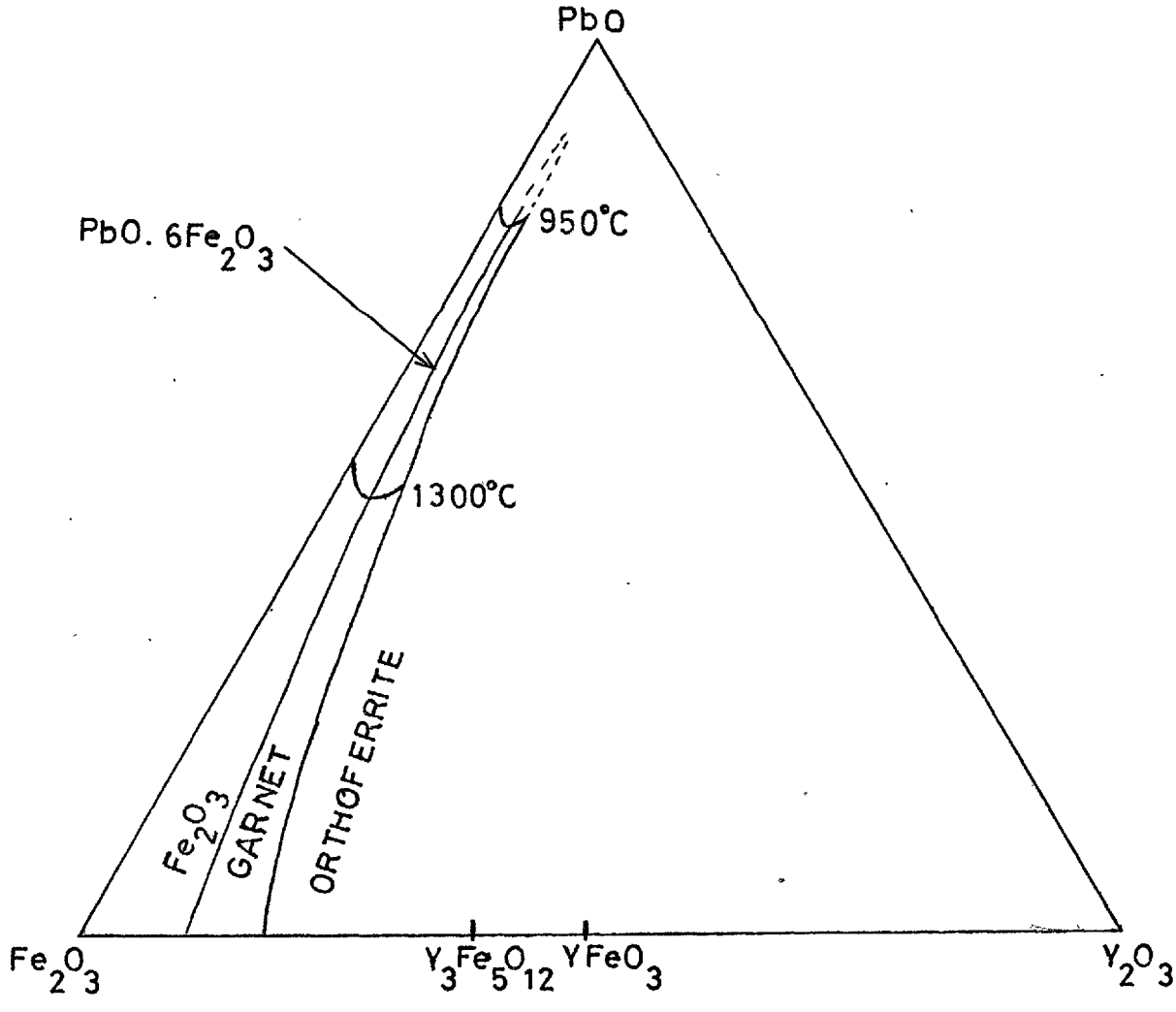

Fig. 2.2 Pseudo-ternary diagram

haematite (Fe_2O_3), magnetoplumbite ($PbO.6Fe_2O_3$), orthoferrite ($YFeO_3$) and garnet ($Y_3Fe_5O_{12}$). To obtain garnet as the primary phase at approximately 950°C, the Fe_2O_3 : Y_2O_3 mole rate must be greater than 12:1. Blank and Nielsen found garnet to exist as the primary phase up to a ratio of 29:1. However, such a high ratio will reduce the amount of yttrium oxide dissolved in the flux and this has two important effects. As garnet is crystallised from the melt the Fe_2O_3 : Y_2O_3 ratio is dramatically increasing; secondly, the yield of garnet is substantially reduced. Since both of these effects are undesirable, it is preferable to work as near to the 12:1 ratio as possible while still ensuring that orthoferrite does not crystallise from melt. The composition given in figure 2.1 has a 12.5:1 mole ratio of $(Fe_2O_3 + Ga_2O_3)$: $(Y_2O_3 + Eu_2O_3)$.

Clearly a full investigation of the solubility curves in the garnet-stable region of the phase diagram would require an enormous amount of data in view of the large number of variables involved. Consequently this section is devoted only to the determination of the liquidus temperature of the melt given in figure 2.1 and the effect of removing garnet during growth on its value. In addition, since lead oxide is known to be slightly volatile, it is useful to know the effect of loss of lead oxide on the garnet liquidus temperature.

The technique used for determining the liquid temperatures was similar to that described by Smith and Elwell (6) and is shown in figure 2.3. Smith and Elwell

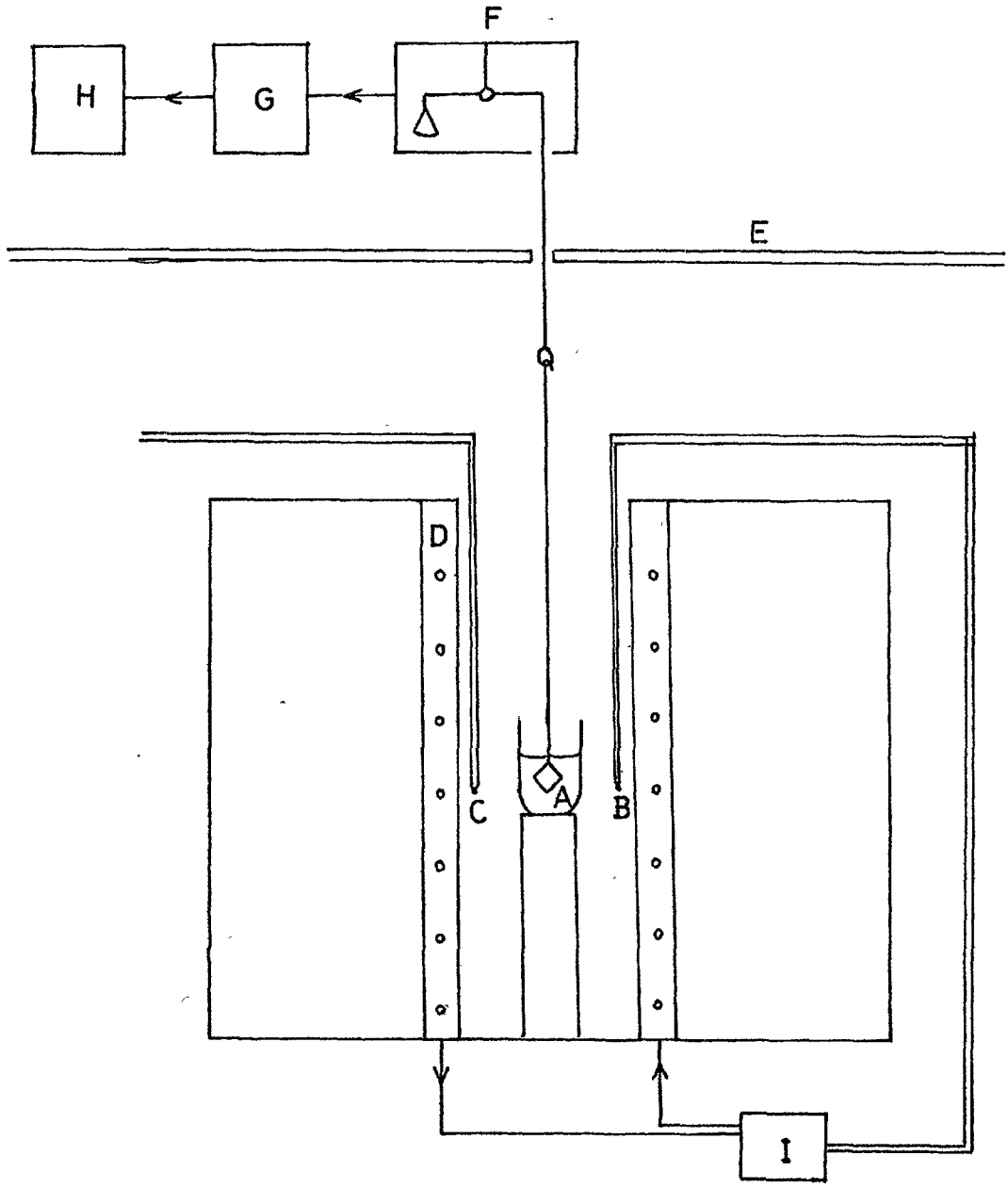

A Garnet Crystal
B Control Thermocouple
C Reader Thermocouple
D Furnace Windings
E Radiation Shield
F Electrobalance
G Control Unit
H Chart Recorder
I Furnace Controller

Fig. 2.3 Apparatus for Solubility Determinations

continuously monitered the weight of a platinum wire dipping into the melt. On slow cooling of melt, crystallisation occurred on the platinum wire producing a change in slope of the weight/time plot. The temperature at which this just took place was taken as the liquidus temperature. However, a notable feature of the melts based on lead oxide/boric oxide is their ability to support large undercoolings without producing spontaneous nucleation, as was reported by Levinstein et al. (7). Although this is a very desirable feature as far as epitaxial growth is concerned it means that the technique of Smith and Elwell will give a low, irreproducible value of liquidus temperature in this case. The technique was therefore slightly adapted so as to weigh continuously a garnet crystal dipping into the melt.

In order to do this, bulk garnet crystals of approximately the same lattice parameter as the crystallising garnet phase were needed. Attempts to grow these by slow cooling of the melt itself yielded extremely small crystals because of the limited cooling range, the ability of the melt to support large undercoolings and the low garnet solubility. Therefore, using the same Fe_2O_3 : Ga_2O_3 and Y_2O_3 : Eu_2O_3 mole ratios as in figure 2.1 the flux was modified by adding a large amount of lead fluoride. The melt used was as follows:

Fig. 2.4

CONSTITUENT	WEIGHT (g.)
PbF_2	100.00
PbO	70.00
B_2O_3	4.00
Eu_2O_3	8.22
Y_2O_3	19.20
Fe_2O_3	29.70
Ga_2O_3	5.06

The dried constituent oxides were weighed, mixed by shaking together in a glass jar and the melt homogenised at 1260°C for 16 hours in a 100 ml. covered platinum crucible. The melt was then cooled to 780°C at 3.5° per hour and then the furnace switched off. The flux was then leached out in dilute acetic acid at 80°C. A total weight of 40 grams of garnet crystals were obtained, some of which are shown in figure 2.5 on mm. graph paper. Their lattice parameter was determined by the powder technique using a Debye-Sherrer camera of radium 11.46 cm and cobalt K_α radiation. The value obtained was 12.38Å which was considered sufficiently close to the lattice parameter of the GGG substrates for them to be used in these solubility studies.

A crystal of approximately 1g. was weighted down with platinum wire so that it would not float on the surface of the melt and immersed in the melt, suspended from one arm of a Cahn RG Electrobalance. The

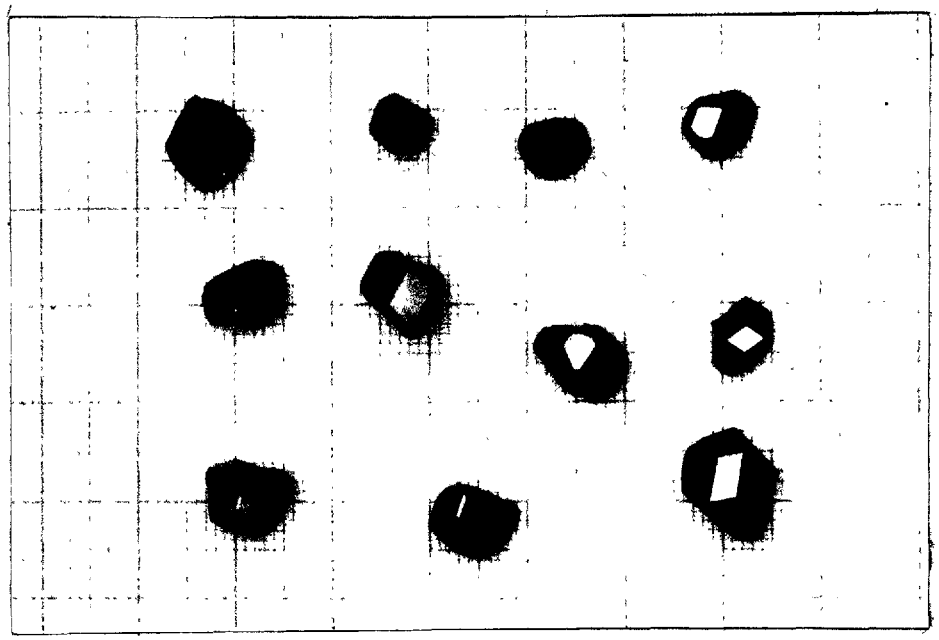

Fig. 2.5 Bulk Garnet Crystals used for Solubility Studies

balance had been previously calibrated with standard weights and its output was fed into a control unit on which large changes in weight of the suspended crystal could be accommodated. Smaller (1 mg. maximum) changes in weight were monitered on a chart recorder (Bryans 27000). On slow cooling, the highest temperature at which the weight of the suspended crystal showed negligible change over a period of one hour was taken as the liquidus temperature. Subsequent runs indicated a reproducibility of $\pm 1^{o}C$.

In order that the change in liquidus temperature on removing garnet from the melt could be determined, various melt were made up, all based on the composition given in figure 2.1 only with small amount of the solute oxides added or removed in ratios corresponding to the garnet formula $Eu_{0.65}Y_{2.35}Fe_{3.9}Ga_{1.1}O_{12}$. The results are summarised in figure 2.6 and their accuracy is to $\pm 1^{o}C$ which represents the control of the temperature within the melt, read by a platinum-sheathed thermocouple.

Fig. 2.6

COMPOSITION BASED ON FIG. 2.1	LIQUIDUS TEMP. (^{o}C)
MELT MINUS 0.68 g. GARNET	969.5
MELT	992
MELT PLUS 0.72 g. GARNET	1012
MELT PLUS 1.41 g. GARNET	1032

It was also determined that for every 10 g.

of lead oxide lost by evaporation the liquidus temperature rose by 7°C. The result is interesting since during the homogenisation period and the growth run, approximately 0.3 g. of lead oxide is lost by evaporation which causes the liquidus temperature to rise by 0.2°C. The growth of an epilayer of 7 microns thickness will remove 7 mg. of garnet from the melt, thus lowering the liquidus temperature by 0.2°C. Therefore the same melt may be used for a large number of growth runs without any significant change in its liquidus temperature.

2.2 Density and Coefficients of Expansion of the Melt and the Flux.

The technique chosen to measure the densities is an Archimedean two-bob system as described by J.L.White (8). Two bobs of approximate weight 0.5 gm and 1.5 gm were fabricated by melting pure (99.9%) platinum metal into balls using an oxy-hydrogen torch. Identical support wires of 0.3 mm diameter thermocouple wire were welded to each bob,

The experimental set up was the same as that shown in figure 2.3, except that a platinum bob was being weighed instead of a garnet crystal. A bob was cleaned in nitric acid and then degreased in isopropyl alcohol. It was then suspended from the electrobalance and weighed firstly in air and secondly immersed in deionised water at a known temperature. The same procedure was repeated for the other bob, using the same depth of water.

An air-cooled copper coil was placed at the

mouth of the furnace so that any lead oxide vapour would condense on this rather than on the suspension wire of the bob. The furnace was switched on and the melt homogenised at 1160°C for 3 hours. A bob was then weighed when immersed in the melt and the procedure repeated, cooling the melt in steps of 20°C. The lowest temperature used was 1000°C. The same procedure was repeated for the other bob. The density of the flux was determined likewise only in that case temperatures as low as 900°C were used since crystallisation of garnet onto the support wire could not occur.

The upthrust, U, acting on the bob can be related to its volume, V, the density of the fluid in which it is immersed, ρ , and the surface tension, S, acting on the wire by:

$$U = \rho V + S$$

If the two bobs are designated by the substrates 1 and 2 then

$$U_1 = \rho V_1 + S_1$$

$$U_2 = \rho V_2 + S_2$$

Since the suspension wires are equal, $S_1 = S_2$ and so :

$$U_1 - U_2 = \rho(V_1 - V_2)$$

Therefore the quantity $V_1 - V_2$ was calculated from the calibration using deionised water. In obtaining the densities of the melt and flux, corrections for the change in magnitude of $V_1 - V_2$ were applied since although

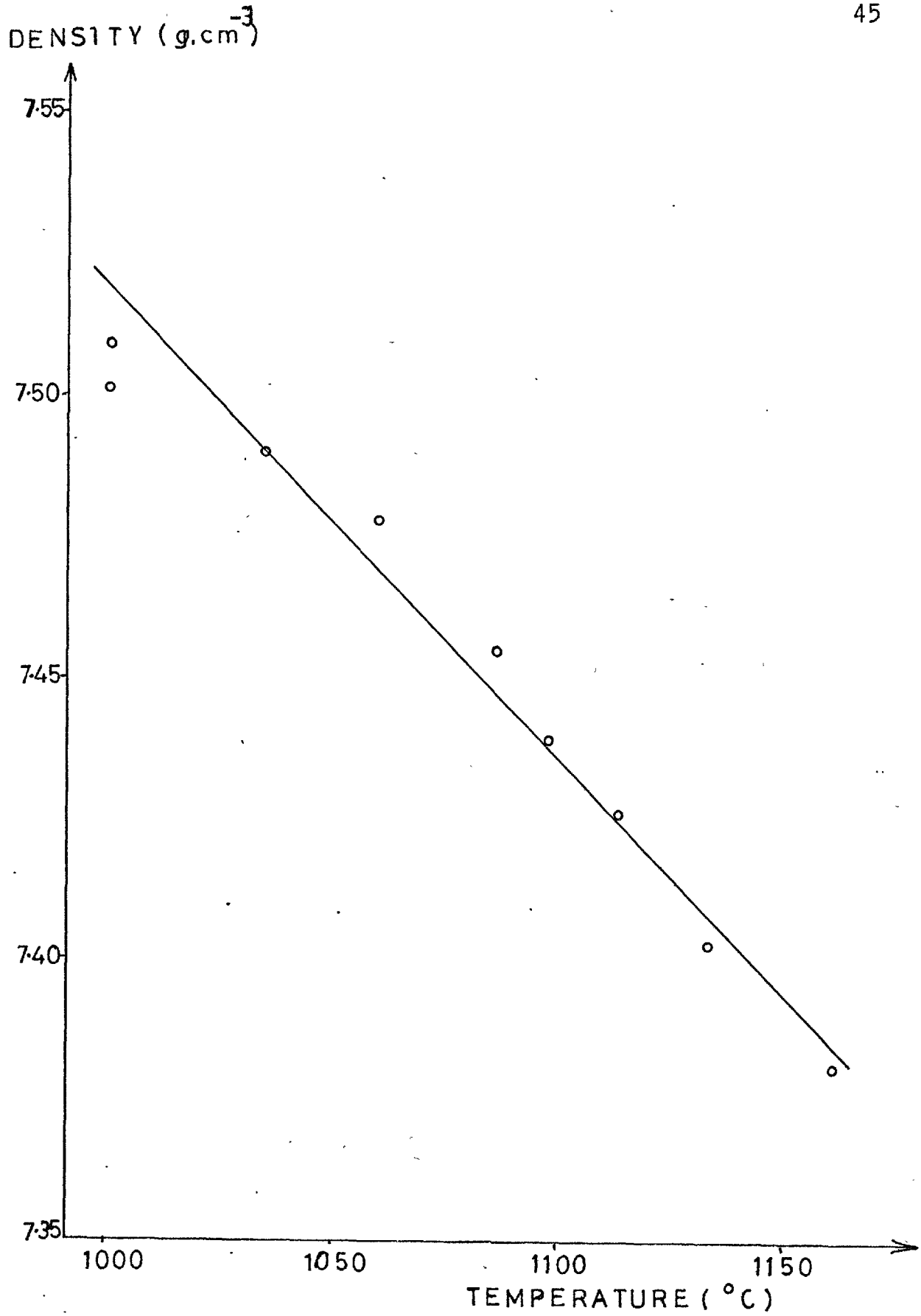

Fig. 2.7 Density of the Melt vs. Temperature

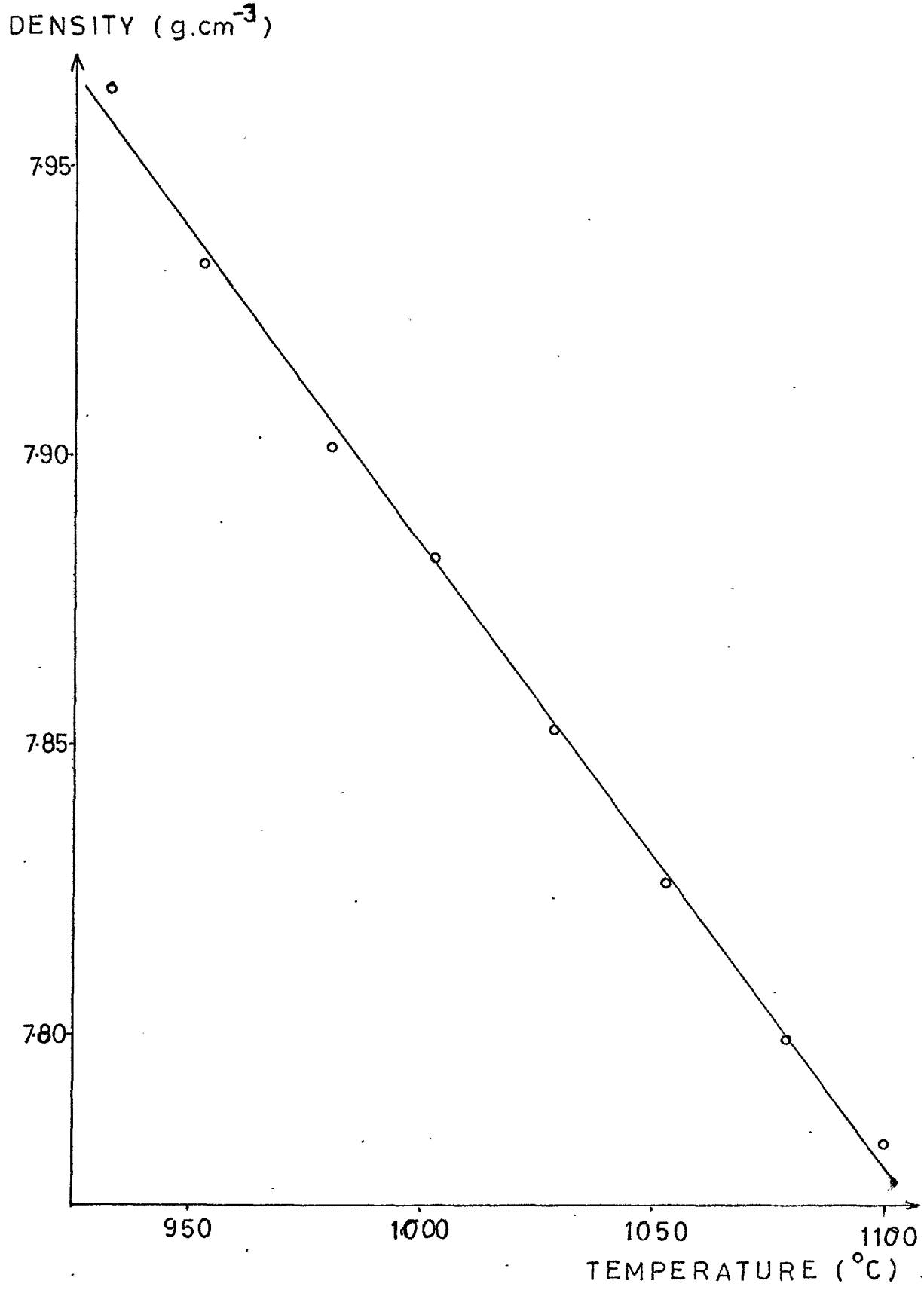

Fig. 2.8 Density of the Flux vs. Temperature

this produced an insignificant error when measuring densities it was very significant when calculating the coeffieients of expansion.

The densities of the melt and flux, including their temperature dependance, are shown in figures 2.7 and 2.8 respectively. The accuracy of the density measurements was estimated at $\pm$ 1%, the major part of which was caused by oscillations in the upthrust on the bob when immersed in the melt or flux. These oscillations are probably due to natural convection. The coefficients of volume expansion of the melt and flux were calculated from the slopes of the density versus temperature plots. Over the temperature ranges used, the coefficients of expansion were 0.99×10^{-4} per ^{o}K for the melt and 1.27×10^{-4} per ^{o}K for the flux.

2.3 Viscosity of the Melt and the Flux.

A review of the methods available for the viscosity determination of high temperature solutions has been given by Bockris et al.(8). Since all apparatus coming into contact with the flux must be made of platinum, the most convenient methods were judged to be the oscillating-bob or the rotating-crucible techniques. Both of these were tried using the experimental arrangement shown in figure 2.9.

A platinum bob was fabricated by melting pieces of platinum in an alumina mould using radio-frequency induction heating. The solidified platinum mass was then

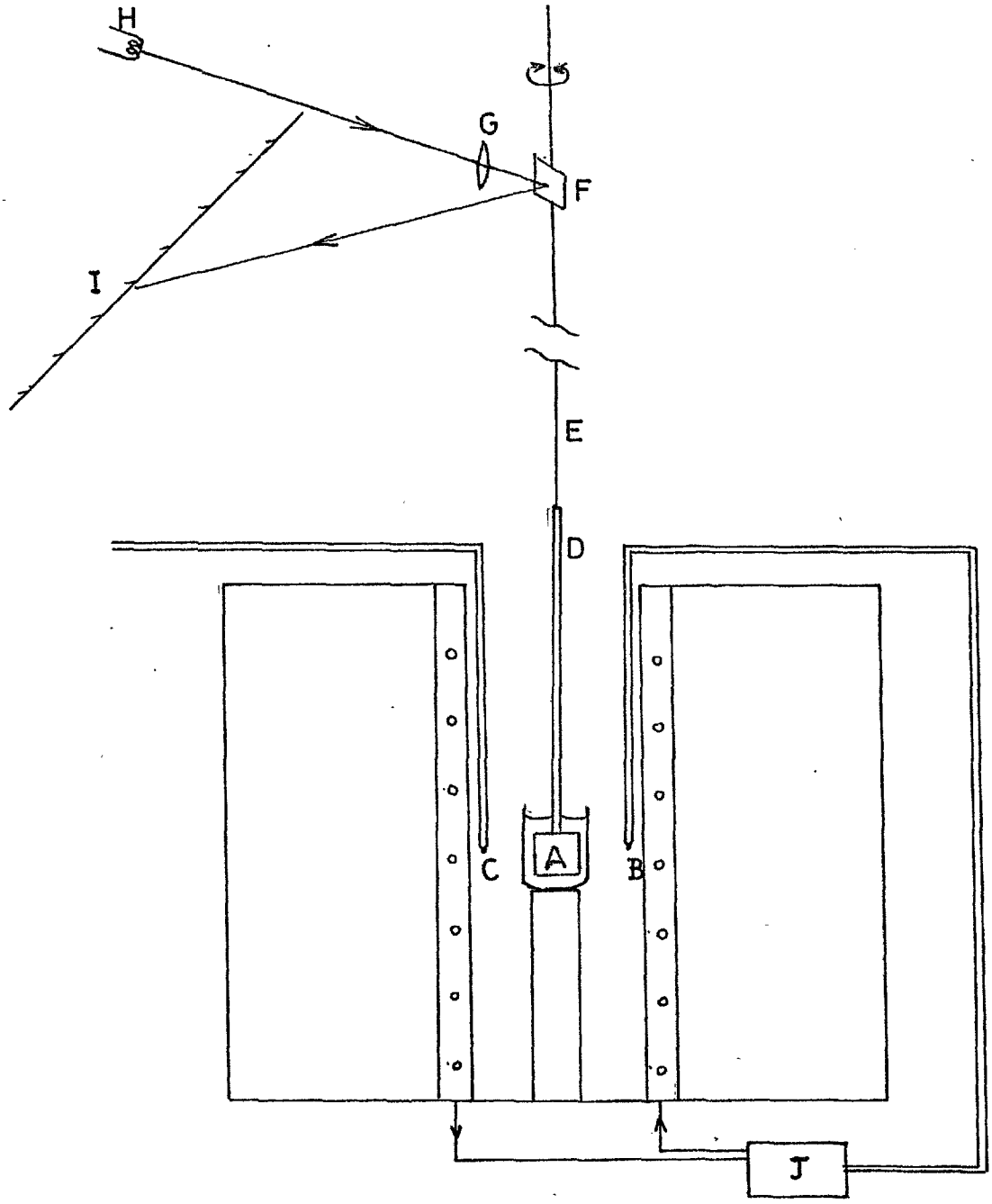

A	Platinum bob	F	Mirror
B	Control Thermocouple	G	Lens
C	Reader Thermocouple	H	Lamp
D	Platinum/Rhodium Rod	I	Scale
E	Torsion Wire	J	Controller

Fig. 2.9 Apparatus for Viscosity Determination

machined into a solid cylinder of diameter 2 cm. and height 1.5 cm. A rigid rod of platinum-rhodium alloy was then welded to the bob and to the top of this rod was connected 1 metre of platinum-rhodium wire to act as a torsion wire. The purpose of the rigid rod was so the torsion wire was kept well out of the furnace enabling the apparatus to be calibrated using room-temperature liquids as viscosity standards. A small mirror was glued to the torsion wire so that the relative twist in the wire could be measured by an optical lever.

The first method tried was to rotate the crucible at a constant speed and measure the twist in wire, the magnitude of which is directly proportional to the viscosity of the liquid in which the bob is immersed. Calibration was made using various water/glycerol mixtures at room temperature. The viscosities of such mixtures were accurately known (9).

For the rotating crucible system the dimensionless Reynold's number, Re is given by (8);

$$Re = \frac{\Omega (a^2 - ab) \rho}{\eta}$$

where a and b are the radii of the crucible and bob respectively, Ω is the angular rotation rate of the crucible, ρ is the density of the melt and η is the dynamic viscosity of the melt. Using an estimated value of 4 centipoise for the dynamic viscosity, a crucible rotation rate just in excess of 20 rpm is enough to give a Reynold's number of 2000 at which the onset of turbulence

in the melt just occurs. Therefore the method is only valid as long as the crucible rotation rate does not exceed the estimated 20 rpm. However, it was found that for rotation rates of below 20 rpm. the angular twist in the torsion wire was very small and results obtained by this method were considered to be of low accuracy. It was concluded that this method would prove far more suitable for liquids of a higher viscosity, although it did indicate that the viscosities of the melt and flux were of the order of five to ten centipoise.

Consequently the oscillating-bob technique, which had previously proved successful (1, 2, 10) for determining viscosities of a few centipoise, was chosen. If a bob is immersed in a liquid and set into oscillation by twisting the torsion wire, the oscillations are damped by the viscosity of the liquid and the amplitudes of oscillation decrease. As long as the damping is light the natural logarithm of the ratio of successive amplitudes, λ, is a constant and related to the properties of the liquid by:

$$\lambda - \lambda_o = C_1(\eta\rho)^{\frac{1}{2}} + C_2\eta + C_3\eta\rho$$

where λ_o is the logarithmic decrement for oscillations in air and the constants C_1, C_2, C_3, are dependant on the shape of the bob and its clearances in the liquid.

In order to determine the values of the three constants, three calibrating liquids were necessary. Special care was taken to ensure that all calibrations and viscosity measurements were performed using the same

crucible, depth of liquid and clearances. For maximum accuracy the calibrating liquids were chosen to exhibit a wide spread of densities and viscosities whilst still remaining in the same order of magnitude as those of the melt and flux. This condition was easily met for viscosity but most room temperature liquids have densities close to 1 g./cc so it was necessary to use a dense molten salt as one of the calibrants. The following calibrants were used:

Fig. 2.10

CALIBRANT	TEMP.(°C)	ρ(g.cm^{-3})	η(cp.)	Ref.
WATER	24.0	1.000	0.913	9
WATER/GLYCEROL (50:50, Weight)	24.0	1.127	5.226	9
MOLTEN LEAD CHLORIDE	577	4.830	3.071	11

The values of C_1, C_2, and C_3 were found to be 0.224, 0.960 and -0.0366 respectively. Using these values the dynamic viscosity of both the melt and flux were determined over a range of temperatures. The temperature dependance of viscosity is usually represented by an arrhenius-type of relationship:

$$\eta \propto \exp\left[-\frac{\Delta E}{RT}\right]$$

Where R is the gas constant, T is the absolute temperature and ΔE is the activation energy required for viscous flow. The results obtained for both the melt and flux are

analysed according to this type of relationship in figure 2.11. (The vertical scale is logarithmic in viscosity whereas the horizontal scale is the reciprocal of absolute temperature). Both the melt and flux show linear plots in figure 2.11, indicating that the Arrhenius type relationship is valid. The activation energies required for viscous flow for the flux and melt are 11.5 kcals $mole^{-1}$ and 11.8 kcals $mole^{-1}$ respectively. These values are typical of molten salts and may be compared with a value of 9.1 kcals $mole^{-1}$ for molten sodium chloride (11).

Owing to the facts that the viscosity measurements required three independant calibrations and that small uncertainties in the measurement of the logarithmic decrement lead to larger uncertainties in the values of the calibration constants, the absolute accuracy of the results is estimated as $\pm$ 15%, although the relative agreement between measurements is much better than this. However this absolute accuracy was considered adequate for calculations based on boundary layer theory since the boundary layer thickness depends on the one-sixth root of viscosity.

It has been commented (12) that the viscosities of most molten salts are the same order of magnitude as that of water (1cp.). Clearly this is true for both the flux and the melt and has also been found valid for other crystal growth systems; a solution of alumina in lanthanum trifluoride has a viscosity of 8 cp. at 1450°C (1) and a solution of lead tantalate in lead vanadate has a viscosity of 2.2 cp at 1200°C (2).

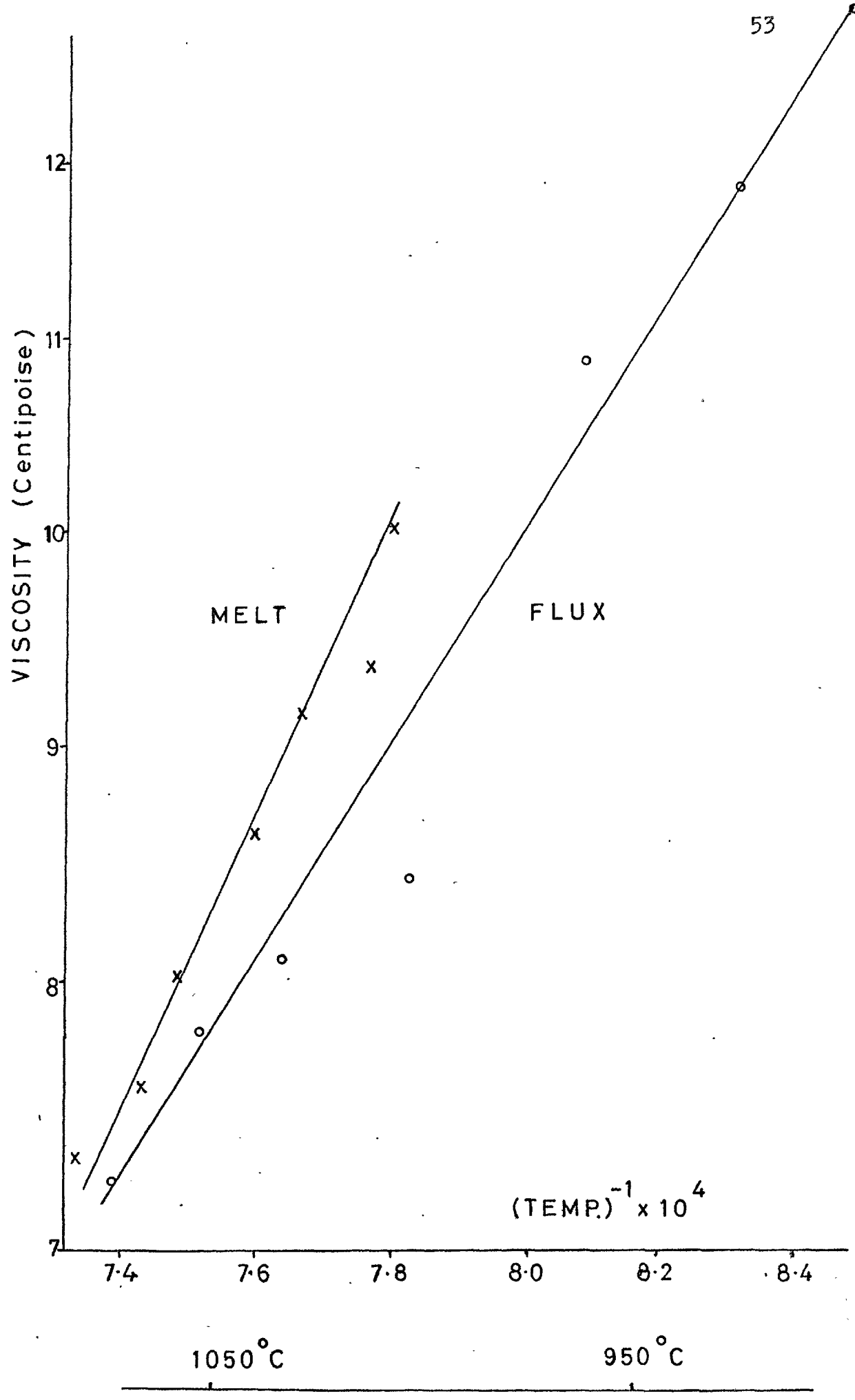

Fig. 2.11 Viscosity of Flux and Melt vs. Reciprocal of Absolute Temperature

2.4 Heat of Solution of Garnet in the Flux.

A knowledge of the value of this parameter is necessary for two reasons. Firstly, it is equal in magnitude, but opposite in sign to the heat of crystallisation, the value of which is needed to determine if heat dissipation is an important factor in the growth process. In addition, since its value for an ideal solution can be calculated from the slope of the solubility curve then comparison of the ideal and measured values may give an estimate of the activity coefficient of garnet in the flux.

The apparatus used is shown in figure 2.12. It consisted of a large thermal mass in which was contained two recrystallised alumina tubes of 2 cm. diameter. Around the base of each tube was arranged a series of thermopiles. The outputs of these two series were connected in opposition and the resultant fed into an integrator. In this way, the apparatus was similar to that used in differential thermal analysis so that any heat changes inside one tube relative to the other produced a signal on the integrator proportional to the magnitude of the change.

Two crucibles of diameter 1 cm. and height 6 cm. were fabricated from platinum sheet and into each of these 25 g. of the flux was premelted. They were then placed in each of the alumina tubes and the calorimeter set at 950°C. A small garnet crystal was suspended just above the surface of one of the crucibles and when thermal equilibrium had been reached was lowered into the flux.

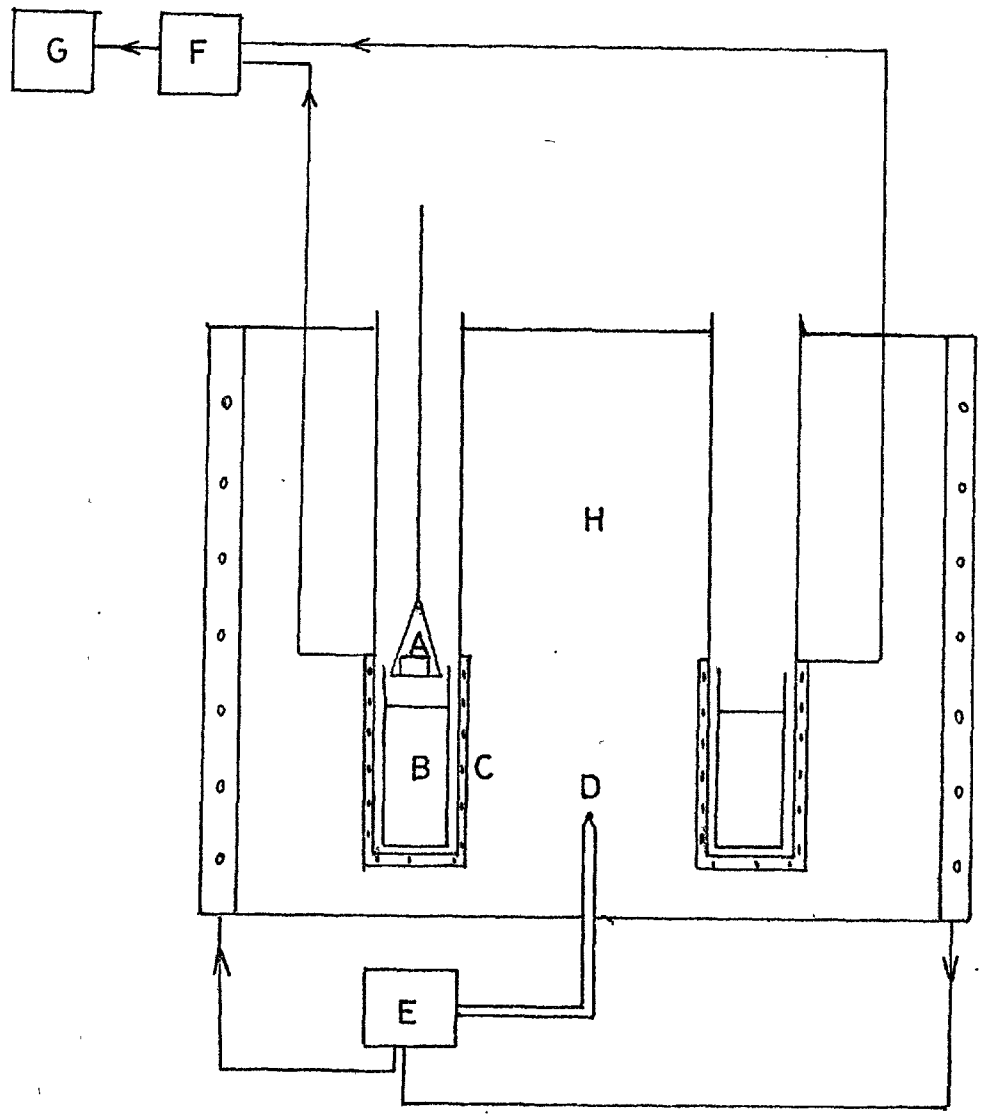

A Garnet Pellet
B Flux
C Thermopile
D Control Thermocouple
E Controller
F Integrator
G Chart Recorder
H Thermal Insulation

Fig. 2.12 Calorimeter for Measuring Heat of Solution

However, it was found that the time taken for dissolution was long so that a reasonably-sized signal was never recorded on the integrator. Subsequently the small garnet crystals, of the same composition as those used in the liquidus temperature studies, were ground to a fine powder and pressed into pellets of approximately 0.1 g. When these pellets, resting on a platinum pan just above the surface of the flux, were lowered into the flux then rapid dissolution occurred. The integrator reading was recorded until the constant background value was reached at which time dissolution was complete. Calibration was made by dropping small pieces of pure platinum of known weight into either of the alumina tubes. The heat absorbed by the platinum in heating up from room temperature to 950°C was calculated from standard tables (13).

Over four runs the mean value determined for heat of solution was 94.1 kcals $mole^{-1}$ (endothermic) and the spread of readings was $\pm$ 11.5 kcals $mole^{-1}$.

The heat of solution for an ideal solution of garnet in the flux was then calculated from the solubility data obtained in section 2.1. Calculation of the actual garnet concentration at each temperature was based on the rare earth constituents since both iron and gallium oxides were in excess. For an ideal solution the Van't Hoff relationship is applicable:

$$\ln N = -\frac{\Delta H}{RT}$$

Where N is the molarity of the solution and ΔH is the

heat of solution. A plot of the natural logarithm of molarity against the reciprocal of absolute temperature was linear and gave an ideal value of ΔH as 24.5 Kcals. $mole^{-1}$. This enormous discrepancy between the measured and the value calculated for an ideal solution can be used to give a model of the garnet species that exist in solution. It can easily be shown that if garnet is dissociated into n species of unit activity when dissolved in the flux then the Van't Hoff relationship may be modified to the following form:

$$\ln N = - \frac{\Delta H}{nRT}$$

Therefore from the slope of the plot of natural logarithm of molarity against reciprocal of absolute temperature the value of 24.5 kcals per mole is in fact the quantity $\Delta H \div n$.

The measured value of ΔH is 94.1 ± 11.5 kcals.$mole^{-1}$ and so the value of n is 3.85 ± 0.45.

Considering yttrium iron garnet for simplicity, a model with accounts for the production of approximately four species from each garnet molecule is

$$Y_3Fe_5O_{12} = {}^{3}/_{2}Y_2O_3 + {}^{5}/_{2}Fe_2O_3$$

This is fairly strong evidence that when garnet is dissolved in the flux the species produced are the constituent oxides rather than complete garnet molecules. There is also a large amount of indirect evidence in favour of this model. The composition of garnet that crystallises

from the melt is usually substantially different from the ratios of constituent oxides present in the melt. In addition, the diffusion coefficient, as determined in chapter 4, of the garnet in solution is relatively large (1.6×10^{-5} $cm.^2 sec.^{-1}$ at 950°C) and is unlikely to be representative of the huge garnet molecule diffusing through the melt.

Using the value of 94.1 $kcals.mole^{-1}$ (endothermic) for the heat of solution of garnet, the heat of crystallisation must be 94.1 $kcals.mole^{-1}$ (exothermic). When a six micron thick epilayer is grown the total heat evolved is less than one calorie. Clearly this is insignificant compared to the heat capacity of the system and so it appears most unlikely that the dissipation of heat of crystallisation provides a rate-limitation on the growth process.

2.5 Diffusion Coefficient of Garnet in the Melt.

As mentioned in the previous section, the constituent oxides rather than complete garnet molecules exist in the melt. Therefore a complete description of the growth process must involve the diffusion of the rare earth, iron and gallium oxides to the crystal interface. Without the use of isotopic tracer techniques, the diffusion coefficients for the constituent oxides are extremely difficult to separate and so it was decided that a diffusion coefficient representative of the complete growth process would be a more useful parameter. This parameter is easily calculated from growth rate data

and a full account of its determination can be found in chapter 4.

2.6 Specific Heat of the Flux and the Melt.

Since lead oxide forms 90% of the melt and 98% of the flux by weight it was considered a good approximation to simply use the published specific heat values for pure lead oxide (14). Accordingly a value of 0.07 cal. $g.^{-1}$ $degree^{-1}$ at 950°C was taken.

2.7 Thermal Conductivity of the Flux and Melt.

Although a reasonable knowledge of this parameter is useful in many crystal growth systems, its measurement at high temperatures is usually difficult. Methods for determining its magnitude all rely on the measurement of heat flow through a section of the melt in the absence of convection. This presents the difficulties since the melt can only be contained in platinum vessels which are much better heat conductors than the melt itself. In addition, ensuring the absence of convection is not always possible. For the onset of thermal convection the dimensionless Rayleigh number, Ra, must exceed 2000. The Rayleigh number is given by

$$Ra = \frac{g \beta \Delta T L^3}{\alpha \nu}$$

where g is the gravitation constant, β is the coefficient of volume expansion, ΔT is the temperature difference across the melt of depth, L, α is the thermal diffusivity

and ν is the kinematic viscosity. Using an estimated value of thermal diffusivity it was calculated that a temperature gradient in excess of only 0.1^{o} cm^{-1} from the bottom to the top of the melt would be enough to cause thermal convection. Consequently it was decided to use an estimated value of thermal conductivity. The majority of reported values for molten salts are in the region of 2×10^{-3} cal. $cm.^{-1}$ $sec.^{-1}$ $degree^{-1}$ (11) and so this value was taken.

CHAPTER 2 : REFERENCES

1) C.M.Cobb and E.Wallis, Report Number AFCRL-67-0196,(1967)

2) T.M.Bruton and E.A.D.White, J.Cryst.Growth 19,(1973),341

3) J.S.Berkes and W.B.White, J.Cryst.Growth 6, (1969), 29

4) E.A.Giess, J.D.Kuptsis and E.A.D.White, J.Cryst.Growth 16, (1972), 36

5) S.L.Blank and J.W.Nielsen, J.Cryst.Growth 17, (1972), 302

6) S.H.Smith and D.Elwell, J. Mat. Sci 2, (1967), 297

7) H.J.Levinstein, S.Licht, R.W.Landort and S.L.Blank, Appl. Phys. Letters 19(11), (1971), 486

8) J.Bockris, J.L.White and J.D.Mackenzie, Physicochemical Measurements at High Temperatures (Butterworths, 1959)

9) G.W.Kay and G.H.Laby, Physical and Chemical Tables (Longmans, 1959)

10) Fawsitt, Proc. Roy. Soc. A80, (1908), 290

11) G.J.Janz, Molten Salts Handbook (Academic Press, 1967)

12) H.Bloom, Chemistry of Molten Salts (W.A.Benjamin, 1967)

13) K.K.Kelley, Entropies of Elements and Inorganic Compounds, (USGPO, 1961)

14) Janaf Thermochemical Tables (National Bureau of Standards 1971)

CHAPTER 3.

3. Growth and Assessment of the Magnetic Garnet Epilayers.

3.1 The Furnace.

The complete furnace is shown in figures 3.1.A and 3.1.B. It consisted of an 18 inch long vertical alumina tube of internal diameter 3.7 inches, which was resistively heated by "Kanthal" Al windings and thermally insulated by "Kaowool". It had a "Sindanyo" lid with two small holes through which the thermocouples passed and a larger central hole through which the substrate could be lowered. The 100 ml. platinum crucible rested on an alumina pedestal which could be rotated about its axis at 25 rpm. to accelerate homogenisation of the melt prior to growth. Thermocouples were of platinum/platinum - 13% rhodium and the controller was a Eurotherm PID/SCR type. Rotation of the substrate in a horizontal plane was achieved by a variable speed Citenco motor which was thyristor controlled to stabilise low rotation rates and could be rotated as fast as 2000 rpm. to remove any droplets of melt which had adhered to the epilayer surface after growth.

In order that the temperature of the melt could be accurately determined, a thermocouple sheath was fabricated out of platinum sheet. Using this platinum-sheathed thermocouple, the crucible was positioned as to be in the hottest part of the furnace with the bottom

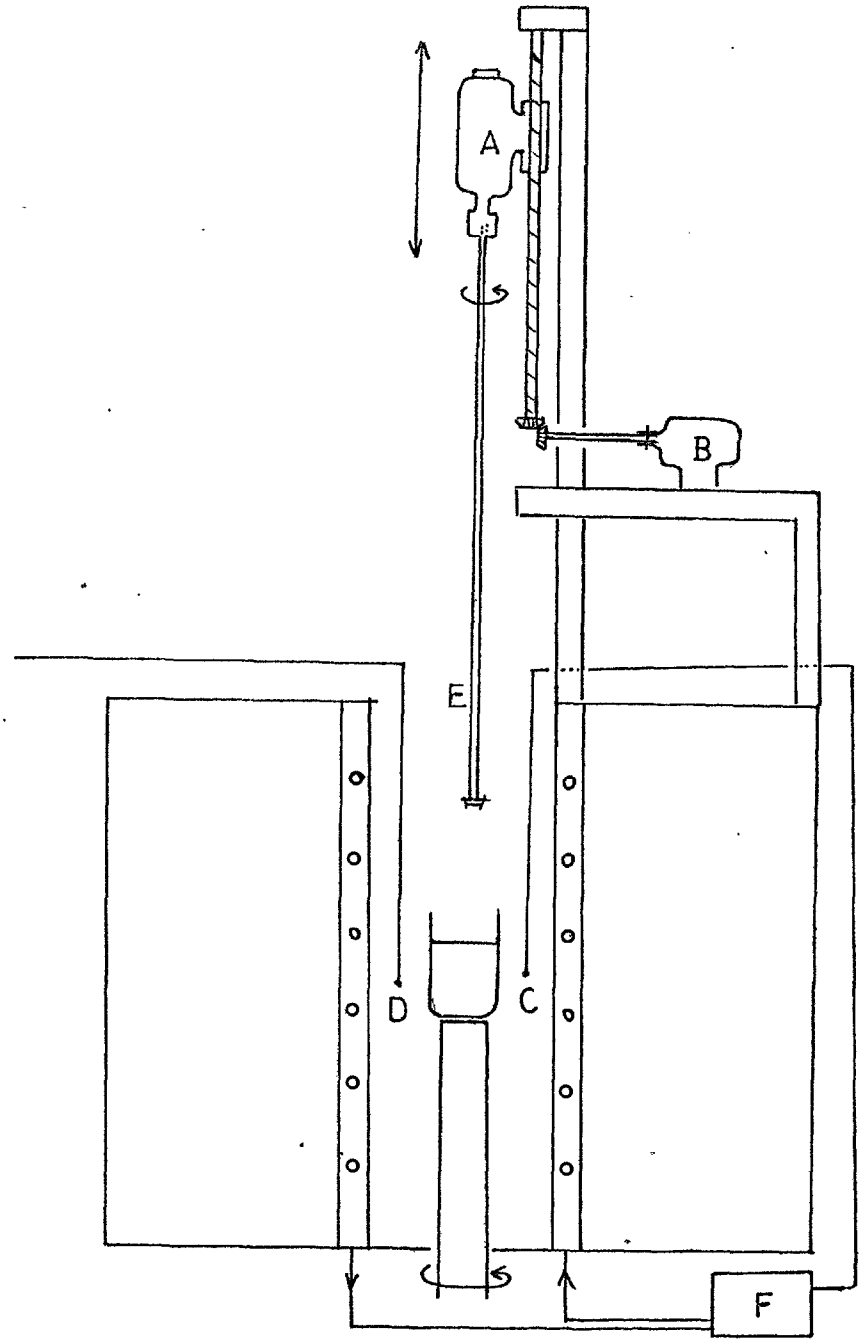

A Variable Speed Motor
B Lowering Motor
C Control Thermocouple
D Reader Thermocouple
E Substrate Holder
F Controller

Fig. 3.1 A Growth Furnace

Fig. 3.1 B

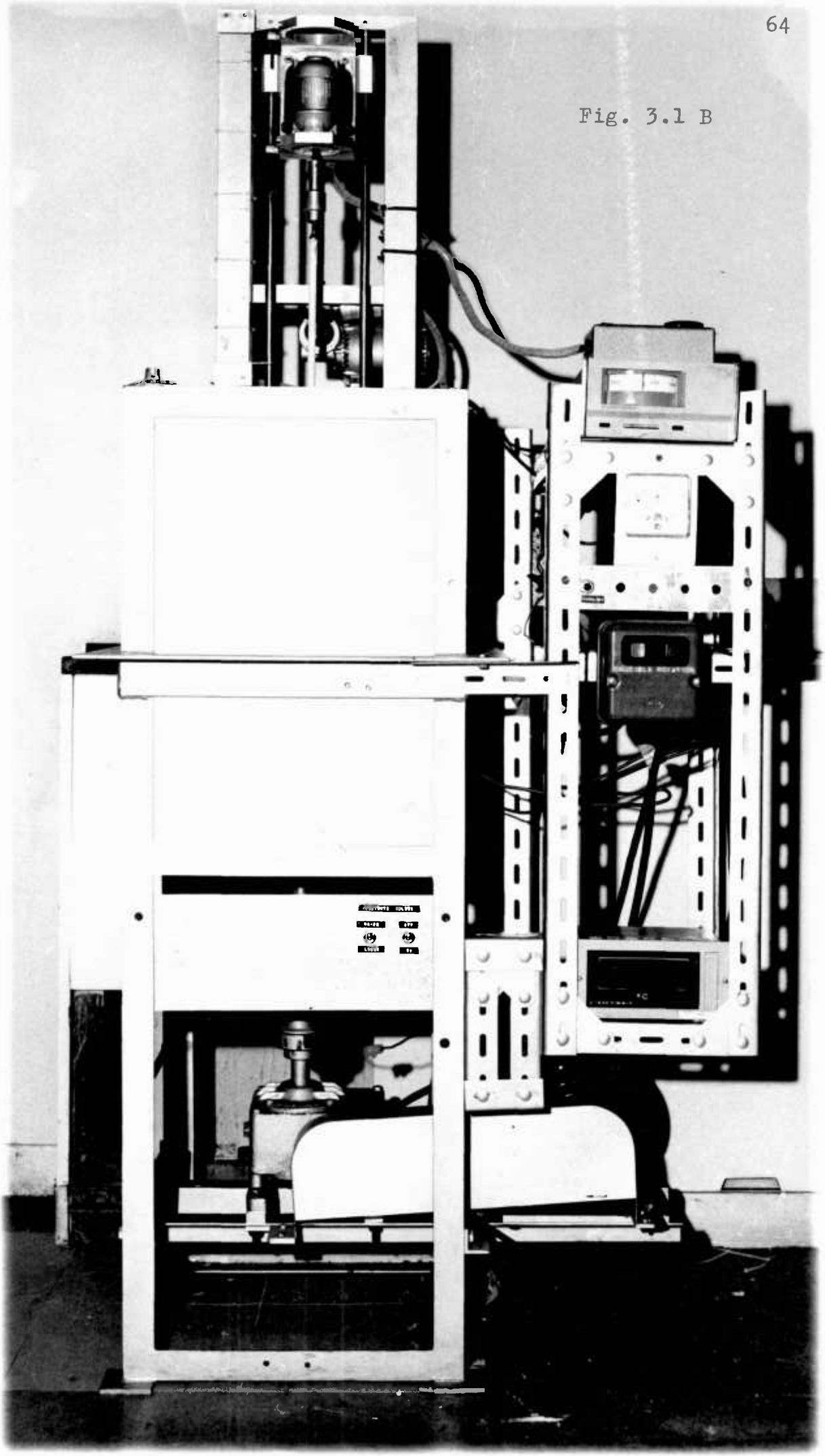

of the melt 1°C hotter than the top. It has already been shown in section 2.7 that a temperature gradient of only 0.1° cm^{-1} in the same sense is enough to promote thermal convection. By modification of the dimensionless Rayleigh number, a similar result is obtained for solutal convection. Therefore a 1°C temperature difference across 2 cm. depth of melt was considered enough to promote solutal convection. This was considered necessary to homogenise the melt because of the large density difference between the flux (8 $g.cm^{-3}$) and the garnet (5.6 $g.cm^{-3}$). In addition, the sheathed thermocouple was used to plot a calibration curve of the temperature in the melt against the temperature of the monitoring thermocouple, so that during growth runs the temperature of the melt was always accurately known. Over a period of two months continuous operation it was found that thermocouples fabricated from 0.3 mm. diameter wire began to give falsely high readings of the temperature, presumably because of attack by lead oxide vapour. To overcome this, thermocouples were fabricated from 1 mm. wire and periodically checked against a third (reference) thermocouple in a furnace free from corrosive vapour.

3.2 Growth Procedure.

The melt composition used is given in figure 2.1. Except for the lead monoxide which was BDH Analar grade, all of the starting materials were of 99.9% purity or better. Prior to weighing, all starting materials were

dried overnight at 250°C. Once weighed they were mixed by shaking vigorously in a glass jar and the mixture then homogenised at 1100°C. for 16 hours in a tightly covered 100 ml. platinum crucible.

The substrate holder, together with a substrate before and after epitaxy, is shown in figure 3.2. It consisted of a fourteen inch long recrystallised alumina tube, one end of which was covered with a closed-end platinum tube, to which was attached four 1 mm. thick platinum tabs to hold the substrate in position. Substrates were purchased from the Union Carbide Company in form of GGG discs of diameter 1 cm. and thickness 0.6 mm. These had been highly polished on one side only. A substrate was mounted onto a 1.1 cm. platinum backing disc and positioned between the four tabs so that only a slight bending inwards of these tabs was sufficient to hold both the substrate and the backing disc tightly to the holder (figure 3.2). With this arrangement, the whole area of the substrate was in good thermal contact with the machined backing disc and both the stress exerted on the substrate and the area covered by the holding tabs were minimal.

As in all cases of epitaxial growth, substrate preparation is of prime importance. Once mounted on the holder, substrates were boiled in a dilute solution of Alconox (sodium phosphate/sodium carbonate) for 10 minutes and then in deionised water for 10 minutes. Finally, substrates were treated in a vapour degreasing bath of "Genklene" (111 trichloroethane). As pointed

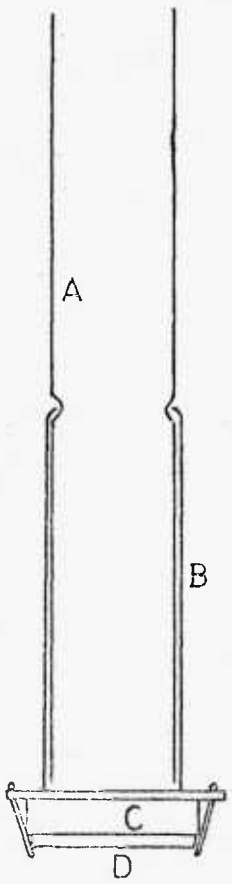

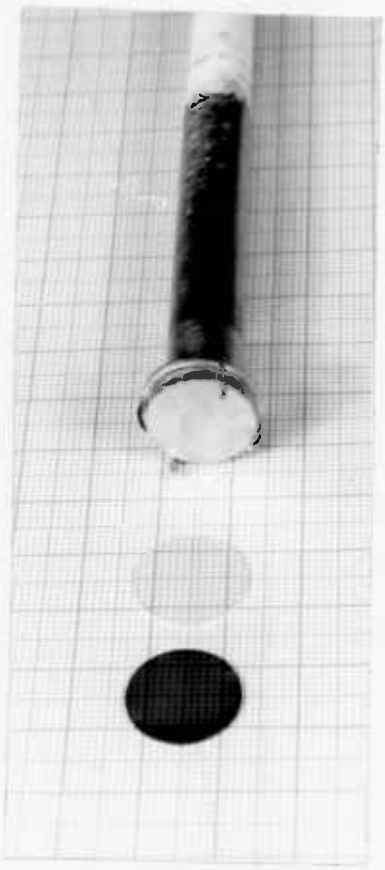

A Alumina Tube
B Platinum Tube
C Platinum Backing Disc
D Substrate

Fig. 3.2 Substrate Holder, Substrate and Epilayer

out by Blank and Nielsen (1), any small particles on the substrate surface may become trapped in the epilayer where they can impede the motion of bubble domains. Therefore immediately after cleaning the substrate the growth process was commenced.

An interesting adaptation of the cleaning procedure has been reported by Robertson et al.(2). It involves dipping a substrate, which need not be highly polished, into a solution of the same material in a lead oxide/boric oxide flux at 60°C above the garnet liquidus temperature. The solution is then cooled linearly by 80°C in 10 minutes so that initially 50 micron of substrate disolves and then a small amount of growth occurs. The substrate thus has an extremely clean surface and should be immediately used for epitaxy. However, it is probable that this method is only applicable when extremely perfect substrates are used since preferential dissolution must occur at the sites of strained regions, leaving the surface pitted. The effect on striations, coring and dislocations on dissolution rate is shown in figure 3.9.

Prior to growth the melt was homogenised at 1100°C for 4 hours and then cooled to the initial growth temperature, allowing 30 minutes for stabilisation at this temperature. The substrate holder was then rotated axially and lowered into the furnace until the substrate was 1 cm. above the surface of the melt. Rapid heating of the substrate to the growth temperature was essential to prevent corrosive lead oxide droplets from condensing

on its surface. For this reason a separate substrate preheat chamber, as described by Ghez and Giess (3), is desirable. After 15 minutes, crucible rotation was stopped and the substrate lowered into the melt, still maintaining the preselected axial rotation rate. The depth of immersion in the melt was 0.5 cm. and was controlled by a microswitch on the lowering mechanism so that this value could be accurately reproduced. After growth the substrate was raised to just above the surface of the melt and spun at 1000 rpm for 30 seconds to remove any droplets of melt from the epilayer surface. The epilayer was then slowly withdrawn from the furnace, allowed to cool to room temperature and then boiled in 50% acetic acid to dissolve any solidified melt trapped between the substrate and the backing disc. When all the melt had dissolved the platinum holding tabs were bent back and the epilayer removed from the holder. The back of the substrate was lapped smooth with 30 micron and then 6 micron diamond paste to allow examination of the domain patterns using transmitted polarised light.

The supersaturation required for growth may be generated in four ways, all of which are illustrated in figure 3.3. Originally, method (ii) was used which involved dipping the substrate into the melt at or above the garnet liquidus temperature and cooling at a linear rate of a few degrees a minute. This method suffered from the disadvantages that etching of the substrate could occur and both the gallium segregation coefficient and distribution between octahedral and tetrahedral

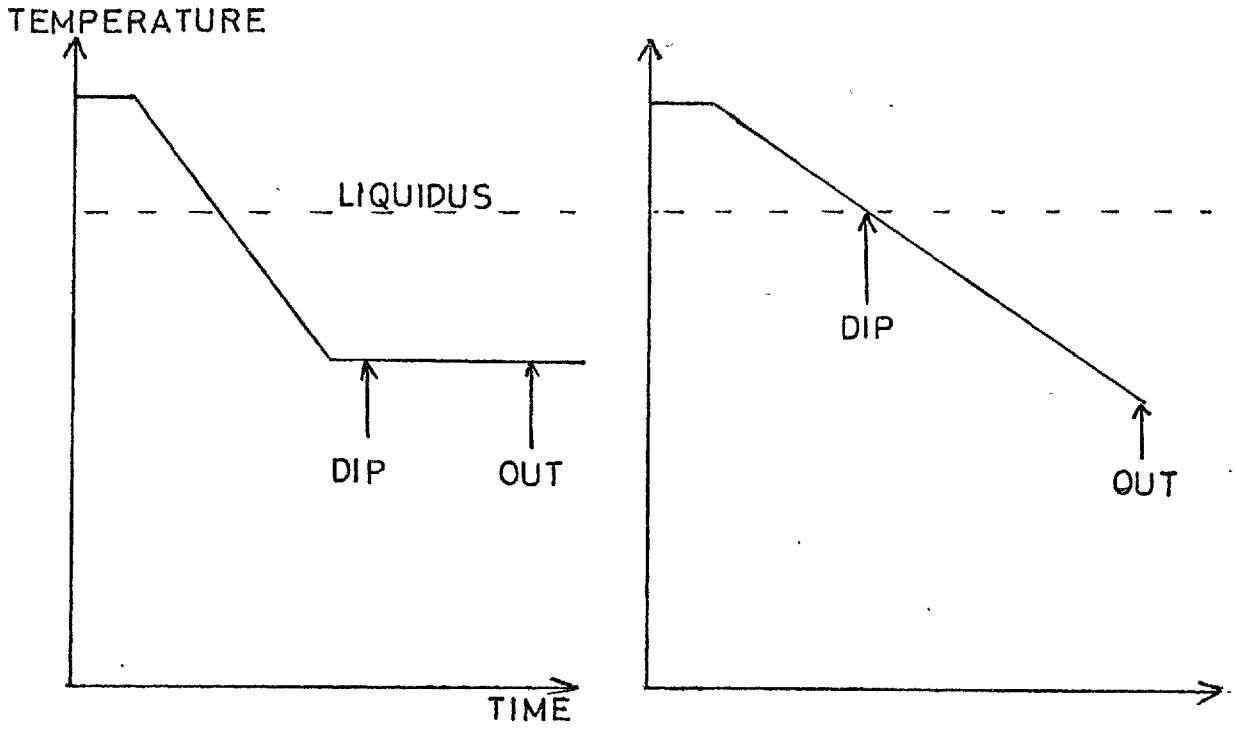

(i) Supersaturated Melt (ii) Linear Cooling

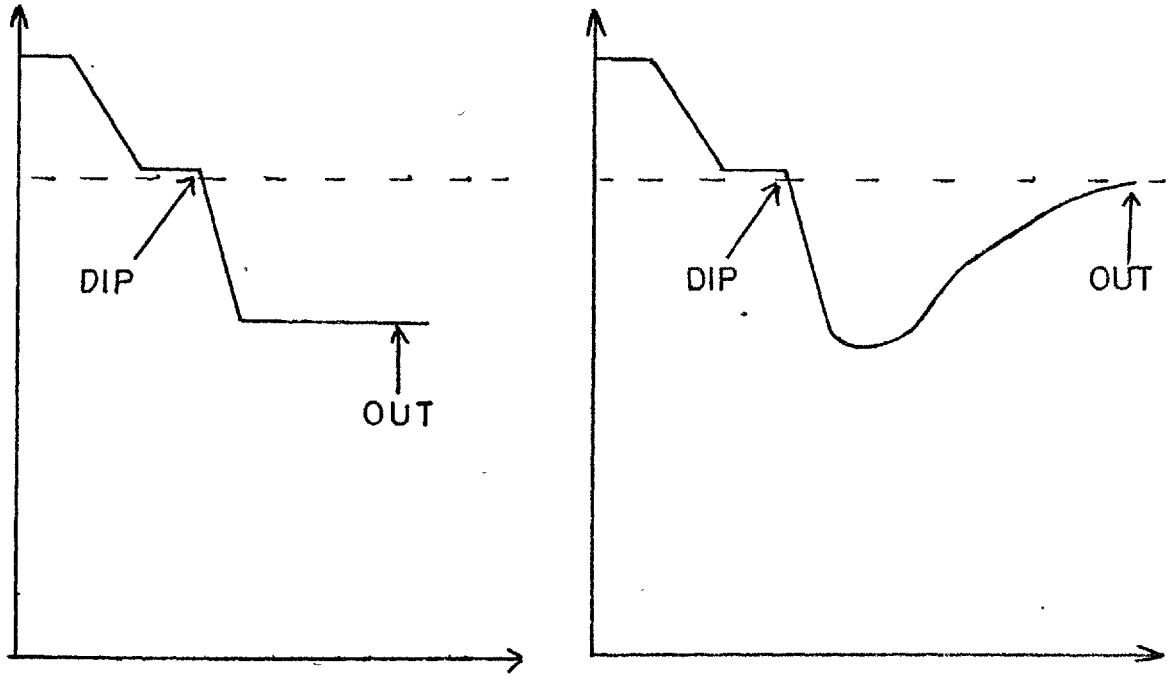

(iii) Back-cooling (iv) Transient Mode

Fig. 3.3 Ways of Generating Supersaturation

sites are functions of temperature.

Fortunately, it was reported by Levinstein (4) that these melts would readily support undercoolings of 40°C without the spontaneous nucleation of garnet. Since the amount of garnet removed from the melt in growing an epilayer is extremely small, Levinstein's discovery meant that growth could take place from a supersaturated melt isothermally and at a constant rate. The optimum undercooling was found to be in the region of 20°C. This gave the most reproducible results, since spontaneous nucleation rarely occurred at such value of undercooling and yet these values were large compared to short term fluctuations in the temperature of the melt. As well as its effect on growth rate, spontaneous nucleation has a more damaging effect, since tiny nucleii may be incorporated in the epilayer (figure 3.11) where they seriously hinder the motion of bubble domains.

Method (iii) offered an alternative mode of isothermal growth. The melt was kept at or above the garnet liquidus temperature and the substrate cooled by blowing a stream of nitrogen down the alumina shaft onto the substrate backing disc. The gas flow rate was adjusted to give the required supersaturation at the crystal interface. For the growth of thin (approximately 5 micron) epilayers, this method was found to have no advantages over method (i) and had the disadvantage of requiring very careful control. However, for the growth of thick epilayers, this method provides a potential way of overcoming interface breakdown which is a serious

problem for extended growth on the (111) garnet face. A full discussion of growth by substrate cooling is given in chapter five.

Finally, method (iv), transient mode LPE, occurs when a cooled substrate is dipped into the melt so as to cool the melt by the desired amount necessary for growth. As yet, this method has not been applied to the epitaxial growth of garnets. However it has been successfully used by Dietch (5) for the epitaxial growth of gallium arsenide, in which case the steep temperature gradient ahead of the interface can prevent the onset of interface instability.

3.3 Assessment of the Epilayer.

3.3.1 Analysis.

Compositional uniformity across the surface of the epilayer is easily determined since the saturation magnetisation is a function of composition. Therefore measurements of bubble-burst field and domain run-out field over the whole area of an epilayer are a good measure of compositional fluctuations. It was found that epilayers grown from supersaturated melts with substrate rotation were always of very unform composition.

However, absolute chemical analysis is far more difficult. Atomic absorption spectroscopy is destructive whilst electron microprobe analysis requires standards for all the components in the epilayer and, in addition, need tedious corrections including allowance for the

presence of the substrate. A radioactive tracer technique has been used by Janssen et al. (6) with some success but even this requires as many isotopes as there are constituents in the epilayer and is especially difficult for gallium since the radioactive isotope ^{67}Ga has a half life of three days only.

A fair estimate of composition can be obtained from the physical properties of the epilayer. Saturation magnetisation is particularly sensitive to the gallium : iron ratio. Lattice parameter, Curie temperature and Faraday rotation measurements are also informative if sufficient accuracy can be obtained. Even this may be complicated by the presence of a small amount of impurity. For example the garnet lattice can incorate lead from the flux on rare earth (dodecahedral) sites and this greatly increases the lattice parameter of the epilayer. The quantity of substituted lead depends on both temperature and growth rate.

Using a melt composition almost identical to that given in figure 2.1 and similar growth conditions, Giess et al. (7) have grown epilayers of approximate composition $Eu_{0.65}Y_{2.35}Fe_{3.9}Ga_{1.1}O_{12}$, as measured by careful electron microprobe analysis. This composition is significantly removed from that of the melt which contains the solute oxides in ratios corresponding to a garnet of formula $Eu_{0.7}Y_{2.3}Fe_{4.4}Ga_{0.6}O_{12}$. In order to simplify an explanation of this discrepancy it is convenient to define segregation coefficients such that gallium, for example, has a segregation coefficient, α_{Ga}, given by

the mole fraction :

$$\alpha_{Ga} = \frac{\left[\frac{Ga}{Ga + Fe}\right]_{epilayer}}{\left[\frac{Ga}{Ga + Fe}\right]_{melt}}$$

It is noticeable that the larger of the two rare earths, europium has the smaller segregation coefficient. This is consistent with the general trend that the larger the rare earth, the smaller is its segregation coefficient, the extreme example of this being lanthanum, the largest rare earth, which has a segregation coefficient of 0.1 in the garnet system $(La,Y)_3(Fe,Ga)_5O_{12}$ (8). However, the more striking effect of segregation is for gallium which has a coefficient of 1.9. This value decreases for increasing growth rates (7) and is consistent with the expected trend that the faster the growth rate the nearer the composition of the epilayer approaches that of the melt (i.e. segregation coefficients tend to unity as the growth rate tends to infinity).

It has already been shown (section 2.4) that constituent oxide species, rather than complete garnet molecules, exist in solution and it is shown in chapter four that the rate-limiting step in the growth process is the diffusion of solute from the bulk solution through a thin boundary layer to the crystal interface. Therefore a tentative explanation of the significance of segregation coefficients is that they are a measure of the rate of diffusion of each species through the boundary

layer. Clearly this explains the effects of rare earth size and growth rate of the values of segregation coefficients. It can even be adapted to explain why the value for gallium is much higher than that of iron if it is assumed that iron oxide is solvated to greater extent than gallium oxide. This assumption is not unreasonable since magnetoplumbite ($PbO.6Fe_2O_3$) can be crystallised from these melts and, in addition, Timofeeva (9) has shown that the solubility of iron oxide in lead oxide fluxes is much higher than the other garnet constituents. Further supporting evidence is that in the barium oxide/boric oxide flux (chapter 6), where presumably the solvation mechanism is different to that in the lead oxide/boric oxide flux, the segregation coefficients for both iron and gallium are approximately unity.

The compositional uniformity of an epilayer grown at Imperial College has been analysed by the General Electric Company (10). Electron microprobe analysis showed that although the gallium concentration was very uniform through the thickness of the epilayer, the first 0.5 micron grown was anomolous is having almost 50% more gallium than the rest of the epilayer. It is unlikely that this could be due to solid state diffusion of gallium from the substrate since gadolinium was not detected in the anomolous layer. Therefore it is likely that this anomolous layer represents the amount of growth before steady state growth conditions were set up. The

presence of the anomolous layer was confirmed by X-ray multiple diffraction.

3.3.2 Thickness determination.

The thickness of epilayers was measured by an interference technique in the infra-red region 4000 $cm.^{-1}$ to 1700 $cm.^{-1}$ using a Perkin-Elmer 357 spectrometer. The sample was placed at right angles to the incident beam and the spectrometer scanned over the given region. The interference scheme is shown in figure 3.4.A. Measurements of thickness using interference peaks at the extremes of the scanned range showed the refractive index of the epilayer was constant in the range 4000 $cm.^{-1}$ to 1700 cm^{-1}.

The intensity of the interference peaks is a good measure of the thickness uniformity of the epilayer. Generally it was found that epilayers grown with substrate rotation were far flatter than those grown without substrate rotation. This was confirmed by using a monochromatic (sodium) light source and measuring the interference fringes obtained by putting an optical flat at a low angle to the epilayer surface. The interference fringes then gave the surface contours of the epilayer. Figure 3.5 shows an epilayer of thickness 18 microns grown with a substrate rotation rate of 200 rpm. The surface is flat to within one fringe ($\pm$ 0.3 micron).

The validity of the infra-red interference technique was confirmed by grinding a section at a small angle from the edge of an epilayer so that the interface

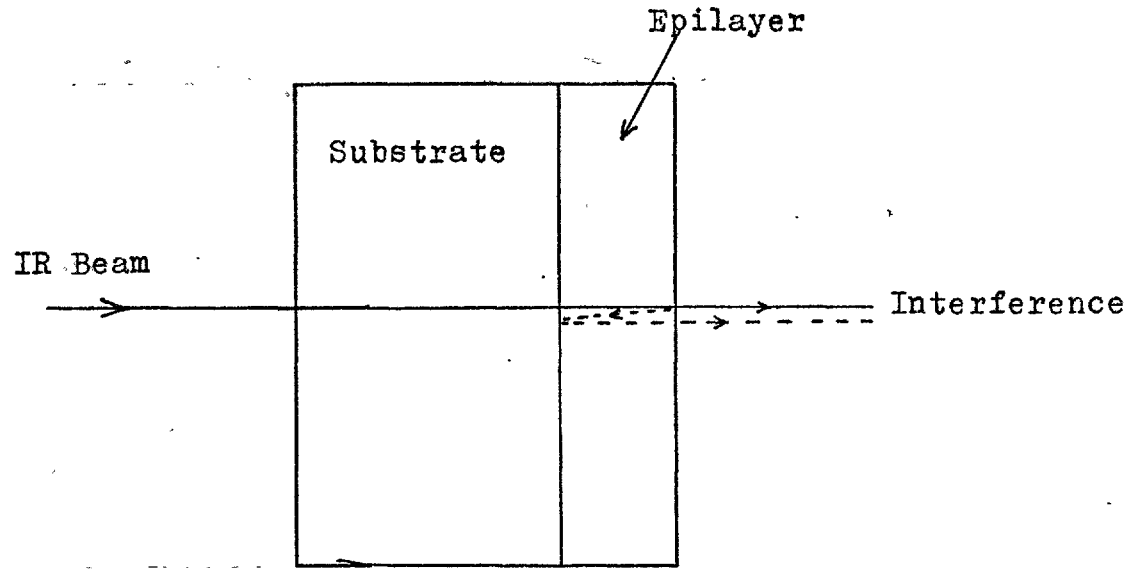

Fig. 3.4 A

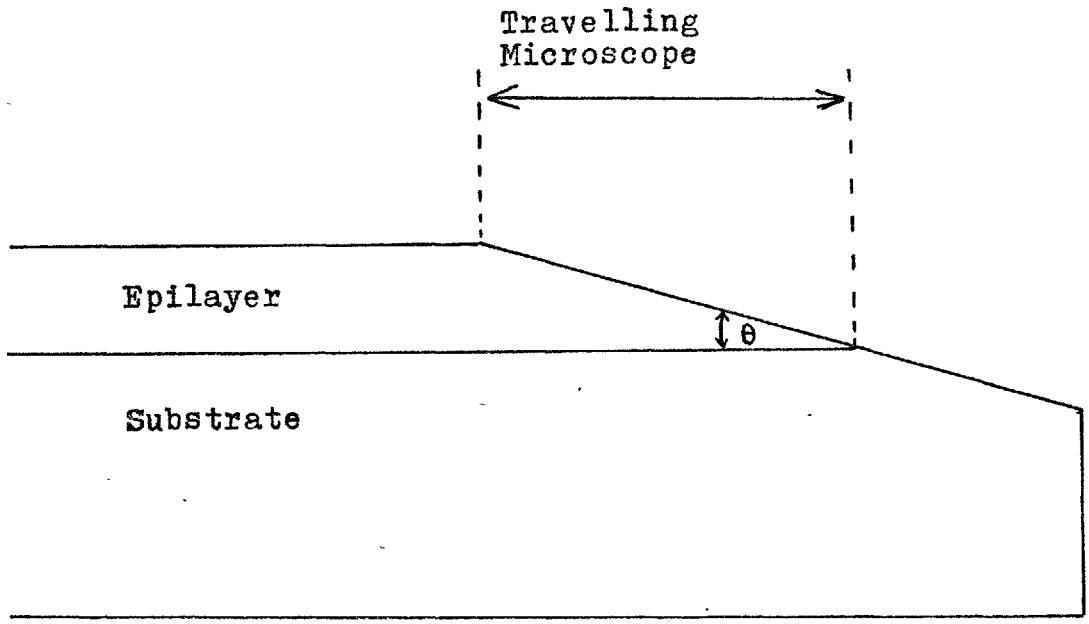

Fig. 3.4 B

Ways of Measuring Epilayer Thickness

with the substrate was visible. The angle was measured by a "Talysurf" and the length of the bevel measured using a travelling microscope, Hence the epilayer thickness was deduced (figure 3.4.B).

3.3.3 Crystal Perfection.

Defects in the epilayer are conveniently divided into two classes. Gross defects such as cracks, grain boundaries and second phase particles may completely prohibit the motion of bubbles across their paths. Minor defects such as dislocations, microscratches, thickness discontinuities and striations only affect bubble stability and mobility in varying degrees thus reducing operating margins in a working device. In addition to this sub-division, defects can also be classified according to their origin:

(i) Those present in the substrate that have propogated into the epilayer during growth.

(ii) Those actually generated during the growth process.

(iii) Those originating at the substrate/epilayer interface caused by too large a lattice mismatch or ineffective cleaning.

Substrate defects were easily assessable. When substrates were polished on both sides and viewed between crossed polaroids, strained regions caused by bunches of dislocations or parts of the boule which grew with a facetted interface could be seen by strain

birefringence. Figures 3.6 and 3.7 show the strain in the parts of the substrate which grew beneath the (211) and (110) facets respectively. More destructively, a one minute etch in phosphoric acid at 200°C was also used to pinpoint dislocations (figure 3.8 shows a particularly acute example). However, phosphoric acid etching was found to be more useful when a low quality epilayer was ground off and the substrate repolished for reuse. During polishing, the amorphous garnet removed from the surface may fill in any scratches thus creating a deceptively good surface appearance. A one minute etch in phosphoric acid at 200°C was used to dissolve this amorphous material and show the true surface appearance. It was found that a final chemical-mechanical polish on a lap flooded with "Syton" (colloidal silica in alkaline solution) was extremely effective in removing the last traces of surface damage.

Etching of the substrate in the fluxed melt slightly above the garnet liquidus temperature was also used to highlight defects. As well as showing up the facetted regions and dislocations, the technique showed remarkable sensitivity to striations. Figure 3.9 shows a highly polished substrate surface which has been immersed in the growth solution at 5°C above the garnet liquidus temperature for one hour. The substrate rotation rate was 200 rpm. The information shown in figure 3.9 could also have been obtained by X-ray topography, a technique which Stacey and Enz (11) have used with a great

deal of success for the assessment of substrate perfection.

Gross defects in the epilayer were also easily assessable. It has been shown (1) that when the lattice parameter of the epilayer is more than 0.013Å less than that of the substrate, cracking of the epilayer occurs. An example of this is shown in figure 3.10. On the other hand when the epilayer lattice parameter is more than 0.018Å larger than the substrate, the epilayer surface is comprised of a large number of pits and hillocks. This is known as film facetting (1) and is thought to be due to dislocations nucleating at the substrate/epilayer interface to accommodate the large lattice mismatch. These dislocations then provide sites for rapid growth and the interface breaks down. Second phase particles in the epilayer were always small garnet crystallites as shown in figure 3.11. These had spontaneously nucleated in the melt prior to or during growth and were caused by too high a supersaturation, ineffective homogenisation of the melt or contamination by dirty platinum-ware.

Minor epilayer defects such as microscratches were found to cause domains to lie along them. Figure 3.12 shows a particularly good example of this. An increase in domain stability is associated with microscratches since on applying an increasing bias field the domains lying along the scratches are the last to run out and the first to reform on lowering the bias field. When small droplets adhered to the epilayer surface on removal from the melt, growth continued under these droplets

until solidification occurred. The small circular thickness discontinuities that resulted are known as mesas. Large mesas were clearly visible to the naked eye while smaller mesas could be seen by the interference technique used for measuring the flatness of the epilayer surface. Figure 3.13 shows an interferogram illustrating two small mesas.

Defects arising from the substrate/epilayer junction are twofold. Small impurity paricules on the substrate surface may be trapped during growth and cause regions of localised strain. When of sufficiently large size, the strain field around an impurity particle can be detected by strain birefringence. However a far more sensitive technique is X-ray topography. Borrmann anomolous transmission topography is extremely sensitive to tiny regions of strain in highly perfect crystals. Using this technique, Stacey and Enz (11) found that almost all impurity could be removed by vigorous cleaning and handling of the substrates in dust-free rooms and under laminar flow hoods.

Secondly, too large a lattice mismatch at the substrate/epilayer interface results in cracking or film facetting, as previously mentioned. Fortunately, lattice parameters of mixed garnets obey Vegard's rule of additivity and thus can be easily calculated. The composition $Eu_{0.65}Y_{2.35}Fe_{3.9}Ga_{1.1}O_{12}$ has a calculated lattice parameter of 12.3862Å. However, electron microprobe analysis (10) has shown epilayers to contain approximately 0.2% by weight of lead. It has been

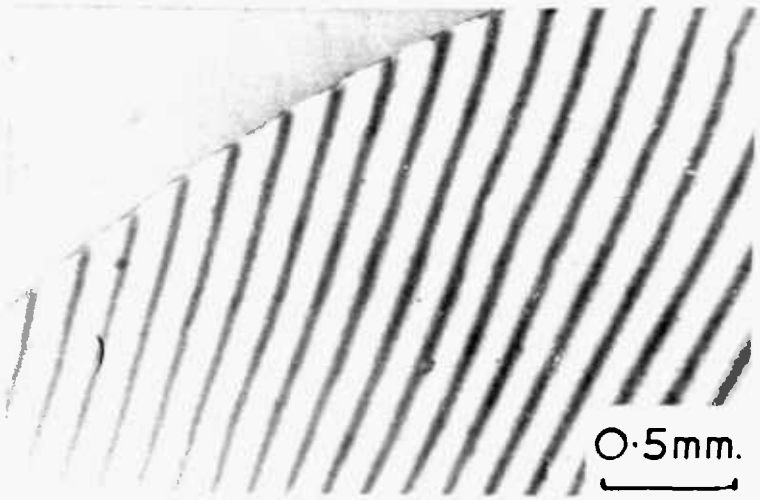

FIG 3.5

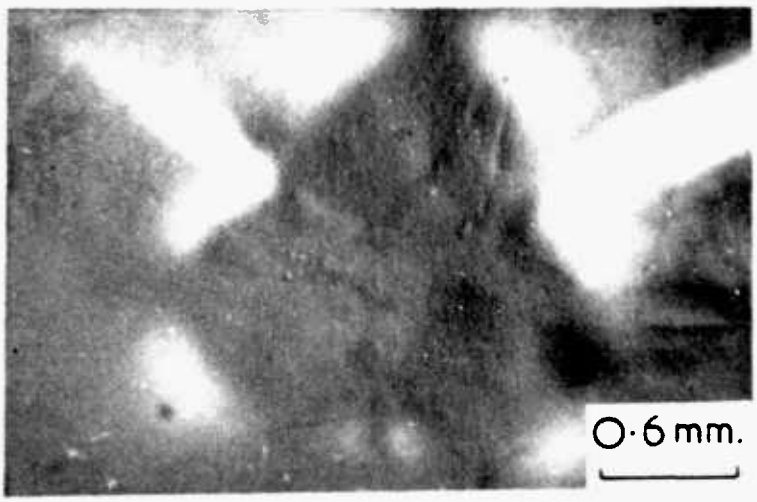

FIG 3.6

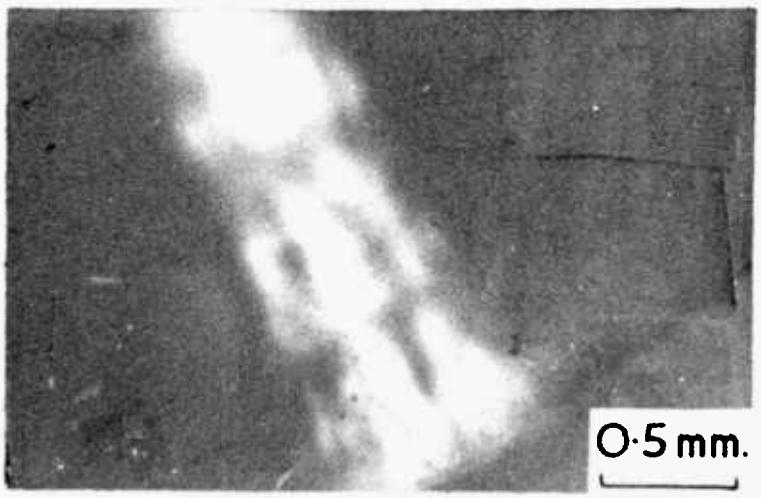

FIG 3.7

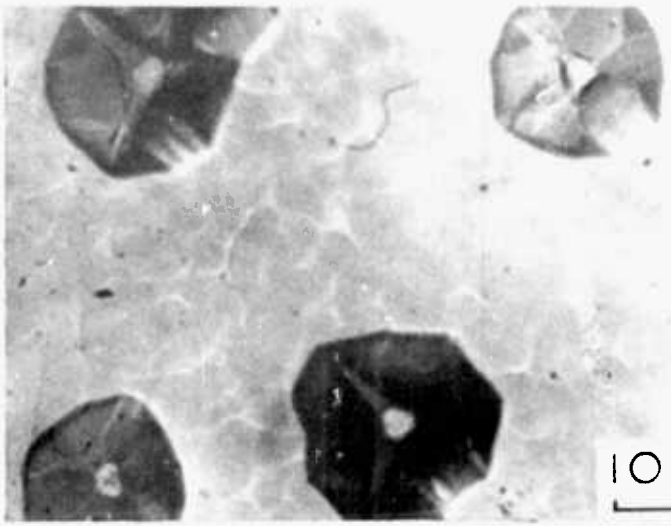

FIG 3.8

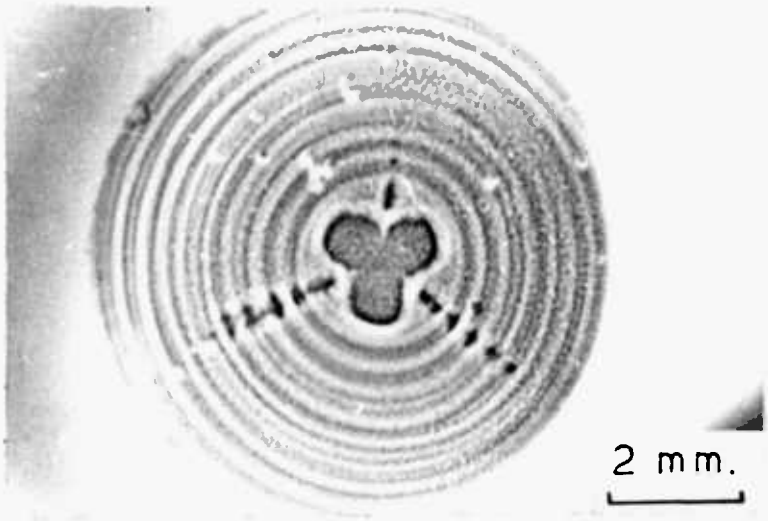

FIG 3.9

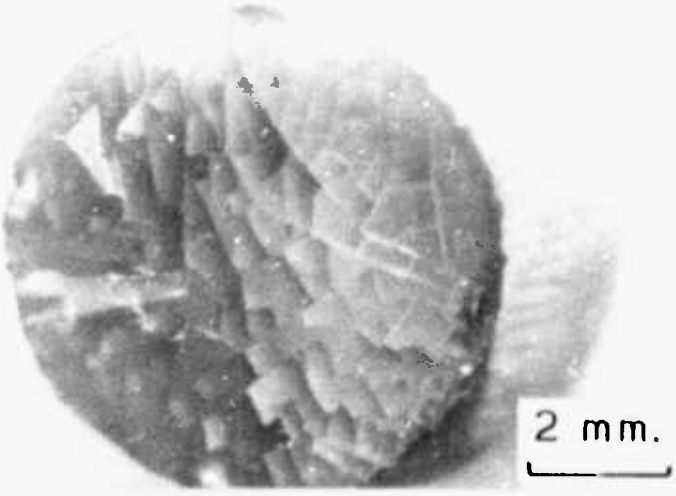

FIG 3.10

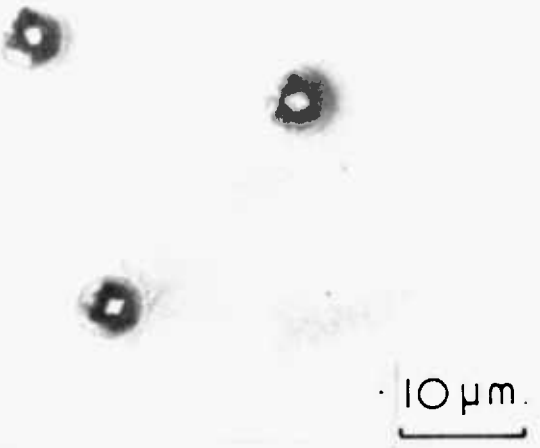

FIG 3.11

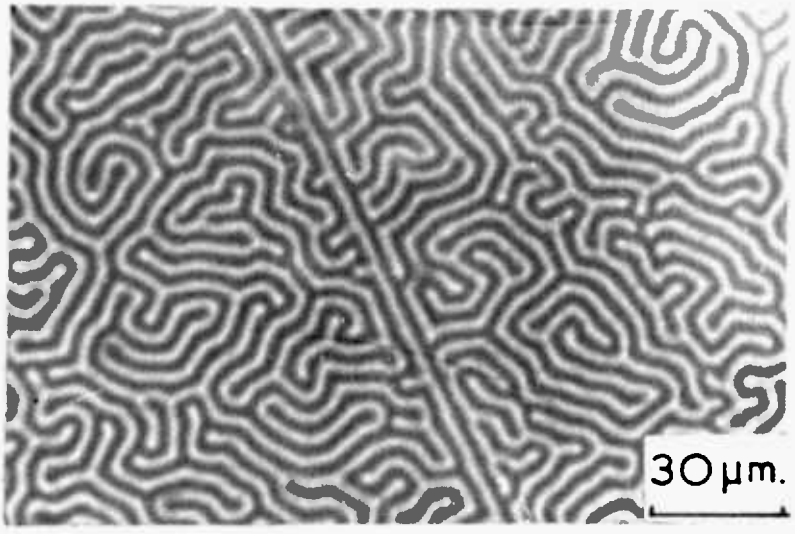

FIG 3.12

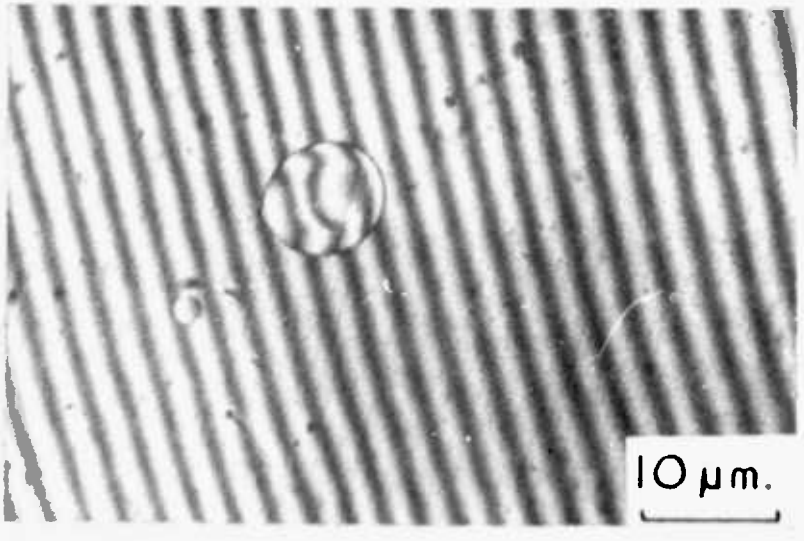

FIG 3.13

shown (12) that lead causes an increase in lattice parameter of 0.013Å for each weight percent. Therefore the corrected value of the calculated lattice parameter is 12.3888Å, which compares extremely well with the measured value of 12.3893Å (10). Therefore the substrate/epilayer mismatch was approximately 0.007Å which is large compared to any local variations in the substrate (± 0.001Å). However it has been shown by accurate electron microprobe analysis (12) that the segregation coefficients of the solute oxides depend on the growth rate. This is supported by magnetic measurements (figure 4.1). Slower growth rates produce epilayers containing relatively more gallium, more yttrium and less lead, all of which decreases the lattice parameter and consequently the mismatch with the substrate.

A sensitive technique for measuring the lattice mismatch has been developed by Glass (13). It is known as double crystal topography. As long as the epilayer is only a few microns thick, a beam of incident X-rays can be diffracted by both the epilayer and substrate. Using an extremely highly collimated incident beam of X-rays, the crystal is rocked through its Bragg angle and diffraction peaks are recorded for both the epilayer and substrate. The separation of the peaks gives the lattice mismatch and the sharpness of each peak is a measure of crystalline perfection.

3.3.4 Magnetic Assessment.

Although crystallographic techniques give a good measure of the number of bubble-pinning defects in

an epilayer, the most useful methods of assessment must be based on the behaviour of bubble domains in a given specimen, especially under conditions that would be present in a working device.

The simplest method of magnetic assessment is observation of the serpentine domain pattern. In a highly perfect epilayer the pattern is random whereas compositional fluctuations, thickness discontinuities or scratches will cause definite trends in the serpentine pattern. The effect of a microscratch is shown in figure 3.12. The effect of thickness discontinuities is shown in figure 3.14 which was taken in the presence of an applied bias field of approximately 100 gauss. The perfection of an hexagonal bubble lattice is also a good measure of the magnetic perfection of the epilayer. In figure 1.1.C a few defects in the bubble lattice are clearly visible.

However, in a working device bubbles are being generated and propogated through the crystal lattice. Consequently the best methods of assessment are based on the dynamic, rather than static behaviour of bubble domains. There are two dynamic assessment methods available. In both cases an hexagonal bubble lattice is formed and a pulsed field applied to the epilayer. Depending on the nature of the pulsed field, the bubbles will either flow randomly (1, 14) or vibrate about their equilibrium positions. In both cases domain pinning defects are easily visible or can be highlighted by time-lapse photography if necessary.

It was found that epilayers analysed by these dynamic assessment methods often had a higher density of pinning defects that could be detected by crystallographic methods.

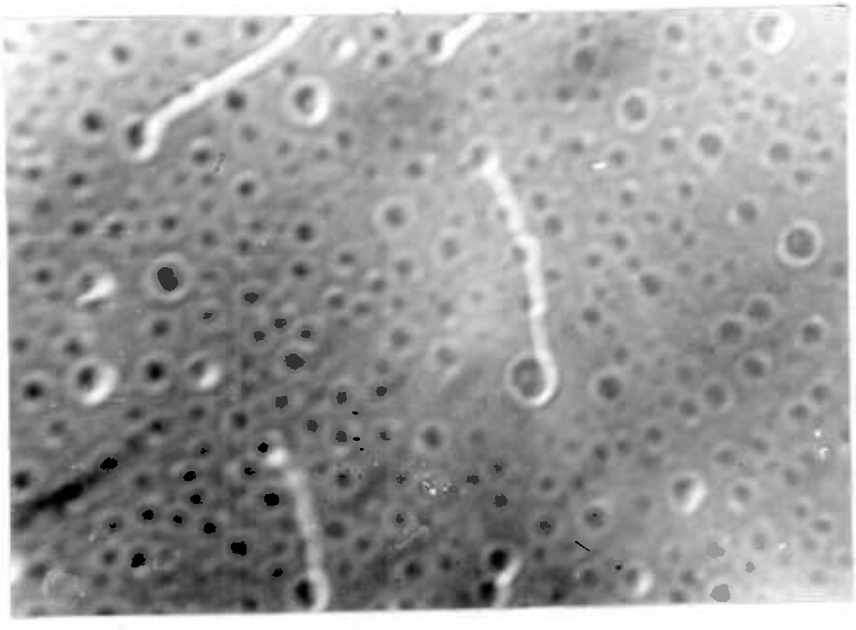

Fig. 3.14 Domain Pinning by Surface Irregularities

CHAPTER 3 : REFERENCES.

1) S.L.Blank and J.W.Nielsen, J.Cryst.Growth 17,(1972),302

2) J.M.Robertson, M.J.G.Van Hout, M.M.Janssen and W.T.Stacy, J.Cryst.Growth 18, (1973), 294

3) R.Ghez and E.A.Giess, Mat. Res. Bull 8, (1973), 31

4) H.J.Levinstein, S.Licht, R.W.Landorf and S.L.Blank Appl. Phys. Letters 19(11), (1971), 486

5) R.H.Dietch, J.Cryst.Growth 7 (1), (1970), 69

6) G.A.M.Janssen, J.M.Robertson and M.L.Verheijka, Mat. Res. Bull 8, (1973), 31

7) E.A.Giess, J.D.Kuptsis and E.A.D.White, J.Cryst.Growth 16, (1972), 136

8) W.Tolksdorf, G.Bartels, G.P.Espinasa, P.Holst, D.Mateika and F.Welz, J.Cryst.Growth 17, (1972), 322

9) V.A.Timofeeva and T.A.Kontova, Soviet Physics - Crystallography 13(3), 1968

10) GEC ANALYSIS 9194/X 109/MA 559/L

11) W.Stacey and U.Enz, IEEE Transactions on Magnetics MAG-8, 268

12) E.A.Giess, D.C.Cronemeyer, R.Ghez, E.Klokholm and J.D.Kuptsis, J.Amer Ceram. Soc.

13) H.L.Glass, Mat, Res. Bull 7, (1972), 385

14) P.Chandhari, Intermag Conference - MAG 8, 333

CHAPTER 4.

4. GROWTH KINETICS.

4.1 The Need for a Kinetic Study.

It has been specified by Thiele (1,2) that a bubble domain has its maximum stability when the epilayer thickness is equal to the bubble diameter. The magnitude of the bubble diameter, d, can be expressed in terms of the magnetic properties of the epilayer and its lattice mismatch with the substrate by

$$d = \frac{10\ (AK_u)^{\frac{1}{2}}}{\pi M_s^{\,2}}$$

where A is the exchange constant (a measure of the force acting to keep adjacent spin vectors aligned) and K_u and M_s are as defined in section 1.4. Consequently for a given epilayer/substrate system the bubble diameter is fixed and only epilayers whose thicknesses are approximately equal to this value will exhibit maximum stability of their bubble domains. Although thickness control may be developed empirically for a given set of growth conditions, the conditions will not be universally applicable since they must depend on the melt composition, the growth temperature, the hydrodynamic conditions in the melt and the geometry of the growth apparatus. Clearly a knowledge of the growth mechanism will assist in the quantitative control of epilayer thickness and

this knowledge can only be gained by a study of the growth kinetics.

In addition to the effect on epilayer thickness, irreproducible growth conditions must lead to irreproducible variations in the magnetic properties of the garnet. To demonstrate this, three epilayers were grown at the same temperature and for the same growth time on (111) oriented GGG substrates. The only parameter varied was the substrate rotation rate. It was found that increasing the rotation rate not only increased the epilayer thickness quite dramatically but also led to a higher saturation magnetisation. The results are shown in figure 4.1. The effect of growth rate on saturation magnetisation can be interpreted in terms of the segregation coefficients of the constituent oxides. The faster the growth rate, the nearer the individual segregation coefficients tend to unity. This causes an increase in the iron : gallium ratio in the epilayer thus producing a higher saturation magnetisation.

4.2 Factors influencing the growth rate.

Since the composition of the epilayer depends on its growth rate, compositional uniformity can only be achieved by maintaining a steady growth rate throughout the dip time. The parameters having the greatest influence on growth rate are temperature, relative supersaturation and the velocity at which the solution flows past the crystal surface. Therefore, as discussed in section 3.2, isothermal growth from a supersaturated melt

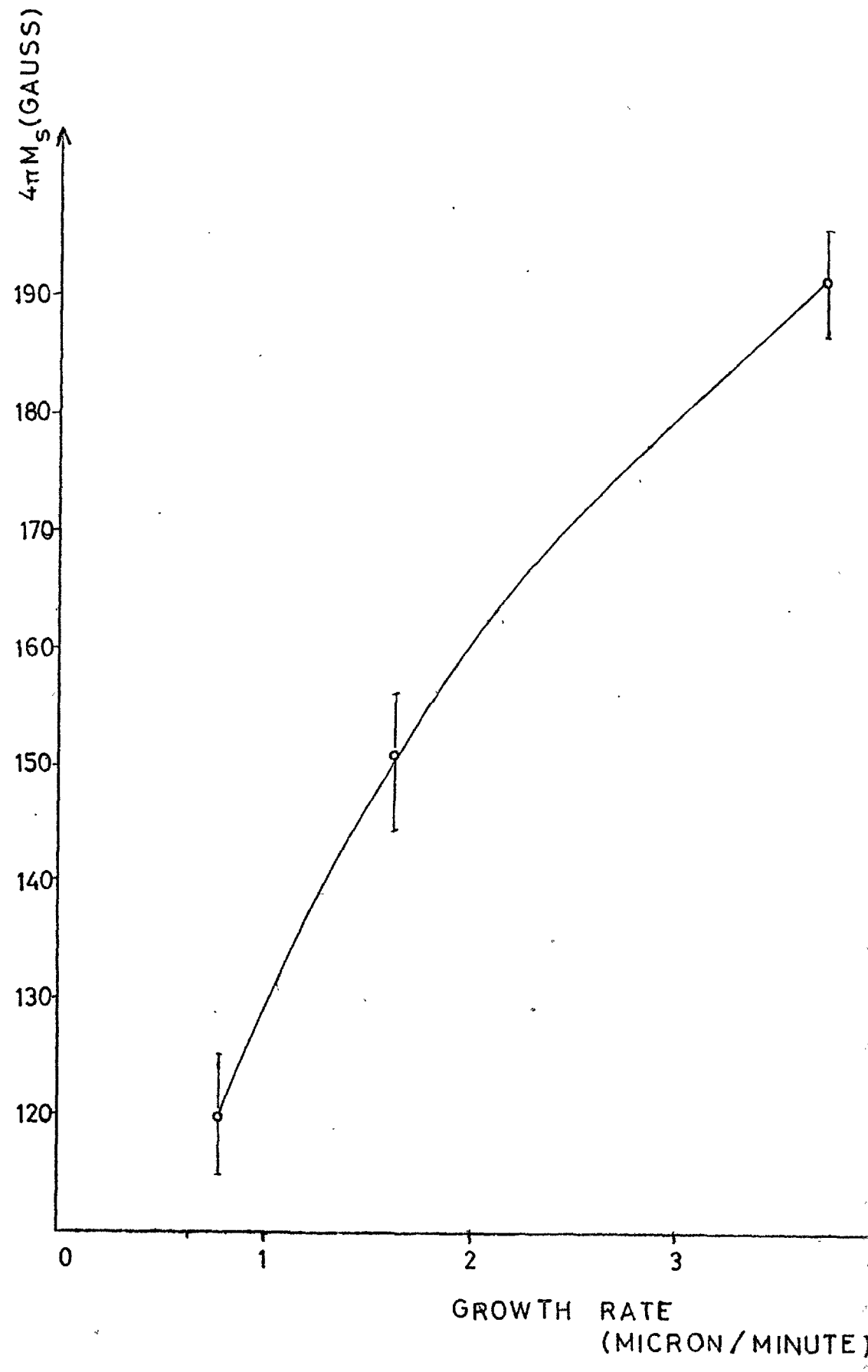

Fig. 4.1 Effect of Growth Rate on Magnetisation

with rotation of the substrate in a horizontal plane is the most suitable method for producing epilayers of uniform composition. The following kinetic study refers entirely to epilayers grown by this method on (111) - oriented GGG substrates. The melt used was of the composition given in figure 2.1 and had a liquidus temperature of 992°C.

In room-temperature solution growth the crystal interface can be visually observed through the growth period and so changes in growth rate with time are easily detected. However, in fluxed-melt growth, such observation is usually impossible and even if this could be achieved the actual thickness of epilayer grown is so small that it would be very difficult to monitor continuously. Therefore it is only possible to determine the average growth rate throughout the dip time by measuring the final thickness of the epilayer.

In order to determine whether the growth rate remained constant throughout the dip time, two series of epilayers were grown varying the growth time but keeping all other parameters constant. The growth temperature used was 973°C, an undercooling of 19°C. For one series a substrate rotation rate of 100 rpm was used whereas for the second series the substrate was not rotated. The thickness of the epilayers were measured by the infrared interference method and the plots of thickness against time are shown in figure 4.2. The following points were noted:

1) The thickness of epilayer grown scaled linearly with time for both series.

2) Both lines pass through the origin to a first approximation.

3) Epilayers grown without substrate rotation showed large thickness variations over their area. In order to estimate their thickness by the interference method, the infra-red beam had to be masked so that it was incident on very small areas (2 mm. square) of the epilayer. In contrast, epilayers grown with a substrate rotation rate of 100 rpm were flat to within half the wavelength of sodium light over at least 90% of their area.

4) On increasing the substrate rotation rate from zero to 100 rpm the growth rate increased by a factor of three.

5) Growth rates were comparable with those of most aqueous solution growth processes.

Once it had been established that growth rate was independant of time, the effects of undercooling were investigated, since it is the least controllable parameter effecting the growth rate. In order to do this, another series of epilayers were grown using a substrate rotation rate of 100 rpm and dip time varying between 5 and 10 minutes. Undercoolings of between $5^{o}C$ and $34^{o}C$ were used and the effect on growth rate is shown in

figure 4.3. Growth rate was found to be proportional to undercooling and consequently supersaturation. However, it appeared that a small undercooling was necessary before epitaxial growth would occur. The magnitude of the critical undercooling was in the region of $3^{o}C$, which corresponds to a supersaturation of 0.025.

The linearity of growth rate with undercooling was found to tail off at high values of undercooling. This reflects both the small curvature in the slope of the garnet solubility curve and the slowing down of mass transfer and surface integration rates with the lower temperatures. In addition, high undercoolings often produced spontaneous nucleation of garnet in the melt prior to or during growth. The presence of garnet nucleii dramatically lowered the growth rate of the epilayer by an irreproducible amount. Therefore it was concluded that undercoolings of between $10^{o}C$ and $20^{o}C$ were the most suitable for reproducible results since as well as inhibiting spontaneous nucleation, these values were large compared to short term fluctuations in the temperature of the furnace ($\pm$ $0.5^{o}C$ maximum).

In order to establish the dependance of growth rate on substrate rotation rate, a series of epilayers were grown at $980^{o}C$ using a dip time of 10 minutes. The substrate rotation rate was varied between 25 rpm and 1000 rpm. At low rotation rates the growth rate was found to be approximately dependant on the square root of rotation rate. Whereas at high rotation rates

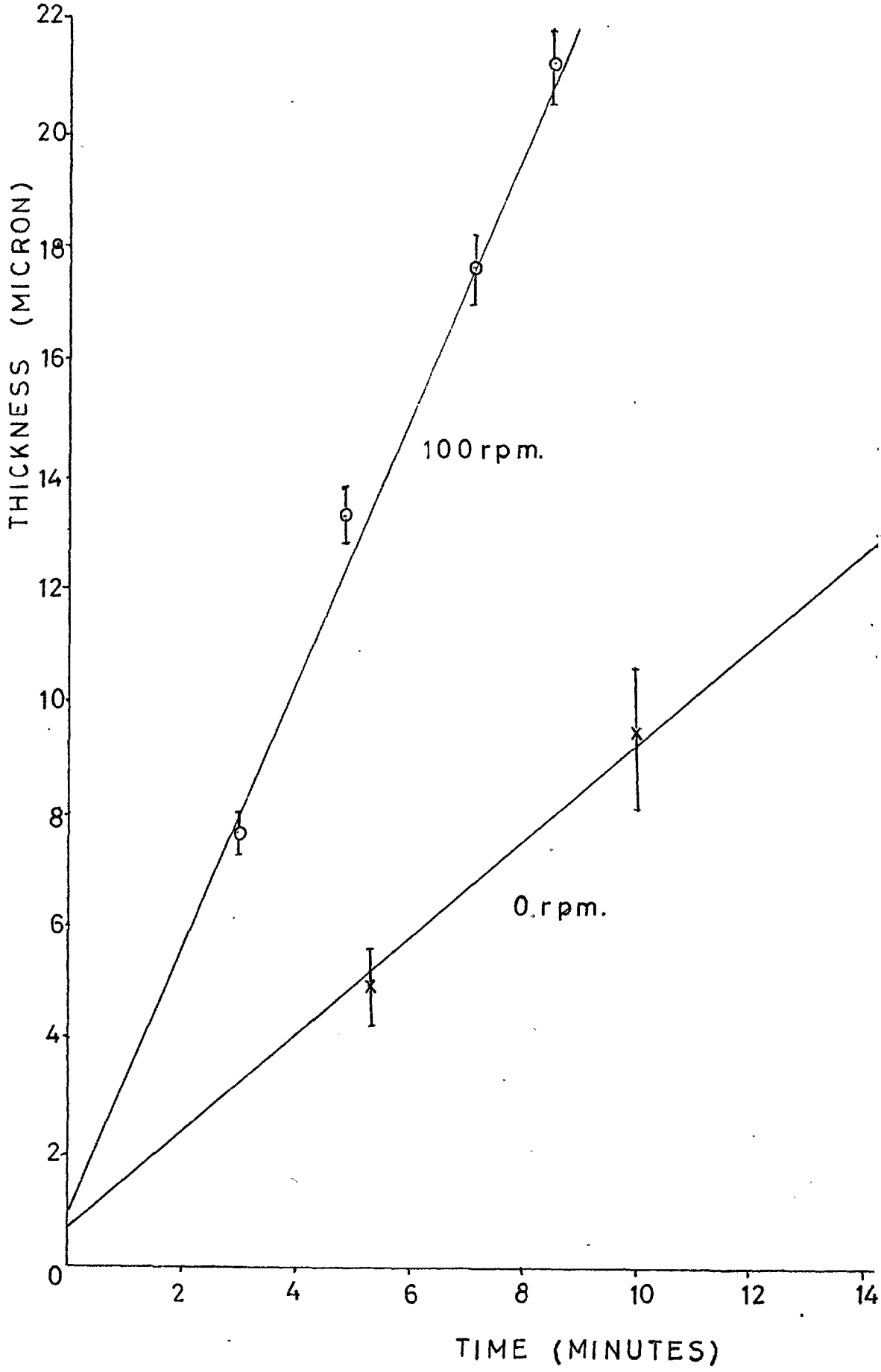

Fig. 4.2 Epilayer Thickness vs. Dip Time

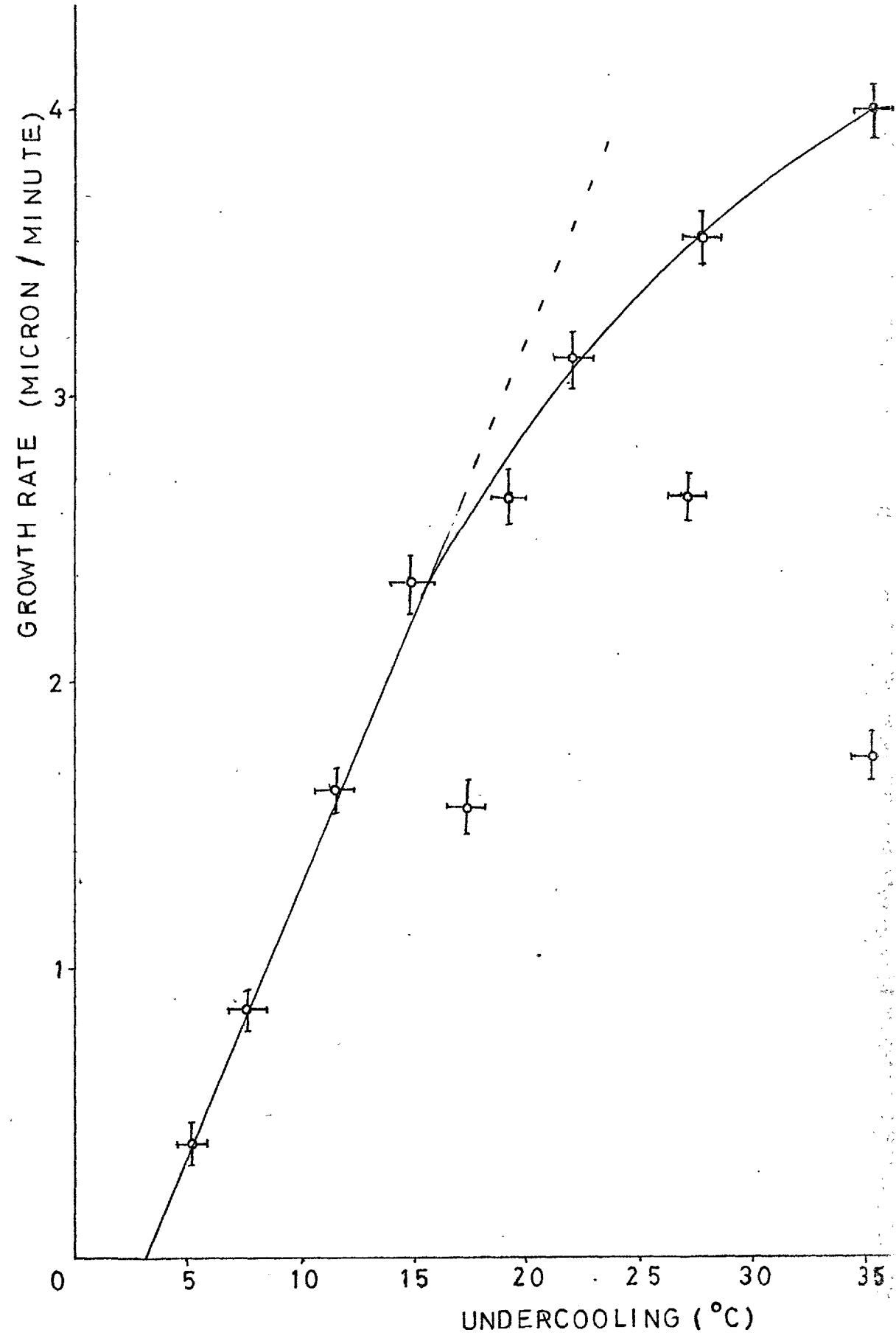

Fig. 4.3 Growth rate vs. Undercooling

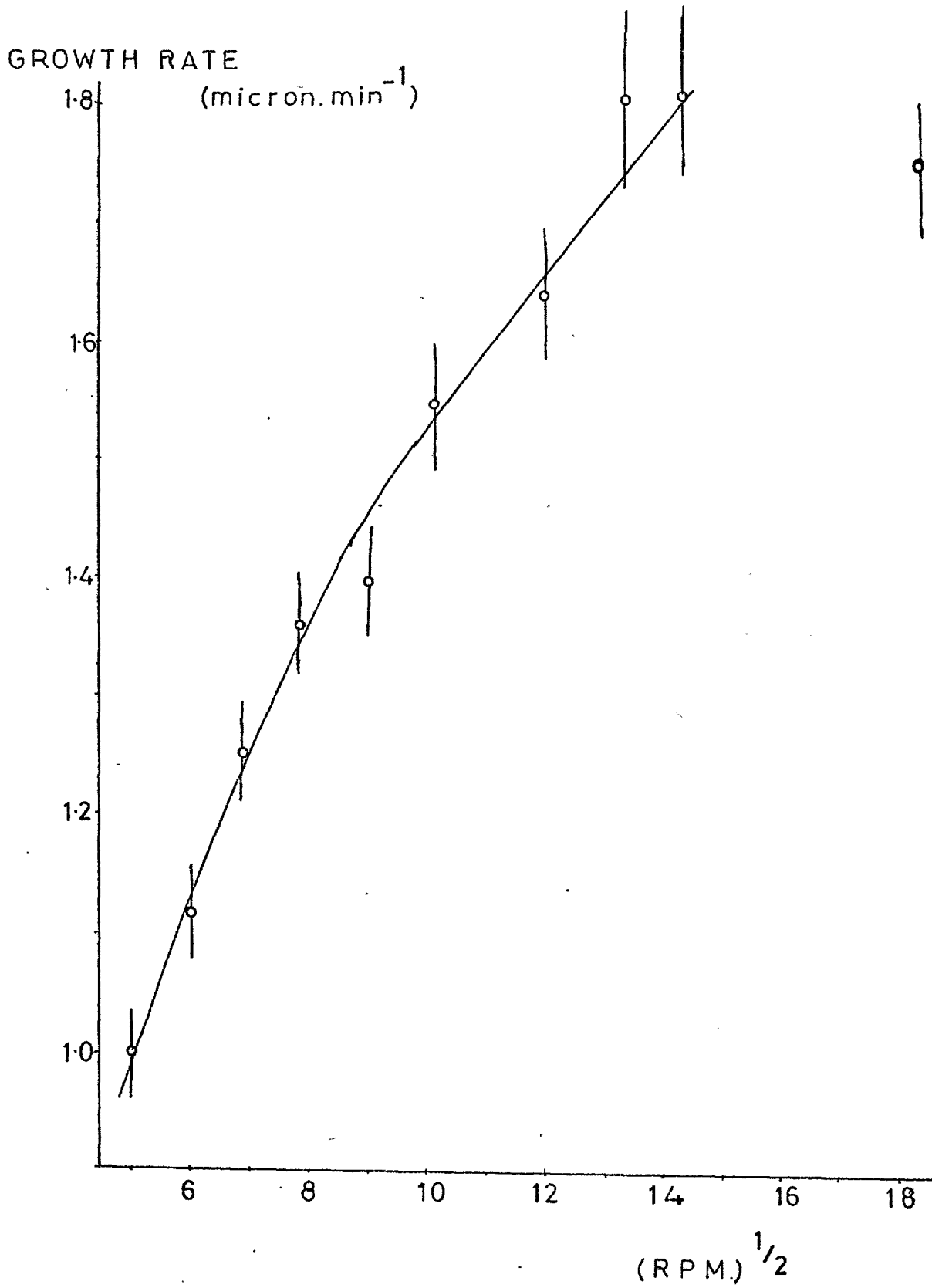

Fig. 4.4 Growth Rate vs. Square root of Rotation Rate

spontaneous nucleation of garnet frequently occurred and the resulting epilayers, although flat to within one fringe across their surface and uniform in magnetisation, contained small garnet crystallites and were of unpredictable thickness. When spontaneous nucleation appeared not be have occurred, growth rates at rotation rates of 1000 rpm were comparable with those at 400 rpm. The results obtained at lower rotation rates are shown in figure 4.4. The error bars on the points are representative of the temperature readout being to the nearest degree and so the actual growth temperature could have been anywhere between 979.5°C and 980.5°C.

4.3 A Model for the Growth Process.

The growth of crystals from solution can be conveniently divided into three processes:

1) Transfer of the solute from the bulk solution to the edge of a thin solutal boundary layer which exists ahead of the crystal interface.

2) Diffusion of solute through the boundary layer to the surface of the crystal.

3) Integration of the solute into the crystal (This step may involve reorientation of the solute species prior to adsorption on the crystal surface, desolvation and diffusion across the surface to a suitable growth site upon which the species is integrated into the crystal structure).

One or more of these three steps may be rate-

limiting depending on the crystal and the growth conditions. If there is no net solution flow relative to the crystal then the solute boundary layer does not have a finite thickness and steps (1) and (2) are combined.

Step (1) cannot be rate determining in the liquid phase epitaxy system for the following reasons. First, the distance, x, that a growth unit can diffuse in a time, t, is approximately given by

$$X = (Dt)^{\frac{1}{2}}$$

where D is the diffusion coefficient. Therefore if bulk diffusion was completely rate limiting the epilayer thickness would scale with the square root of dip time. The data in figure 4.2 shows a linear dependance with time for both substrate rotation rates of 100 rpm and zero. Secondly, if bulk diffusion were rate limiting the growth rate would be independant of substrate rotation rate. Thirdly, it is easily shown that rotation of the substrate in a horizontal plane near the top of the melt is an extremely efficient method of homogenising the melt. This was demonstrated by a controlled growth simulation experiment at room temperature. A glass beaker was used instead of a crucible and the kinematic viscosity of the melt matched by use of an appropriate water/ glycerol mixture. Using the same liquid depth and clearances as for a normal growth run, the substrate holder was rotated at 100 rpm and a small quantity of colouring agent (potassium permanganate solution) injected into the system. Complete homogenisation always occurred

in less than fifteen seconds and took only a few seconds with faster rotation rates. Consequently boundary layer diffusion, surface integration or their combined interaction must be rate-limiting.

It has been well established (1, 2) that when a disc rotates with constant angular velocity in a liquid, a uniform momentum boundary layer, whose thickness can be expressed in terms of the angular velocity and the physical properties of the liquid, is rapidly set up. Burton, Prim and Slichter (3) have extended this to apply to the solute boundary layer in the Czochralski growth of uniformly-doped germanium crystals, in which case the crystal interface approximates to a flat rotating disc. The expression relating to the solute boundary layer thickness, δ_c, to the properties of the system is:

$$\delta_c = 1.6 \; D^{\frac{1}{3}} \nu^{\frac{1}{6}} \omega^{-\frac{1}{2}} \qquad 4.1$$

where D is the diffusion coefficient of the solute, ν is the kinematic viscosity of the solution and ω is the angular rotation rate of the disc. Therefore if boundary layer diffusion provided a limitation on the growth rate of the epilayer, the growth rate should scale with the square root of substrate rotation rate and this is approximately in accordance with the experimentally-obtained data.

However equation 4.1 is only valid as long as the solution flow is laminar around the disc. The transition from laminar to turbulent flow is governed by the magnitude of the dimensionless Reynold's number, Re,

which for a rotating disc is defined by

$$Re = \frac{\omega r^2}{\nu} \qquad 4.2$$

where r is the radius of the disc. At Reynold's numbers in excess of 2000 (1) the flow becomes turbulent. For the liquid phase epitaxy system equation 4.2 predicts turbulent flow at rotation rates of over 650 rpm and, bearing in mind that small protrusions on the disc (such as the platinum holding tabs) will aid the onset of turbulence, it is probable that equation 4.1 is only valid for substrate rotation rates substantially lower than 650 rpm.

A close inspection of the data shown in figure 4.4 reveals that in the region where equation 4.1 is valid, boundary layer diffusion is not the only process which provides a finite impedance to the growth rate. If it were, equation 4.1 predicts a linear plot passing through the origin whereas the data in figure 4.4 does show a distinct deviation from linearity as the rotation rate increases. This can only be the consequence of the surface integration process. As the rotation rate increases, the solute boundary layer becomes thinner and so surface integration becomes relatively more important as a limitation to the growth rate. The surface integration process must proceed at a finite rate since when the constituent oxides have diffused to the surface of the garnet crystal they must become correctly oriented before they are adsorbed and then must take a finite time

to be accommodated on an appropriate growth site. Perhaps the strongest evidence that surface integration is not an instantaneous process is the strong preference of gallium for tetrahedral sites. An instantaneous integration process would provide an even distribution of gallium atoms on octahedral and tetrahedral sites.

A method of estimating the relative impedances of the boundary layer diffusion and surface integration processes has been proposed by Brice (4) and is shown in figure 4.5. In order to apply the model of Brice to the liquid phase epitaxy system, it is necessary to consider the growth process as involving the diffusion and integration of "garnet growth units". This simplification is essential since a complex growth model must now involve each of the four constituent oxides diffusing and integrating at different rates. In figure 4.5 the equilibrium concentration of garnet is C_e and the concentrations in the bulk colution and at the interface are C_b and C_i respectively. The quantity $C_b - C_i$ represents the driving force for boundary layer diffusion and $C_i - C_e$ is the driving force for surface integration. The quantity $C_b - C_e$ is the total supersaturation.

Fick's first law of diffusion states that the number of molecules, J, diffusing through unit area in unit time is given by

$$J = D \frac{dc}{dx} \qquad 4.3$$

where $\frac{dc}{dx}$ is the concentration gradient. Applying this to

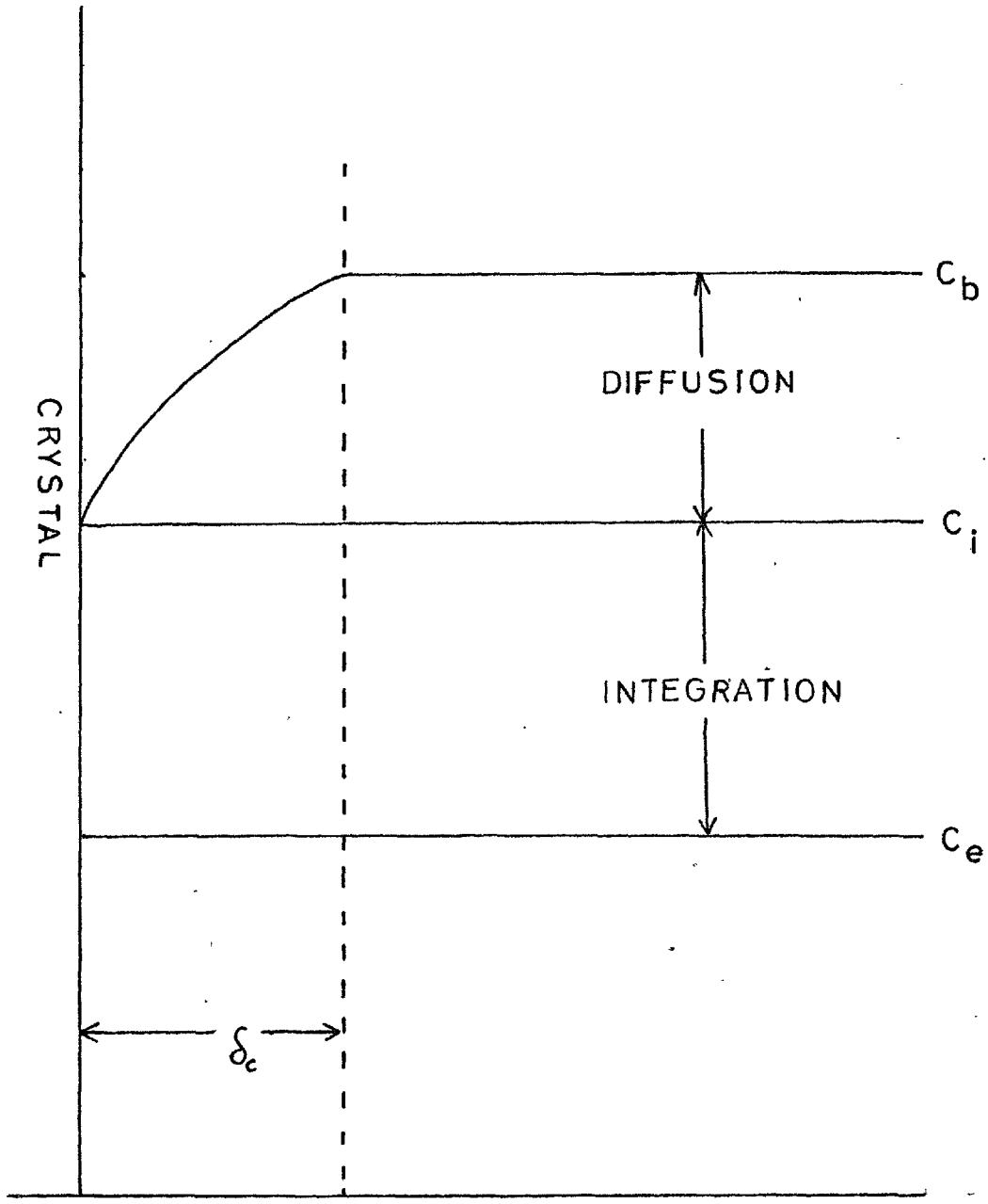

Fig. 4.5 Boundary Layer Diffusion and Surface Integration

the boundary layer diffusion step:

$$J = \frac{D\,(C_b - C_i)}{\delta_c} \qquad 4.4$$

or in terms of the growth rate, f ,

$$f = \rho^{-1} \frac{D\,(C_b - C_i)}{\delta_c} \qquad 4.5$$

where ρ is the density of the garnet.

The thickness of the concentration boundary layer is defined inequation 4.1 so that substitution into equation 4.5 gives

$$f = \frac{\rho^{-1} D^{\frac{2}{3}}\,(C_b - C_i)}{1.6\ \nu^{\frac{1}{6}}\,\omega^{-\frac{1}{2}}} \qquad 4.6$$

The velocity of the surface integration process is given by

$$f = A\,(C_i - C_e)^n \qquad 4.7$$

where A is the surface integration rate constant and n is the order of the reaction.

Since the quantity C_i cannot be directly measured, combination of equations 4.6 and 4.7 with the elimination of C_i gives

$$\frac{f}{\omega^{\frac{1}{2}}} + \frac{1}{B}\left[\frac{f}{A}\right]^{\frac{1}{n}} = \frac{C_b - C_e}{B} \qquad 4.8$$

where $B = 1.6\ D^{-\frac{2}{3}} \nu^{\frac{1}{6}} \rho$

In equation 4.8 the viscosity and density of the melt have already been measured. The density of the epilayer was calculated from its formula and lattice parameter to be 5.59 $g.cm^{-3}$. The magnitude of $C_b - C_e$ was calculated from the slope of the garnet liquidus curve (figure 2.6), allowing for the fact that approximately 3^o undercooling is necessary to initiate epitaxial growth. Therefore the unknown parameters in equation 4.8 are diffusion coefficient, surface reaction constant and the order of the surface reaction.

For growth on an atomically rough crystal surface it has been suggested by Brice (5) that the reaction is first order. It is reasonable to assume that the garnet (111) face is atomically rough on account of its fast growth rates, which are not dependant on the presence of spiral disolcations or other growth features. In addition, the growth rate varies linearly with undercooling which also suggests the reaction is first order with respect to supersaturation.

When the data in figure 4.4 was analysed by plotting $f\omega^{-\frac{1}{2}}$ against f, a straight line was obtained as shown in figure 4.6. However, this is not in itself complete proof that the reaction is first order, since if $f^{\frac{1}{2}}$ is plotted along the horizontal axis then, although a slight curvature is apparent, a straight line can still be drawn through six of the nine points. Therefore it is an assumption, although a very probable one, that the surface reaction is first order.

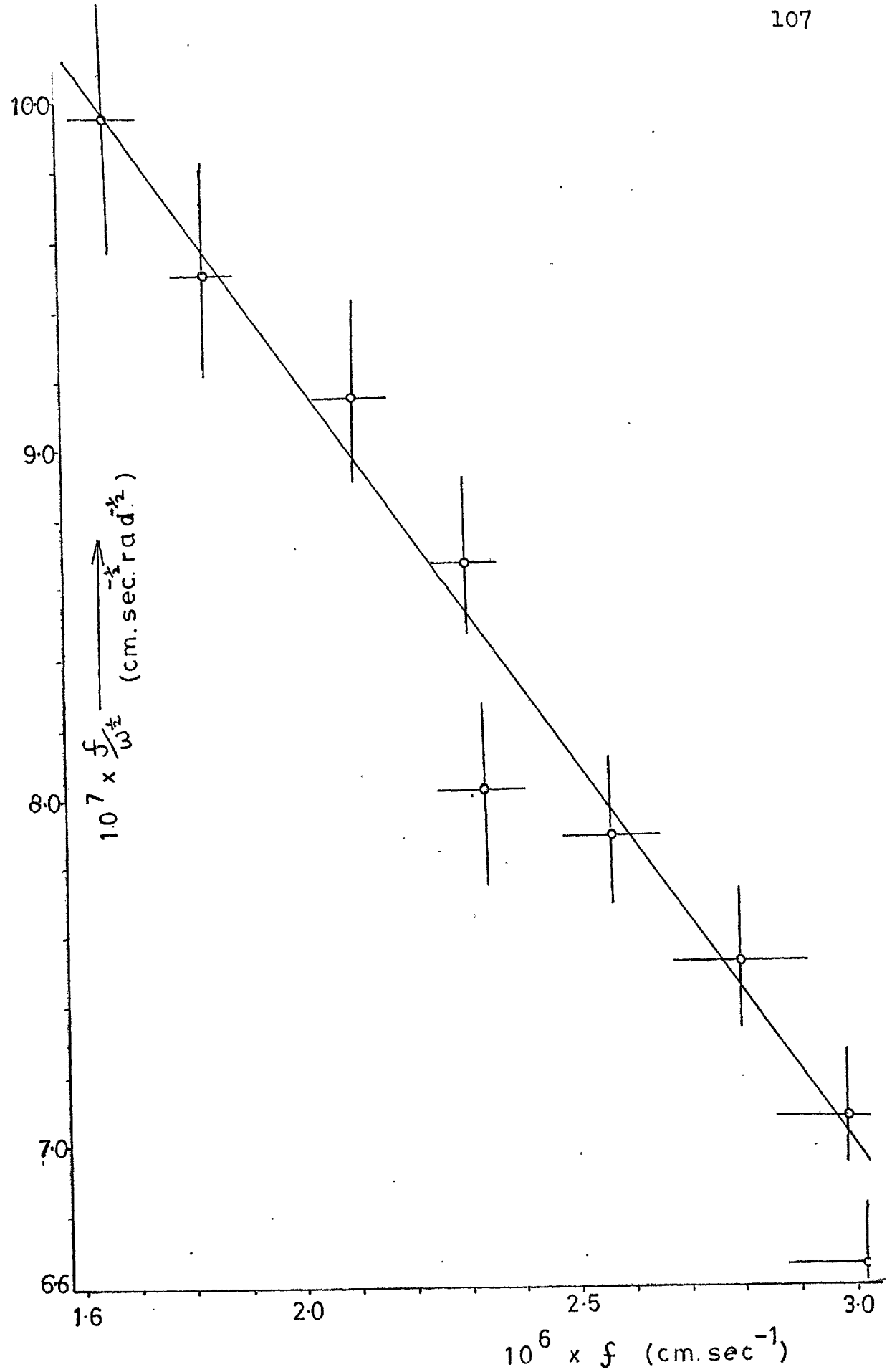

Fig. 4.6 Analysis of Growth Kinetics

According to equation 4.8 the line in figure 4.6 is characterised by:

$$\text{Slope} = -\frac{1}{AB}$$

$$\text{Intercept on } \frac{f}{\omega^{\frac{1}{2}}} \text{ axis} = \frac{C_b - C_e}{B} \quad \text{at } f = 0$$

The following values were obtained from the graph:

$$\text{Slope} = -0.214 \pm 0.04 \text{ radian}^{-\frac{1}{2}} \text{ sec}^{\frac{1}{2}}$$

$$\text{Intercept} = (1.343 \pm 0.12) \times 10^{-6} \text{ cm.sec}^{-\frac{1}{2}}\text{radian}^{-\frac{1}{2}}$$

Consequently at 980°C the values of diffusion coefficient and surface integration constant that provide the best fit to the available growth rate data are

$$D = (1.6 \pm 0.3) \times 10^{-5} \text{ cm}^2 \text{ sec}^{-1}$$

$$A = (7.1 \pm 2) \times 10^{-4} \text{ cm}^4 \text{ sec}^{-1} \text{ g.}^{-1}$$

To compare these results with those obtained by Ghez and Giess (6) for the garnet system of composition $Eu_{1.1}Yb_{1.9}Fe_5O_{12}$, it is necessary to define another surface integration constant, k, such that

$$k = \rho A \qquad 4.9$$

Therefore the value of k is $(4 \pm 1.2) \times 10^{-3}$ cm.sec^{-1}, which together with the diffusion coefficient are in reasonable agreement with those of Ghez and Giess who,

using a growth temperature of 880°C, obtained :

$$D = 3 \times 10^{-5} \text{ cm.}^2 \text{ sec}^{-1}$$

$$k = 3 \times 10^{-3} \text{ cm. sec}^{-1}$$

It is interesting to note that the value of the diffusion coefficient is comparable with diffusion coefficients in aqueous solution at room temperature. However, it is more difficult to grasp the physical significance of the value of the surface integration constant. Rearrangement of equation 4.8 for n = 1 and expressing the parameters in terms of the solute boundary layer thickness gives

$$f = \frac{\rho^{-1} (C_b - C_e)}{\frac{\delta c}{D} + \frac{1}{k}} \qquad 4.10$$

The relative impedances of the diffusion and integration processes are very approximately given by the magnitudes of $\frac{\delta c}{D}$ and $\frac{1}{k}$. When the substrate rotation rate is 36 rpm, $\frac{\delta c}{D}$ is about three times larger than $\frac{1}{k}$. However, at faster substrate rotation rates, the solutal boundary layer is thinner and so the surface integration step becomes relatively more important as a rate-limiting process. At 144 rpm the magnitude of $\frac{\delta c}{D}$ is only a factor of 1.3 larger than $\frac{1}{k}$ so that surface integration is almost as important as boundary layer diffusion. Confirmation of this can be obtained by close examination of the data in figure 4.4. At 36 rpm the growth rate

is 1.1 microns/minute and at 144 rpm is 1.7 microns/minute. If boundary layer diffusion was the only limitation on the growth rate, equation 4.5 predicts the growth rate would double on increasing the substrate rotation rate from 36 rpm to 144 rpm.

It is interesting to note that Robertson (7) has measured growth rates using a number of different substrate orientations. Under identical growth conditions the (111) substrate orientation was always faster growing that the (211) and (110) orientation by up to a factor of two. Since the boundary layer thickness does not depend on substrate orientation, these results indicate that surface integration on the (211) and (110) garnet faces is appreciably slower than on the (111) face. Again this is consistent with the model that the garnet (111) face is atomically rough, therefore providing a high density of easy growth sites.

From equation 4.1 it is now possible to obtain an estimate of the thickness of the solute boundary layer. For a substrate rotation rate of 100 rpm its thickness is approximately 60 microns. However, it is also evident from equation 4.1 that in the absence of substrate rotation the solutal boundary layer should be of infinite thickness. In this case, boundary layer diffusion would be equivalent to bulk diffusion and the epilayer thickness would scale with the square root of growth time. The experimental data (figure 4.2) shows thickness to have a linear dependance on time which means that a finite boundary layer must exist even in the absence of substrate

rotation. This can only be stabilised by the presence of natural convection in the melt and explains why the epilayers grown without substrate rotation had irreproducible thickness variations across their surfaces. Solution flow due to natural convection is seldom regular or reproducible and consequently produces thickness variations in the solutal boundary layer.

Using the growth rate data of figure 4.2 and the calculated values of diffusion coefficient and surface integration constant, the thickness of the solutal boundary layer can be calculated from equation 4.10. For the case of natural convection its thickness is approximately 260 microns at the centre of the epilayer. It has been shown by Carlson (8) that when solution flows across a flat crystal surface with a velocity, V, the rate of solute transfer to the surface is given by

$$J = \tfrac{1}{3} Sc^{\frac{1}{3}} D(C_b - C_i) \left[\frac{V}{\nu x}\right]^{\frac{1}{2}} \qquad 4.11$$

where x is the distance along the surface from the leading edge and Sc is the dimensionless Schmidt number as defined by

$$Sc = \frac{\nu}{D} \qquad 4.12$$

From equation 4.4 we have

$$J = D \frac{(C_b - C_i)}{\delta_c}$$

Equating this with equation 4.11 and taking x as the distance of the centre of the substrate from its edge (0.5 cm.) the solution flow velocity past the centre of

the substrate was calculated as 1 cm/sec. This value is reasonable for fluid flow due to natural convection and is large enough to maintain a homogeneous melt prior to growth. This is especially important in view of the appreciable density difference between the flux and the garnet.

CHAPTER 4 : REFERENCES

1) W.G.Cochran, Proc. Camb. Phil. Soc.30, (1934), 365

2) V.G.Levich, Physicochemical Hydrodynamics,(Prentice Hall, 1962)

3) J.A.Burton, R.C.Prior and W.P.Slichter, J.Chem.Phys. 21(11),(1953), 1987

4) J.C.Brice, J.Cryst.Growth 1, (1967), 161

5) J.C.Brice, J.Cryst.Growth 1, (1967), 218

6) R.Ghez and E.A.Giess, Mat. Res. Bull 8, (1973), 31

7) J.M.Robertson, Private Communication.

8) A.Carlson, Growth and Perfection of Crystals Edited by R.H.Doremus, B.W.Roberts and D.Turnbull (Wiley, 1958)

CHAPTER 5.

5. Interface Instability.

5.1 The Structure of the (111) Garnet Plane.

The equilibrium (habit) faces of fluxed melt grown garnet crystals are always of the form (211) and (110). These are therefore the slowest growing garnet faces since the faster growing directions will be eliminated during growth. The mechanism by which these (211) and (110) faces grow is well understood and has been studied in detail by Lefever et al. (1, 2). When a small garnet nucleus has formed the supersaturation is high and so the initial growth of the crystal is usually dendritic. As the crystal grows the supersaturation decreases and the dendritic growth changes to normal growth, producing a garnet crystal which has a dendritic core and an external morphology comprised of (211) and (110) faces. The habit faces then grow either by the spreading of layers, if the supersaturation is high enough, or, more commonly, by active growth centres from which series of growth steps radiate creating vicinal faces. Figure 5.1 shows an interferogram on a (110) face of one of the garnet crystals grown for the solubility determinations of section 2.1. Four interacting active growth centres are clearly visible. Lefever has proposed that this type of active growth centre is comprised of screw dislocations.

Fig. 5.1 Growth Features on a Garnet (110) Face

There is considerable evidence that the (111) garnet face grows by a different mechanism to those of the habit faces. (111) - oriented GGG boules are frequently grown free from dislocations (3,4,5). Since epitaxial growth proceed at the same rate on such substrate material as on substrates containing dislocation, it can only be concluded that dislocations do not contribute to the growth mechanism. In addition, the surfaces of some thin epilayers were coated with a 20Å layer of evaporated gold and observed in a scanning electron microscope (Cambridge Stereoscan Mark II). Over the whole of the surfaces no microscopic growth features were ever detected.

However, as discussed in section 4.3, surface integration on the (111) face is appreciably faster than on either the (211) or the (110) faces. Therefore the (111) face must provide a high density of preferred growth sites and the only way of accounting for this is that the surface is relatively rough on an atomic scale. An atomically rough surface is shown in figure 5.2 and as can be seen from this much simplified model, a growth unit (represented by a cube) arriving at the surface has a larger number of nearest neighbour atoms than if it were arriving at an atomically smooth surface. Consequently the growth unit is tightly bound to the surface and integrated into the crystal.

5.2 Constitutional Supercooling.

Constitutional supercooling is often encountered

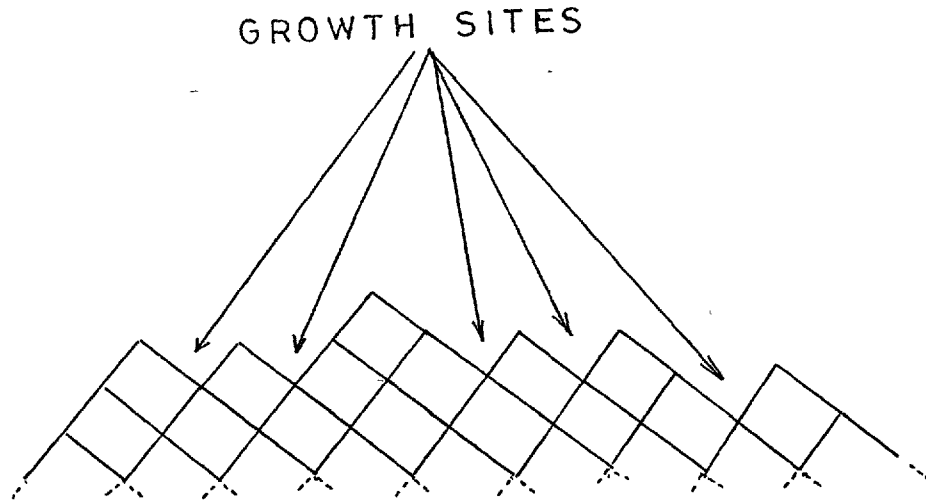

Atomically rough Interface

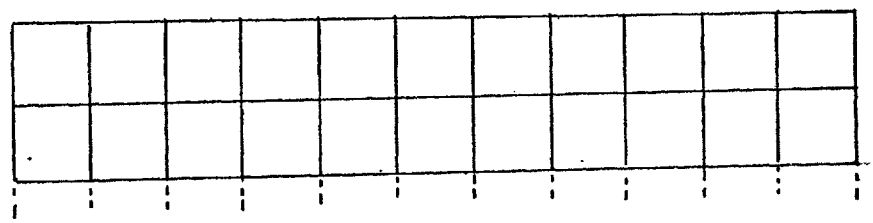

Atomically Smooth Interface

Fig. 5.2

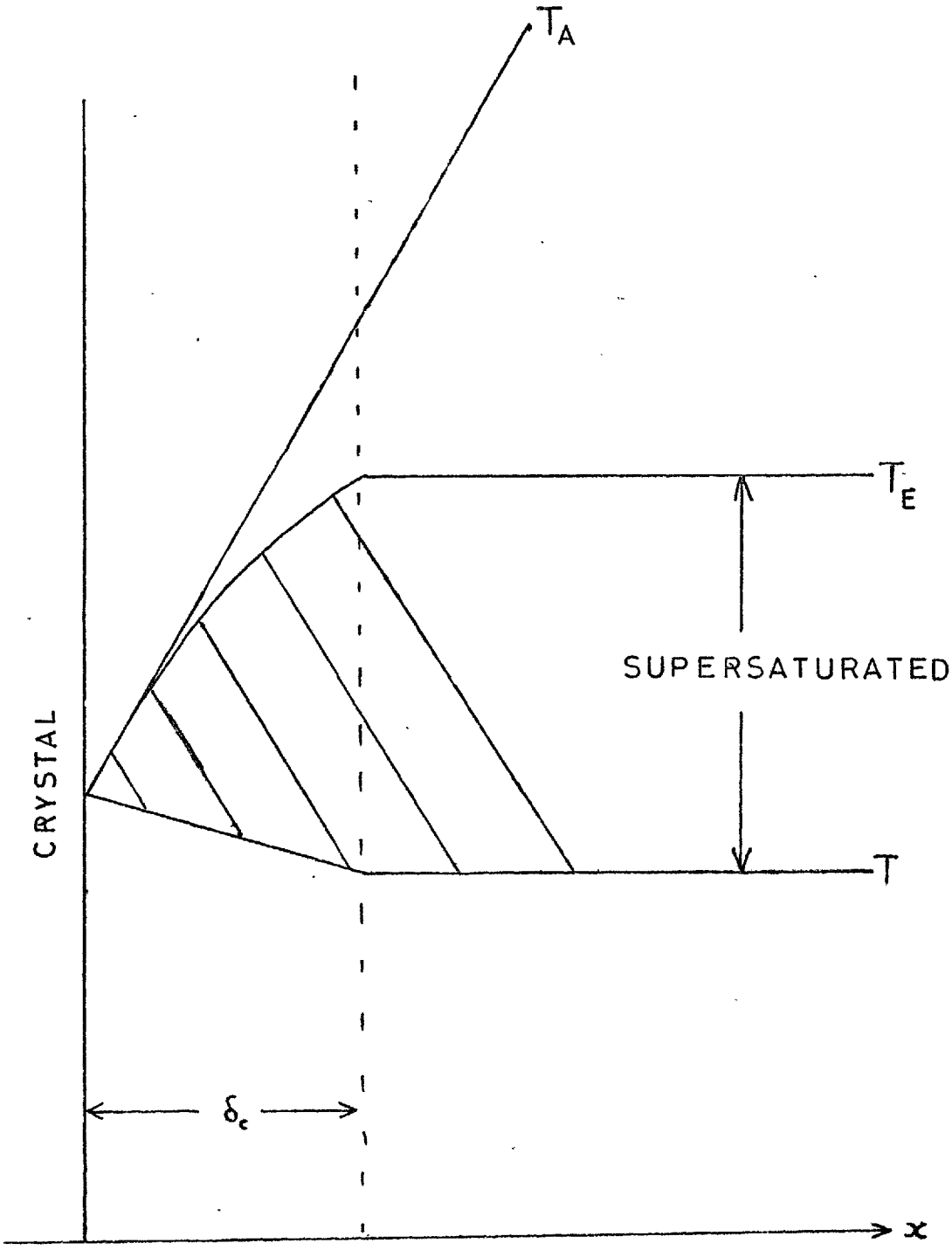

Fig. 5.3 Constitutional Supersaturation

in the growth of crystals from heavily doped melts (6). In solution growth, both at low temperature and for fluxed melts (7) the same phenomenon can also be encountered, in which case it is known as constitutional supersaturation. In all cases, the cause of the phenomenon is the same; namely the partial or complete rejection of one component at the crystal interface. Figure 5.3 depits the case for the epitaxial growth of garnets. At the interface the constituent garnet oxides are incorporated into the crystal whereas the flux is rejected and accumulates there. This causes a lowering in the garnet liquidus temperature, T_E, at the interface. Consequently the region immediately ahead of the interface is one of increasing supersaturation (as shown by the shaded region in figure 5.3). If a small perturbation developes on the interface it is protruding into a region of increasing supersaturation and must grow faster than the rest of the interface. Eventually the interface breaks down into a series of ridges between which large volumes of flux become trapped.

Although almost all growth of crystals from solution occurs under conditions of constitutional supersaturation, interface instability is seldom a problem for habit faces as long as growth rates are not excessively high. The reason for this can be explained in terms of the relative surface free energies. The habit faces of crystals are those with the lowest surface free energies and are therefore thermodynamically more stable

than any perturbations which may develop on them. As long as this stabilising effect is greater than the destabilising effect of constitutional supersaturation, the interface will remain planar.

Since it is probable that the garnet (111) face is atomically rough it will contain a relatively large fraction of free bonds directed outwards from the surface. Therefore the (111) face should have a high surface free energy in comparison with the habit faces and growth on such a face under conditions of constitutional supersaturation should lead to interface instabilities. The reason that interface breakdown is not observed on epilayers grown for bubble domain applications is that the amount of growth on the highly polished substrate surfaces is so small that perturbations on the surface do not have time to develop at the growth rates used. In addition, rotation of the substrate provides both thermal and solutal boundary layers of uniform thickness ahead of the interface. This means that the whole of the substrate receives solute at the same uniform rate and can dissipate heat at the same uniform rate. Both of these factors inhibit the formation of perturbations on the interface.

5.3 The Growth of Thicker Epilayers.

In order to investigate whether or not the (111) epilayer interface grows in a metastable state and would break up on prolonged growth, as predicted, it was decided to grow epilayers up to a thickness of

200 microns and observe their surfaces.

The onset of interface breakdown was observed by growing epilayers for different times using the same growth conditions. An undercooling of 8^{o} was used so that together with a substrate rotation of 100 rpm the resulting growth rates would be in the region of 1 micron $min.^{-1}$. During the growth period the furnace was cooled at a linear rate of 2^{o} $hr.^{-1}$ in order to balance the rate of removal of garnet from the melt and keep the growth rate constant. Epilayer thicknesses were measured by accurately weighing the substrate before and after growth since although iron garnets are far more transparent in the infra-red than in the visible spectrum, the infra-red interference technique for measuring thickness only works for specimens with flat surfaces.

The surfaces of the epilayers were observed by phase contrast microscopy. Figure 5.4 shows the surfaces of three epitaxial layers of approximate thicknesses 50, 100 and 150 microns. After 50 microns growth the interface is just beginning to show signs of a few ripples. At 150 microns growth the ripples have developed into a series of sharp parallel ridges, between which flux can be trapped and included in the crystal. In addition to the parallel ridges, another morphology was often encountered under the same growth conditions. This was a series of flat-sided, approximately triangular hillocks (figure 5.5). It was not uncommon to find both morphologies of interface breakdown on the same epilayer surface.

FIG 5.4 Interface Breakdown Sequence

FIG 5.5

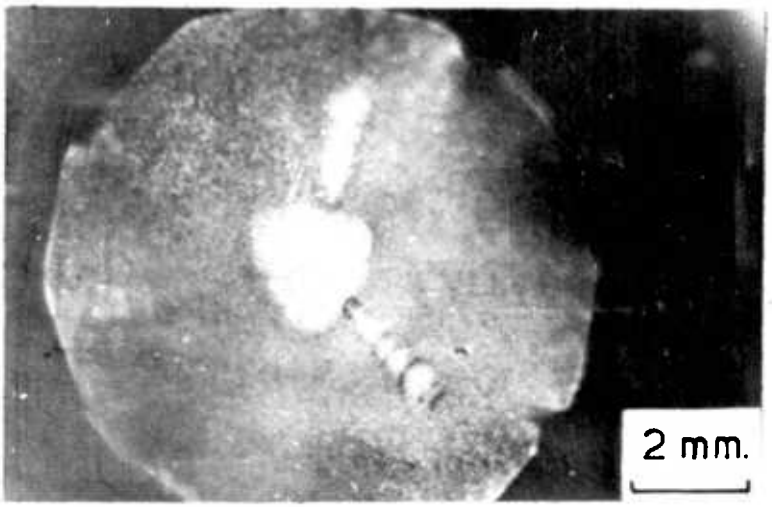

FIG 5.6

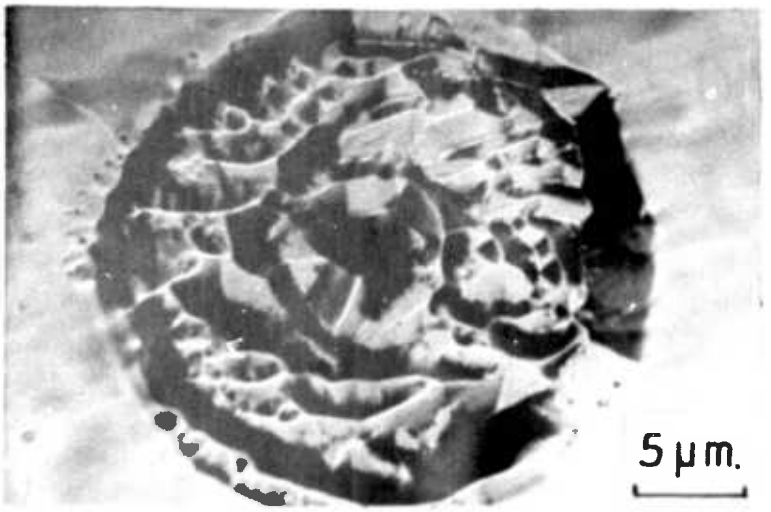

FIG 5.7

It is essential to distinguish between these triangular hillocks and the ones of a similar morphology known as film facetting. Blank and Nielsen (8) have shown that film facetting occurs when the lattice parameter of the epilayer exceeds that of the substrate by more than 0.018Å. It is probable that when growth occurs under the large compressive force created by such a lattice mismatch, dislocations nucleate as a result of localised slip and these serve as centres for rapid growth.

Since the lattice parameter of the epilayers grown was only 0.007Å larger than that of the substrate, it is unlikely that the specimen shown in figure 5.5 shows film facetting. In addition, film facetting occurs in thin epitaxial layers whereas interface breakdown is only evident after about 50 microns growth. Linares (9) has grown layers up to 100 microns thickness of yttrium iron garnet on various orientations of gadolinium gallium garnet. Even in this case, where the epilayer lattice parameter is 0.006Å less than that of the substrate, regular triangular hillocks were observed on the (111) orientations. Irregular hillocks were observed on the (100) substrates whereas the ($\bar{1}$10), a garnet habit face, always had mirror-smooth surfaces. It is likely that the flat sides of the hillocks on the (111) epilayers are of the form (211) or (110) both of which have three-fold symmetry with respect to the (111) direction and are the natural habit faces of garnet.

In order to prove that dislocations were not

nucleating during the growth of the epilayer and causing interface breakdown, a sample exhibiting the triangular hillocks was carefully polished with finer grades of diamond paste and finally with Syton until surface irregularities were removed. The polished epilayer surface was then given a two minute etch in phosphoric acid at 200°C. Only a few dislocations per square centimetre were detected and these can be attributed to dislocations present originally in the substrate.

Having proved that dislocations were not the cause of interface breakdown, it is worth mentioning that areas of strain in the substrate propogate into the epilayer during growth and have a localised positive influence on interface breakdown. It was noticeable that when substrates were not core-free the pattern of the core was often visible on the surface of the epilayer. This was because the interface broke down at slightly different rates in the cored regions than for the rest of the substrate area. Figure 5.6 shows a particularly acute example of the effect and was photographed by reflecting a light beam from the surface of the epilayer. The effect of isolated dislocations was also noticeable. A clean substrate was lightly etched in phosphoric acid (2 minutes at 200°C) and the positions of the dislocations mapped. The surface was then repolished flat with Syton and a 50 micron thick epilayer grown on to it. When most of the interface was just beginning to break down, a few circular regions corresponding to the sites of dislocations were seen to be in a more advanced state of breakdown (figure 5.7).

It has been shown by Hurle (6) that the magnitude of constitutional supersaturation (as represented by the magnitude of $\left[\frac{\partial T_E}{\partial x}\right]_{x=0} - \left[\frac{\partial T}{\partial x}\right]_{x=0}$ in figure 5.3) increases both with more efficient stirring and faster growth rates. Accordingly a number of thick epilayers were grown with either low or zero substrate rotation rates and small values of undercooling. It was found that even at growth rates as low as 0.1 micron $min.^{-1}$ interface instability was still encountered.

5.4 Back-cooling of the Substrate.

5.4.1 Theoretical Approach.

In order to completely eleminate constitutional supersaturation from the growth process it is necessary that a steep temperature gradient is applied ahead of the growing interface. The applied gradient at which this just occurs is given in figure 5.3 by

$$\left[\frac{\partial T_A}{\partial x}\right]_{x=0} \geqslant \left[\frac{\partial T_E}{\partial x}\right]_{x=0} \qquad 5.1$$

There are two ways in which the steep temperature gradient can be applied and these are represented in figures 3.3 (iii) and 3.3 (iv). In transient mode LPE the steep temperature gradient is created by dipping a cooled substrate into the melt. Clearly the amount of cooling of the melt that can be achieved by this technique is not sufficient for the growth of thick epilayers.

In addition, as growth proceeds, the substrate temperature approaches that of the melt thus reducing the magnitude of the temperature gradient ahead of the interface. However, back-cooling of the substrate is far more suitable since the heat can be extracted continuously at a uniform rate so that growth takes place isothermally. Nitrogen gas can be blown down the aluminia shaft onto the substrate backing disc to provide the cooling. The nitrogen flow rate determines the magnitude of the applied temperature gradient.

In order to calculate the magnitude of the applied temperature gradient needed to eliminate constitutional supersaturation it is necessary to know the value of $\frac{\partial T_E}{\partial x}$ at the interface. This can be calculated according to the growth model shown in figure 4.5. For the LPE growth of garnets the simplifying approximation can be made that the concentration of garnet varies linearly across the thickness of the solutal boundary layer. Although this assumption is not strictly valid for the growth of doped crystals by directional freezing (6,10) it is far better approximation for the LPE system since growth rates are two orders of magnitude lower. In addition, there is a significant rate limitation at the garnet interface due to the surface integration process. This will also tend to limit the curvature of the concentration profile and support the assumption.

Immediately the rotating substrate dips into the

supersaturated melt there is a short transient period during which growth is rapid while the solutal boundary layer builds up to its equilibrium thickness. Brice (11) has commented that the duration, t, of the transient is approximately given by

$$t = \frac{\delta_c^2}{D} \qquad 5.2$$

Therefore for a substrate rotation rate of 100 rpm, steady state growth conditions are achieved in about three seconds. Once steady state growth conditions are reached the rate at which the crystal removes garnet from the melt is equal to the rate of arrival of garnet at the interface:

$$f = \frac{\rho^{-1} D (C_b - C_i)}{\delta_c} \qquad 5.3$$

In addition the growth rate must also be equal to the rate of surface integration of the garnet:

$$f = A (C_i - C_e) \qquad 5.4$$

$$\text{so that } C_i = \frac{f}{A} + C_e \qquad 5.5$$

The concentration gradient at the interface, $\left[\frac{\partial c}{\partial x}\right] x = 0$, is given by $\frac{C_b - C_i}{c}$ so that substituting for C_i from equation 5.5 gives

$$\left[\frac{\partial c}{\partial x}\right]_{x = 0} \quad \frac{C_b - C_e - \frac{f}{A}}{\delta_c} \qquad 5.6$$

For a substrate rotation rate of 100 rpm the value of δ_c is 59 microns (equation 4.1). The magnitude of $(C_b - C_e)$ is determined by the undercooling and the slope of the garnet solubility curve. An undercooling of 8^oC produces a growth rate of one micron a minute (figure 4.3). Consequently evaluation of equation 5.6 gives

$$\left[\frac{\partial c}{\partial x}\right]_{x = 0} = 0.48 \text{ g. cm}^{-4}$$

The value of $\left[\frac{\partial T_E}{\partial x}\right]_{x = 0}$ is then given by

$$\left[\frac{\partial T_E}{\partial x}\right]_{x = 0} = \left[\frac{\partial c}{\partial x}\right]_{x = 0} \times \left[\frac{dT_E}{dc}\right] \qquad 5.7$$

This equation does not take into account the heat of crystallisation liberated at the interface and its dissipation by conduction through both the crystal and the melt. Although this is a significant correction in growth by directional freezing (6, 10) it is insignificant in fluxed melt growth since the growth rates are much lower.

The value of $\left[\frac{\partial T_E}{\partial x}\right]_{x = 0}$ can now be calculated from equation 5.7 since the term $\left[\frac{dT_E}{dc}\right]$ is simply the reciprocal of the slope of the garnet solubility curve. Therefore for the growth temperature of 884^oC, a substrate rotation rate of 100 rpm and consequently a growth rate of 1 micron min^{-1}, the value of $\left[\frac{\partial T_E}{\partial x}\right]_{x = 0}$ is approximately 410^o cm^{-1}. In order to eliminate

constitutional supersaturation for the given growth conditions, the applied temperature gradient must be equal to or greater than this value (equation 5.1).

In order to compare experimental results with this theory it is essential to have a reliable method of measuring the applied temperature gradient ahead of the interface. Direct measurement by a series of thermocouples would be extremely difficult since the substrate is rotating at 100 rpm and the melt is corrosive to platinum-rhodium alloys. In addition, the region over which the applied temperature gradient extends is comparable with the thickness of the thermal boundary layer so that extremely small thermocouples would be required. However, if the bulk of the melt is at a constant temperature, T_B, and the crystal interface is at a lower temperature, T_i, then the temperature difference must occur across the thickness of the thermal boundary layer, δ_T, to that

$$\left[\frac{\partial T_A}{\partial x}\right]_{x=0} = \frac{T_B - T_i}{\delta_T} \qquad 5.8$$

The value of T_B can be measured directly with a platinum sheathed thermocouple. T_i can be deduced from the growth rate of the epilayer and a knowledge of its dependance on undercooling (figure 4.3). The thickness of the thermal boundary layer depends on both the value of the dimensionless Prandtl number and the physical properties of the melt. The dimensionless Prandtl number, Pr, is defined by

$$Pr = \frac{\nu}{\alpha} \qquad 5.9$$

where ν is the kinematic viscosity and α is the thermal diffusivity. The thermal diffusivity is defined in terms of the thermal conductively, K, and specific heat, Cp, by

$$\alpha = \frac{K}{\rho C_p} \qquad 5.10$$

Therefore at the growth temperature the thermal diffusivity of the melt is 3.8×10^{-3} cm.^{2}sec^{-1} and consequently the Prandtl number is 3.2. However the relative uncertainty in both the values is large since the value of thermal conductivity used in their calculation has been estimated rather than measured (see section 2.7).

Sparrow and Gregg (12) have shown that the thickness of the thermal boundary layer can be accurately expressed in terms of the Prandtl number for two limiting cases :

$$Pr > 100 \qquad \delta_T = 1.6\, Pr^{-\frac{1}{3}} \nu^{\frac{1}{2}} \omega^{-\frac{1}{2}} \qquad 5.11$$

$$Pr < 0.01 \qquad \delta_T = 1.13\, Pr^{-1} \nu^{\frac{1}{2}} \omega^{-\frac{1}{2}} \qquad 5.12$$

For a fluid with a Prandtl number of 3.2, although neither of the limiting equations are strictly correct, the best approximation to the actual thickness of the thermal boundary layer can be obtained from equation 5.11 (13). However, it must be emphasised that the value calculated from equation 5.11 will be slightly less than the actual value. For a substrate rotation rate of 100 rpm and a growth temperature of 884°C, equation 5.11 predicts that the thickness of the thermal boundary layer is 370 microns. Therefore constitutional supersaturation is just eliminated

when the magnitude of $(T_B - T_i)$ is 15.2°C (equation 5.8)

5.4.2 Experimental results.

The furnace used is described in section 3.1. A slight modification was made to the way in which the substrate holder was positioned so as to allow rotation of the substrate whilst leaving the top of the holder shaft open for the passage of the cooling gas. This modification is shown in figure 5.8. Substrate rotation was achieved by a pair of interlocking toothed wheels and a motor with a flexible drive. Nitrogen gas was blown down the substrate holder shaft through a 4 mm. bore stainless steel tube. Flow rates of up to 12 litres $min.^{-1}$ were used and were measured with a Rotameter flow gauge. To obtain even growth over the whole surface of the substrate it was necessary to polish the platinum backing disc to a high degree of flatness to ensure good thermal contact with the whole of the substrate.

The growth procedure consisted of cleaning and mounting the substrate as described in section 3.2 and then manually lowering it to just above the surface of the melt. Once the substrate had reached the furnace temperature, it was lowered into the melt and the flow of nitrogen commenced. It was found that if the flow of nitrogen was commenced before the substrate was immersed in the melt, then extreme cooling of the substrate and holder resulted. This frequently caused spontaneous nucleation of garnet at the beginning of the growth process

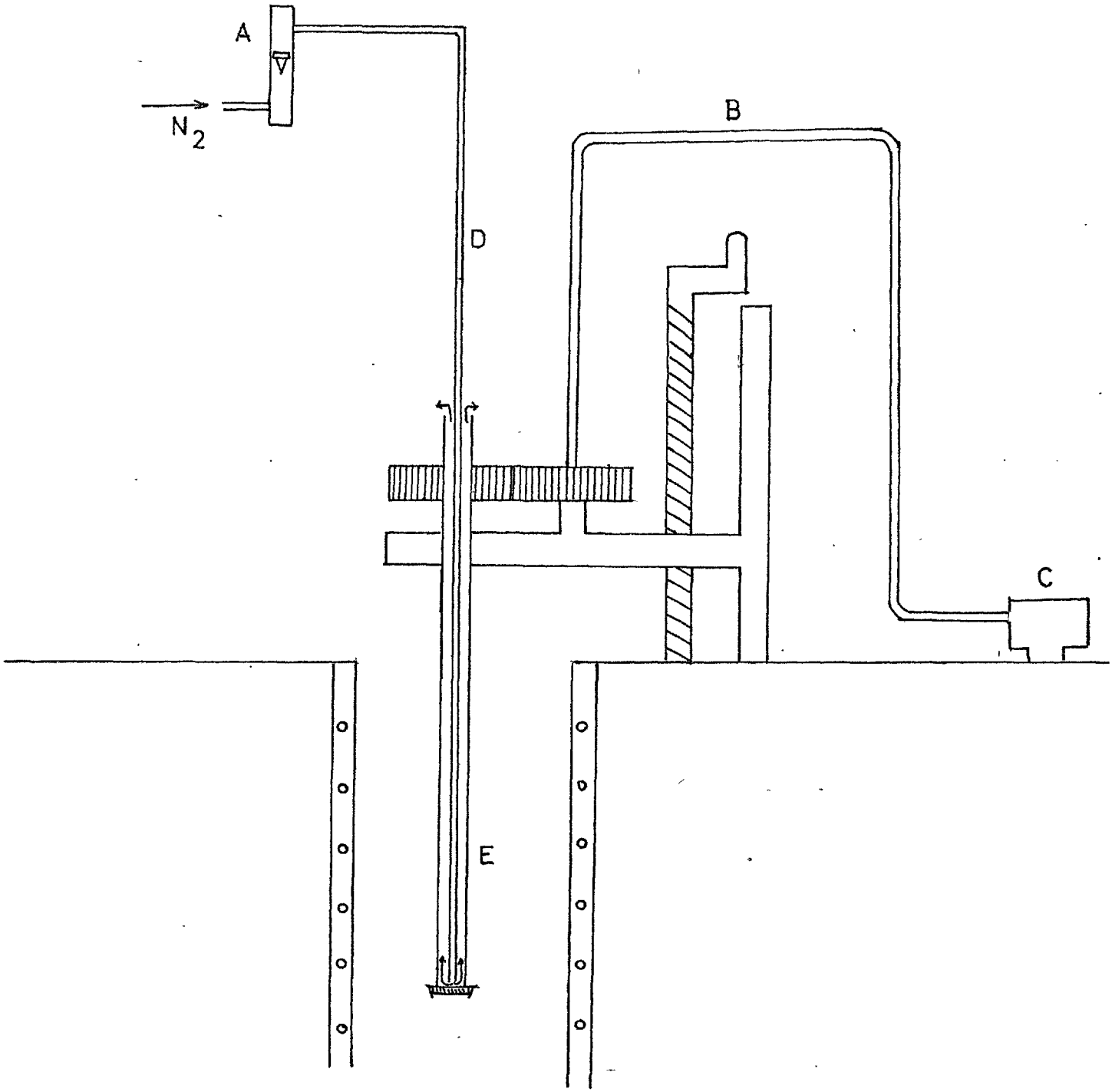

A Rotameter Flow Gauge
B Flexible Drive
C Variable Speed Motor
D Stainless Steel Tube
E Substrate Holder

Fig. 5.8 Back-cooling Apparatus

which not only lowered the growth rates by an irreproducible amount but also caused many garnet crystallites to be contained in the epilayer.

During growth the substrate was rotated at 100 rpm and the furnace cooled linearly at 2^{o} $hr.^{-1}$ to maintain a constant growth rate. The nitrogen flow rate and temperature in the bulk of the melt were set so as to produce both the desired growth rate and cooling at the interface. At the end of the preselected growth period the nitrogen flow was stopped and the epilayer withdrawn from the melt. It was found that if the epilayer was withdrawn from the melt before the gas flow was stopped, the thermal shock was always enough to cause cracking at the already-stressed substrate/epilayer interface.

It was found that a nitrogen flow rate of 5 litres $min.^{-1}$ caused the interface to be $16^{o}C$ cooler than the bulk of the melt. According to equation 5.8 this is just enough to eliminate constitutional supersaturation when the growth rate is 1 micron $min.^{-1}$. In order to achieve this growth rate an undercooling of $8^{o}C$ coupled with the given substrate rotation rate of 100 rpm is necessary. Therefore the temperature in the bulk of the melt must by $8^{o}C$ above the garnet liquidus temperature of $992^{o}C$.

Under these conditions, epilayers of thickness up to 200 microns were grown. Examination of their surfaces showed that interface breakdown had still occurred.

However there was some evidence that the thickness of epilayer that could be grown before surface breakdown occurred was slightly greater than when no back-cooling was applied.

When higher gas flow rates were used, cracking at the substrate/epilayer interface frequently resulted. Therefore in order to obtain any correlation between experimental results and theoretical predictions, lower growth rates had to be used. The reason for this is since the concentration gradient ahead of the interface is proportional to the growth rate (equation 5.3), the same must also be true for the value of $\left[\frac{\partial T_E}{\partial x}\right]$ at $x = 0$ (equation 5.7). These lower growth rates were obtained, without altering the substrate rotation rate or the nitrogen flow rate, by raising the temperature in the bulk of the melt to between 1000°C and 1008°C.

In order to test the theory a number of epilayers were grown at growth rates between 0.2 and 1.0 microns $min.^{-1}$. In general it was found that epilayers could be grown up to thicknesses of 150 microns without surface breakdown when the applied temperature gradient was between two and three times greater than that predicted by the simple theory. This agreement between experiment and theory was considered reasonable, especially since the value for the thermal diffusivity of the melt was only estimated.

CHAPTER 5 : REFERENCES

1) R.A.Lefever, A.B.Chase and K.A.Wickersheim,
J. Appl. Phys. 33, (1962), 2249

2) R.A.Lefever and A.B.Chase,
J.Amer. Ceram. Soc. 45, (1962), 32

3) B.Cockayne, Conference on Magnetic Bubbles, LONDON, 1973

4) J.A.Pistorius, Conference on Magnetic Bubbles,LONDON,1973

5) D.Mateika, Conference on Magnetic Bubbles, LONDON, 1973

6) D.J.T.Hurle, Solid State Elec. 3, (1961), 37

7) E.A.D.White and J.W.Brightwell,
Chem. and Ind., (Sept.25th 1965), 1662

8) S.L.Blank and J.W.Nielsen, J.Cryst.Growth 17, (1972), 302

9) R.C.Linares, J.Cryst.Growth 3/4, (1968), 443

10) J.A.Burton, R.C.Prim and W.P.Slichter,
J.Chem. Phys. 21(11), (1953), 1987

11) J.C.Brice, The Growth of Crystals from Liquids, Page 155,
(North Holland, 1973)

12) E.M.Sparrow and J.L.Gregg,
J. Heat Transfer (August, 1959), 249

13) J.C.Brice, The Growth of Crystals from Liquids, Page 132,
(North Holland, 1973)

CHAPTER 6.

6. Alternative Solvent Systems for the Epitaxial Growth of Garnets.

6.1. The Need for Alternative Solvent Systems.

Although the lead oxide/boric oxide flux is widely used for the epitaxial growth of highly perfect magnetic garnet crystals, the flux does have a number of serious disadvantages. It has been specified by White (1) that an ideal solvent for crystal growth should have the following properties, which are not necessarily in order of importance:

a) dissolve reversibly a high propertion of solute;
b) have a large temperature coefficient of solubility;
c) have a low vapour pressure at the growth temperature;
d) be available in quantity in a high purity form;
e) be containable in available crucible materials;
f) be readily soluble in aqueous media;
g) be non-toxic;
h) have a low viscosity.

In fact, the lead oxide/boric oxide flux only meets requirements (d), (e), (f) and (h). It dissolves at 950°C about 2% by weight of garnet and will only crystallise garnet as the premary phase when a large excess of iron oxide is present. The temperature coeffieient of solubility is low. The flux has an appreciable vapour pressure which gives rise to problems

of toxicity and corrosion of the furnace windings and thermocouples. In addition, small traces of reducing agents may liberate metallic lead which quickly forms a low melting point alloy with the platinum crucible.

As well as these general disadvantages of the flux there are also those specific to the growth of garnet epilayers. Because of the volatility of lead oxide, corrosive droplets can condense on the substrate prior to growth and etch its highly polished surface. Lead can be incorporated into the garnet lattice on rare earth (dodecahedral) sites. The amount depends on the growth conditions but may be as much as 2% by weight, causing a substancial increase in the lattice parameter of the epilayer. In addition, since the lead ion is only divalent, charge compensation must occur in the form of oxygen vacancies or tetravalent iron (2). Although lead can be annealed out of the garnet lattice in the form of lead dioxide at high temperatures, this results in the production of rare earth vacancies and divalent iron, which has the damaging effects of lowering domain wall velocity and increasing coercivity (3). A further disadvantage of lead-based fluxes is that the gallium segregation coefficient is substantially greater than unity and varies considerably with both temperature and growth rate.

In view of the numerous disadvantages of the lead oxide/boric oxide flux, it was decided to see if other of the commonly used fluxes would be more suitable

for garnet epitaxy, whilst still retaining the most desirable property of lead oxide/boric oxide fluxes, their ability to support large undercoolings. This ability is essential for the growth of multicomponent garnets with uniform composition since it allows growth to proceed isothermally and at a constant rate.

6.2 Barium-based Fluxes.

As long ago as 1962, Linares (4) demonstrated the use of fluxes based on boric oxide combined with one of the oxides of the alkaline or alkaline earth metals for the growth of a wide variety of oxide crystals. Of these fluxes, barium oxide/boric oxide was found to be the most suitable for the growth of yttrium iron garnet.

The barium oxide/boric oxide flux has a number of advantages over the more conventional lead oxide fluxes. The garnet solubility and temperature coefficient of solubility are both substantially higher. Flux loss by evaporation and attack on the platinum crucibles are both negligible. The large ionic radius (1.35Å) of divalent barium should prevent it from entering the garnet lattice. Linares found that when the barium oxide : boric oxide mole percentages were between 67:33 and 58:42, yttrium iron garnet could be crystallised when the yttrium : iron ratio in the flux was the stoichiometric 3:5 (i.e. yttrium iron garnet is congruently saturating over this range of flux compositions). At higher concentrations of boric oxide, barium hexaferrite is the primary phase.

According to the phase diagram of Levin and McMurdie (5) the melting points of the fluxes vary linearly from 950°C for the 58:42 composition to 1100°C for the 67:33 composition. In deciding on a suitable flux composition for the epitaxial growth of garnets a compromise must be made between two factors. At high concentrations of boric oxide the fluxes have high viscosities and so cannot be spun off the epilayer immediately after growth. Regions of the epilayer from which the flux is not removed will show both thickness irregularities and a high concentration of magnetic defects. However, at low boric oxide concentrations, the fluxes have high melting points. This is also undesirable since high growth temperatures cause a substancial reduction in the growth-induced magnetic anisotropy of the garnet, which may adversely effect the stability of bubble domains. This is especially important for the case of submicron bubbles which can only exist when the uniaxial anisotropy is high.

Accordingly a flux composition with a 60:40 mole ratio of barium oxide to boric oxide was chosen. This composition of flux has a melting point in the region of 980°C. In order to determine the optimum ratios of solute oxides for the growth of garnet, a number of small melts were made up with different ratios of (iron oxide + gallium oxide) : rare earth oxide. The rare earth, iron and gallium oxides used were all of 99.9% purity or better. Boric oxide was BDH Optran grade. Since barium oxide is extremely hygroscopic and

cannot be easily dehydrated, Analar barium carbonate was used as the starting material. All constituents were dried overnight at 250°C before weighing and then mixed by vigorously shaking in a glass jar. On slow heating, the barium carbonate decomposed to the oxide. After the decomposition was completed the melts were homogenised at 1200°C for 16 hours in a large furnace heated by Silicon carbide elements and then cooled to room temperature. The flux was leached out from each melt with dilute hydrochloric acid and the crystalline products identified using an optical microscope. X-ray diffraction on powdered samples was also used for identification in a few cases.

It was found that the best solute composition for giving garnet crystals was on (iron oxide + gallium oxide): rare earth oxide ratio of 5.5:3. Although garnet was the primary phase when the stoichiometric 5:3 ratio was used, traces of orthoferrite were also present. At much higher ratios than 5.5:3, barium hexaferrite ($BaO.6Fe_2O_3$) in the form of red hexagonal plates was the premary phase.

Having established the position of the garnet stability field there remained the problem that the segregation coefficients of the individual oxides were unknown. Since the garnet stability region in these melts is vastly different to in lead-based melts, it is likely that the solvation mechanisms are different and so no parallels between segregation coefficients can be

drawn. Therefore in order to obtain an epilayer, a melt was made up according to the composition given in figure 6.1.

Figure 6.1

Constituent	Weight (g.)
Eu_2O_3	8.90
Y_2O_3	26.86
Fe_2O_3	28.06
Ga_2O_3	10.45
BaO	149.50
B_2O_3	34.20

This melt contains 27% by weight of the constituent garnet oxides in ratios corresponding to a garnet of formula $Eu_{0.5}Y_{2.5}Fe_{3.9}Ga_{1.1}O_{12}$. These ratios were chosen so that if the segregation coefficients of all the solute oxides were close to unity, the epilayer would have the desired saturation magnetisation and a lattice parameter exactly matching that of the GGG substrate (12.382Å). As long as the segregation coefficients were not markedly different from unity, epitaxial growth would still have been possible. Measurement of the saturation magnetisation of the epilayer would then have given the values for the segregation coefficients of iron oxide and gallium oxide.

Using the technique described in section 2.1, the garnet liquidus temperature was determined at 1048°C and this value increased by 6.5° for each gram of garnet added. Lawrence et al. (6) have measured both the density and viscosity of a flux consisting of barium oxide:boric oxide in a 59:41 mole ratio at 1050°C. Their values for the density was 4.1 $g.cm^{-3}$. Therefore the slope of the garnet solubility curve is 2.4×10^{-3} $g.cm^{-3}$ $degree^{-1}$, a factor of 2.1 higher than for the lead oxide/boric oxide flux. To test if the melt would support larger undercoolings without spontaneous nucleation of garnet, a platinum wire was dipped into the melt at various temperatures. It was found that the melt could support undercoolings of up to 20° for several hours without garnet crystallites forming on the wire.

The technique and furnace used for the growth of epilayers was the same as described in chapter 3, except that due to the high failure rate of Kanthal furnace winding at the homogenisation temperature of 1160°C, these were replaced by platinum - 30% rhodium. In addition, the substrate was spun at 2000 rpm on withdrawal from the melt to remove most of the viscous melt that had adhered to the epilayer surface.

It was found that uncracked epilayers could be grown onto (111) GGG substrates using the melt composition given in figure 6.1. Growth rates obtained were 12% lower than for the lead oxide/boric oxide flux using the same undercoolings and substrate rotation rates. For

reasons which will be discussed later in this chapter, only a few epilayers were grown from this melt and so an accurate kinetic assessment could not be made. However, using the viscosity value obtained by Lawrence et al.(6) (1.5 poise at 1050°C) and assuming the surface integration constant was the same as for the lead oxide/boric oxide flux, a rough estimate of the garnet diffusion coefficient was made using equation 4.10. The value obtained was 4×10^{-6} cm.^{2}sec.$^{-1}$. This value is almost an order of magnitude lower than for the lead oxide/boric oxide flux but is reasonable since the viscosity of the barium-based melt is an order of magnitude higher.

The saturation magnetisation of epilayers grown from this melt was found to be in the region of 150 gauss and showed no dependance in growth rate (cf.figure 4.1.). Since saturation magnetisation is very sensitive to the iron : gallium ratio and a garnet of composition $Eu_{0.5}Y_{2.5}Fe_{3.9}Ga_{1.1}O_{12}$ has a saturation magnetisation in the region of 150 gauss, it was concluded that the segregation coefficients of both iron oxide and gallium oxide were close to unity. This is a distinct advantage over lead-based solvents for epitaxial growth and may, in addition, prove extremely useful for the growth of bulk crystals of gallium substituted iron garnet with uniform magnetisation throughout.

The barium content of an epialyer grown at the rate of 2.1 microns min.$^{-1}$ was analysed using a JXA - 3A electron microprobe. Since garnet is a poor

electrical conductor it was coated with a thin (100Å) layer of graphite to prevent the surface from accumulating charge which would deflect the electron beam. Electrons were accelerated through a potential of 25 KV. and the beam focussed onto a one micron square area of the epilayer surface. The intensity of the barium K_{α} doublet was measured using barium sulphate as a standard. No allowance was made for the substrate since the penetration of the electrons was only about two microns, one-fifth of the epilayer thickness. Large areas of the epilayer surface were viewed on a fluorescent screen using reflected electrons in a manner analogous to scanning electron microscopy. The electron beam could then be focussed onto chosen areas of the epilayer surface and appeared as a bright spot on the screen. It was found that over most of the epilayer surface the barium content was below the level of detection (0.3% by weight). However, at pitted regions in the surface, of the type shown in figure 6.2, up to 1% by weight of barium was detected.

The electron microprobe analysis was supplemented by X-ray fluorescence spectroscopy using a Jeol JSX 60S4 X-ray spectrometer. X-rays were produced by 50 KV. electrons striking a chromium target. The width of the beam produced was comparable with area of the epilayer. Since this technique has a far greater penetration into the sample than does electron microprobe analysis, it was necessary to apply a correction for the presence

of the substrate. This was done with the aid of blank substrate. Using barium sulphate as a standard, it was found the average barium content was (0.02 $\pm$ 0.005)% by weight over the whole of the epilayer. This level of flux contamination is far lower than for epilayers grown from lead-based melts and is small enough to have negligible effect on the lattice parameter match with the substrate.

However, there was one severe disadvantage of the barium-based melts. Because of their high viscosity, melt droplets could not be completely drained from the epilayer surface immediately after growth. On slow withdrawal from the furnace, growth continued under these regions of viscous melt until they finally vitrified. Rapid withdrawl of the epilayer to a cooler part of the furnace minimised the thickness discontinuities but frequently caused the epilayer to crack and part from the substrate. In addition to the extra growth, the present of the viscous melt caused many defects in the epilayer surface. The defects were examined by scanning electron microscopy (Cambridge Stereoscan Mark II microscope) and a selection of the micrographs is shown in figure 6.2. As can be seen, many of the defects are comparable in size with the bubble diameter.

In order to utilise the potential of barium-based melts for the production of device quality garnet films, it was clear that all traces of the melt would have to be removed from the epilayer surface immediately

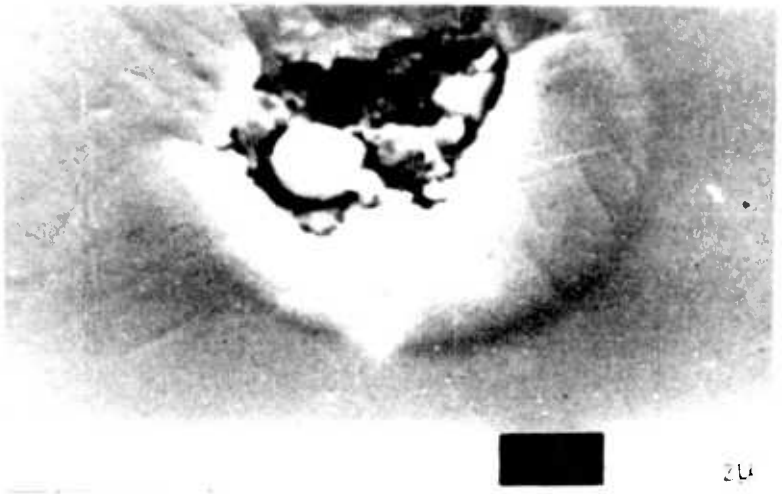

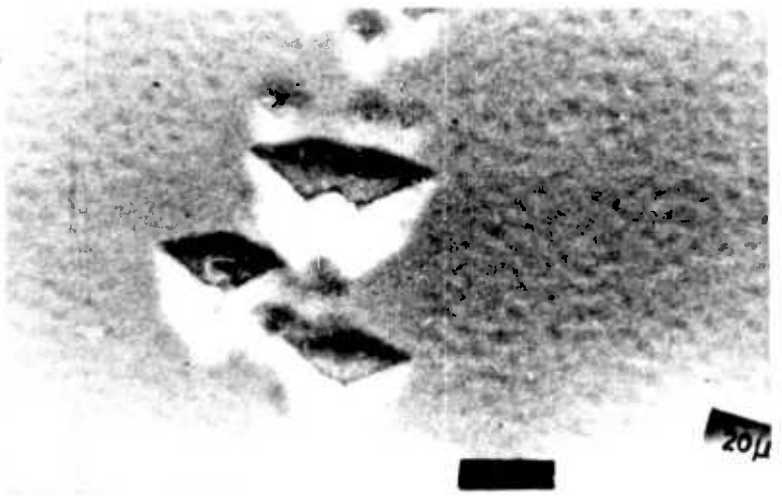

FIG 6.2 Micrographs of surface defects

after growth. Lawrence et al. (6) reported that the a addition of barium fluoride lowers the viscosity of barium borate fluxes and so 50 g. of BDH "extra pure" barium fluoride was added to the melt. The garnet liquidus temperature was remeasured and surprisingly showed no change from the original value of 1048°C. To check that the addition of barium fluoride was not causing two phases to separate, the melt was cooled to room temperature. Examination showed only one glass phase. Therefore it was concluded that barium fluoride plays little part in the garnet solvation mechanism.

Epitaxial growth from this melt was still troubled by the adhesion of droplets to the garnet surface. In fact, the combination of the lower melt viscosity and slightly extended liquid range caused the thickness discontinuities to be even greater than previously encountered. Consequently it was decided to carry out a full viscosity study on the solute/solvent system to see if a melt composition could be found that would have a suitable viscosity at growth temperatures of less than 1050°C.

The experimental set up used is shown in figure 2.9. Because of the viscosity values involved, the rotating-crucible technique, as reported in section 2.3, was found to be more suitable than the oscillating-bob technique. Calibration of the apparatus was made at room-temperature using concentrated sulphuric acid and water/glycerol mixtures. Viscosity values were obtained

for the binary flux and with various additions of barium fluoride and garnet. The data obtained is shown in figure 6.3 which has viscosity plotted on a logarithmic scale against the reciprocal of the absolute temperature (the index to the various symbols is given on the preceeding page). The absolute accuracy of the values was estimated at $\pm$ 10%. The activation energy for viscous flow was in the region of 20 Kcals.mole^{-1} for all compositions investigated.

The results show some interesting trends which as well as giving the most suitable flux composition for garnet epitaxy also provide indirect evidence of the nature of the bonding between the flux and solute. The barium oxide : boric oxide flux in a 60 : 40 mole ratio has a viscosity of 60 cp. at 1050^{o}C. The addition of 15% by weight of garnet dramatically increases this value to 190 cp. Although the addition of barium fluoride does lower the viscosity, the effect is not substantial. The lowest value found was for barium oxide : barium fluoride : boric oxide in a 30 : 50 : 20 mole ratio containing 15% by weight of garnet, which has a viscosity of 50 cp at 1050^{o}C. Compositions with higher barium fluoride or lower boric oxide contents are unsuitable because of their high melting points. It is interesting to note that hardly any benefit is gained by working at higher temperatures since as the temperature increases, so does the garnet solubility and this acts to raise the viscosity of the system.

The trends in the viscosity date can be explained.

INDEX TO VISCOSITY MEASUREMENTS

o	BaO (60)	B_2O_3 (40)				
□	BaO (60)	B_2O_3 (40)	+	15 weight % YIG		
✳	BaO (60)	B_2O_3 (40)	+	25 weight % YIG		
x	BaO (51)	B_2O_3 (34)	BaF_2 (15)	+	15 weight % YIG	
△	BaO (30)	B_2O_3 (20)	BaF_2 (50)	+	15 weight % YIG	

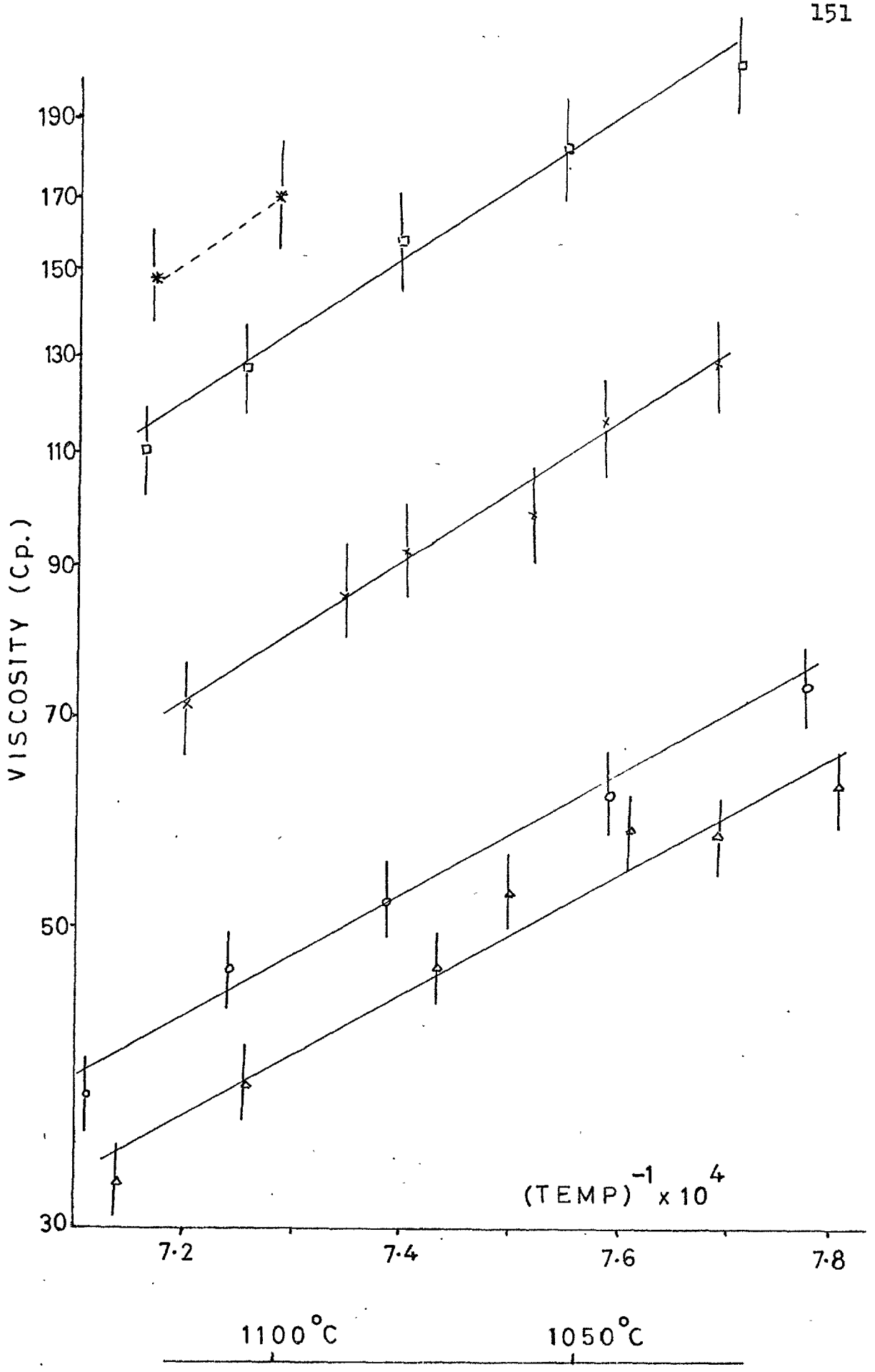

Fig. 6.3 Viscosity of Various Compositions vs. the Reciprocal of the Absolute Temperature

by the following model. Molten boric oxide exists not in the form of discrete molecules but as large complex networks of boron-oxygen bonds. Consequently it has an extremely high viscosity. Barium oxide can complex with the boric oxide to reduce the average network size and in doing so lowers the melt viscosity. When iron oxide is added it is solvated not by the boric oxide but by the barium oxide. The fact that barium hexaferrite ($BaO.6Fe_2O_3$) is easily crystallised from these melts is good evidence for this. Therefore both the iron oxide and boric oxide compete for the limited amount of barium oxide:

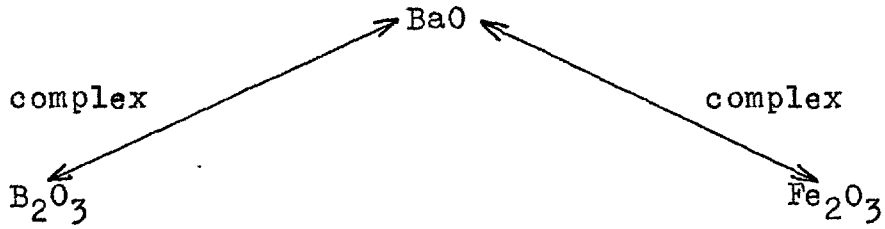

The more iron oxide that is added, the more boric oxide is liberated to reform networks thus causing an increase in viscosity. This model also explains why, for a given rare earth odixe : iron oxide ratio in the melt, increasing the boric oxide concentration causes the primary phase to contain a higher concentration of iron oxide (i.e. orthoferrite, garnet, barium hexaferrite and finally iron oxide itself). Barium fluoride plays no part in the solvation mechanism but is effective in reducing the average size of the boric oxide networks.

In view of the viscosity data it was felt that

the flux consisting of barium oxide : barium fluoride : boric oxide in a mole ratio of 30 : 50 : 20 was the most promising for the epitaxial growth of garnets. When a melt was made using this flux and containing a (iron oxide + gallium oxide) : rare earth oxide of 5 : 3, barium hexaferrite was the primary phase. In order to crystallise garnet it was necessary to use a slight excess of the rare earth components, an (iron oxide + gallium oxide) : rare earth oxide ratio of 4.3 : 3 proving the most suitable.

It was found that even from this system, the adhesion of melt to the epilayer surface was still a serious problem. Therefore it was concluded that although the growth of garnet crystals from barium-based fluxes does have a number of advantages over the more conventional lead-based fluxes, their high viscosity at the low growth temperature required for bubble domain garnet materials makes them unattrative. However for top-seeded solution growth or epitaxial growth at higher temperatures, barium-based fluxes have a high potential.

6.3 Bismuth-based fluxes.

It has been reported by Robertson (7) that when bismuth partially substitutes on dodecahedral sites in rare earth iron garnets their magneto-optic effect is greatly enhanced. When the magnetic domains of such materials are viewed between nearly-crossed polarisers, the contrast between domains of opposite spin polarity

is high. As well as the attractive possibility of optical display, optical methods for the detection of magnetic bubble domains can be envisaged. At present this detection is based on magnetoresistance and involves greatly expanding the size of a bubble beneath a series of permalloy chevrons. This is not only time-consuming but also involves large areas of the epilayer surface, thereby reducing the density of data stored.

Robertson found that neither lead-based nor barium-based fluxes were entirely suitable for the growth of bismuth-substituted garnets, the former because the incorporated lead in the garnet lattice is detrimental to the optical properties and the latter because of their high viscosities. In addition, bismuth oxide is readily reduced to the metal, forming a low melting point alloy with platinum and destroying the crucible.

Garton el al. (8) have reported that a bismuth oxide/vanadium pentoxide flux is suitable for the growth of a variety of oxide crystals. The flux is non-volatile, soluble in dilute acids and has the further advantage that any traces of organic matter will reduce the vanadium pentoxide to a lower oxide rather than liberate free bismuth metal. Therefore it was decided to see if this flux would be useful for the growth of bismuth-substituted garnets.

To do this, a number of melts of various compositions were made up using analar bismuth oxide, analar vanadium pentoxide and 99.9% pure yttrium oxide and iron oxide as starting materials. These melts were

homogenised at 1200°C for 16 hours and then cooled to room temperature overnight. It was found that when vanadium pentoxide formed greater than 25 mole % of the flux, yellow plates and rods of yttrium vanadate were always the primary phase. For a flux consisting of a bismuth oxide : vanadium pentoxide in a 4 : 1 mole ratio, garnet was the primary phase when the iron oxide : yttrium oxide mole ratio was 3 : 1. Ratios of greater than 5 : 1 gave iron oxide whereas ratios in the region of 2 : 1 gave orthoferrite.

Before attempting epitaxial growth from these melts, their viscosity was measured by the rotating crucible method. For a bismuth oxide : vanadium pentoxide flux in a 4 : 1 mole ratio containing 10% by weight of solute oxides, the viscosity was 4 poise at 1100°C and as high as 7 poise at 950°C. Therefore it was concluded that this system would not be suitable for the epitaxial growth of garnets for bubble domain applications.

6.4 Molybdate Fluxes.

Because of the rejection of both barium-based and bismuth-based fluxes on account of their high viscosities, it was decided to concentrate on low viscosity molybdate fluxes. Although these have an appreciable volatility at 1000°C, certain entectic compositions would permit growth at less than 600°C. Such low growth temperatures are advantageous for both process control and producing garnet with high growth-induced anisotropies.

The system potassium oxide : molybdenum trioxide was chosen because the large ionic radius of the potassium ion (1.39Å) should prevent it from entering the garnet lattice.

Melts were made up using analar potassium carbonate, analar molybdenum trioxide and 99.9% purity iron and yttrium oxides. On heating, the potassium carbonate decomposed to the oxide with the evolution of carbon dioxide. Melts were then homogenised at 1000°C for 16 hours, cooled to room temperature overnight and the crystalline products identified. The potassium oxide : molybdenum trioxide mole ratio was varied between 1 : 1 and 1 : 5 and the iron oxide : yttrium oxide mole ratio varied from 1 : 1 to as high as 30 : 1. However, it was found that invariably orthoferrite was the primary phase. Even the addition of small amounts (less than 10% by weight) of boric oxide to the melt was unsuccessful in producing garnet, although this did give red hexagonal crystals of presumably potassium ferrite at high concentrations of iron oxide.

CHAPTER 6 : REFERENCES

1) E.A.D.White and J.W.Brightwell,
Chem. and Ind. (Sept, 1965), 1662

2) D.L.Wood and J.P.Remeika,
J. Appl. Phys. 37, (1966), 1232

3) P.W.Shumate, J. Appl. Phys. 43, (1972), 30

4) R.C.Linares, J.Amer. Ceram. Soc. 45(7), (1962), 307

5) E.M.Levin and H.F.McMurdie,
J. Res. Nat. Bur. Standards 42(2), (1949), 135

6) C.M.Lawrence, P.Capper, I.M.Coe and D.Elwell,
BACG Conference of Crystal Growth (York,1973)

7) J.M.Robertson,
BACG Conference of Crystal Growth (York,1973)

8) G.Garton, S.H.Smith and B.M.Wanklyn,
J.Cryst.Growth 13/14, (1972), 588

CHAPTER 7

7. CONCLUSIONS

During the past few years there has been great interest shown in thin slices of magnetic oxide crystals for bubble domain device applications. The materials requirements for such applications are numerous and have been discussed in the opening chapter of this thesis. At the present time, by far the most promising materials belong to the garnet family. Thin slices of these are conveniently fabricated by liquid phase epitaxial growth onto non-magnetic garnet substrates. By the use of highly perfect substrates, careful preparation and control of growth conditions, epilayers with extremely low concentrations of magnetic defects can be grown.

Regrettably, due to lack of time in an industrial environment, the LPE growth process has been developed empirically. Therefore correlation of results obtained in different laboratories is difficult since these must depend on the individual details of the growth conditions such as furnace geometry, temperature gradients and the hydrodynamic conditions in the melt, all of which are not always accurately known. The main objective of this research project has been to gain a more precise knowledge of the growth process. This knowledge may enable the optimum growth conditions to be specified and consequently improve both correlation and reproducibility of results. Establishing the optimum growth conditions is especially important for the controlled growth of multicomponent

garnet epilayers with both compositionaland thickness uniformity and may, in addition, prove useful for the future scaling up of the growth process, if this should become necessary.

The fundamental physical properties of the lead-based melt such as density, expansivity and viscosity have been measured. Where necessary, their values have been used to calculate the dimensionless numbers which characterise the hydrodynamic conditions in the melt prior to and during growth. The garnet solubility curve has been measured in the appropriate region of the phase diagram and the effects of flux loss by evaporation determined. The heat of solution of garnet in the flux has been measured and comparison of the value obtained with the theoretical value for an ideal solution, calculated from the garnet solubility curve, is consistent with the constituent oxide species, rather than complete garnet molecules, existing in solution. There is a large amount of indirect evidence in favour of this model.

As previously stated, the choice of growth conditions is extremely important for the reproducible growth of epilayers of uniform composition and thickness. Of the LPE processes available, dipping is the most suitable since it offers the greatest control of heat and mass transfer. The mode in which the substrate is held during dipping is also important. Rotation of the substrate in a horizontal plane produces solutal and thermal boundary layers of uniform thickness over the whole of its growth

surface. This is ideal for the production of epilayers of uniform thickness and composition. If the substrate is not rotated or is held in a vertical plane (1), both compositional and thickness irregularities may result. For both geometries the transfer of solute to the crystal interface can take place either by natural convection followed by diffusion through the resulting boundary layer or, in the absence of convection, by bulk diffusion. The disadvantages of natural convection have already been discussed in section 4.3. Bulk diffusion has the disadvantage that steady state growth conditions are never attained. Growth rate steadily decreases with dip time, producing a drift in both composition and the distribution of gallium between octahedral and tetrahedral sites through the thickness of the epilayer. In addition, since more solute is within a "diffusional length" of the edge of the epilayer than the centre, thickness gradients result.

The ability of the melts to support large undercoolings has proved beneficial on two accounts. It enables growth to take place isothermally at a preselected temperature and at a constant rate. Secondly, it has allowed the effects of supersaturation, solution flow velocity and time on crystal growth rate to be analysed independently. Investigations of this nature had previously been restricted to low temperature solution growth in all but a few cases (2, 3).

For the case of substrate rotation in a horizontal plane, the following data is relevant to the growth process;

growth rate varies linearly with supersaturation and it appears that a small supersaturation is necessary to initiate epitaxial growth. At undercoolings of greater than about 25°C, spontaneous nucleation of garnet may occur in the melt. Immediately the substrate is dipped into the supersaturated melt, growth is relatively rapid for an initial transient period of approximately three seconds, after which steady state growth conditions are attained and the epilayer thickness then scales linearly with time. The duration of the transient decreases with increasing substrate rotation rate.

The growth process essentially comprises of two rate-limiting steps; diffusion of solute through a boundary layer of typically 100 microns thickness followed by integration at the crystal interface. At low substrate rotation rates (30 rpm), boundary layer diffusion is the slower of the two steps by a factor of between three and four. At higher substrate rotation rate the thickness of the solutal boundary layer is reduced and so the significance of the surface integration process increases.

Much of the kinetic evidence is consistent with the (111) garnet face being rough on an atomic scale and consequently having a relatively high surface free energy. Growth on such an interface under conditions of constitutional supersaturation should lead to interface breakdown. This has been confirmed experimentally and found to hold even at low growth rates. However interface breakdown only began to occur after about 50 microns growth so that

it is not a problem for the growth of thin epilayers although it may be a serious problem for the growth of thicker epilayers for microwave applications.

Back-cooling of the substrate was used to eliminate constitutional supersaturation and thus stabilise the planar growth interface. Reasonable agreement between experimental results and theoretical calculations was obtained. It was found that the use of this method for the growth of thick garnet epilayers was severely limited since the magnitude of the applied temperature gradient needed to stabilise the interface was large and cracking at the substrate/epilayer growth junction frequently resulted. This method of growth may be useful in other systems where interface instability is a serious problem.

Although the lead oxide/boric oxide flux is suitable for garnet epitaxy, it has a number of disadvantages such as volatility, incorporation of lead in the epilayer and a high gallium segregation coefficient. Therefore an investigation of other potential fluxes was carried out. Molybdates had the specific advantage that certain compositions would enable growth at 600°C and yet still have a low melt viscosity. However these failed to yield garnet as the primary phase. Although the bismuth oxide/vanadium pentoxide flux was found to be suitable for the growth of bismuth-doped garnet crystals, its high viscosity made it unsuitable for the growth of thin epilayers.

The barium oxide/boric oxide flux was shown to

possess none of the disadvantages of the lead oxide/ boric oxide flux. Reproducible epitaxial growth was performed using supersaturated solutions of garnet in this flux. Because of the high viscosity at the temperatures used for garnet epitaxy, the adhesion of droplets of melt to the epilayer surface after growth was found to be a serious problem. The addition of barium fluoride lowered the melt viscosity but the effect was not substantial enough, even for large additions. Therefore it was concluded that this flux system was unsuitable for the growth of thin garnet epilayers but had a number of distinct advantages for the top-seeded solution growth of bulk garnet crystals.

CHAPTER 7: REFERENCES

1) W.Tolksdorf, G.Bartels, G.P.Espinosa, P.Holst, D.Mateika and F.Welz. J. Cryst. Growth 17, (1972), 322

2) R.A.Laudise, The Art and Science of Growing Crystals Edited by J.J.Gilman (Wiley 1963)

3) P.A.C.Whiffin, P.W.Whipps and J.C.Brice, BACG Conference (York, 1973).

ACKNOWLEDGEMENTS

I am indebted to my Supervisor, Dr. E.A.D. White, of Imperial College, for his help and encouragement throughout the course of this work. I should like to thank Mr. J.D.C. Wood for many valuable discussions and Dr. J.H.E. Jeffes of the Imperial College for the use of his calorimeter.

Financial support was provided by the Science Research Council, to whom I am deeply grateful.

Finally, I should like to thank my Wife for her patience and my Mother for carefully typing this thesis.